



THE HONG KONG
POLYTECHNIC UNIVERSITY

香港理工大學

Pao Yue-kong Library

包玉剛圖書館

Copyright Undertaking

This thesis is protected by copyright, with all rights reserved.

By reading and using the thesis, the reader understands and agrees to the following terms:

1. The reader will abide by the rules and legal ordinances governing copyright regarding the use of the thesis.
2. The reader will use the thesis for the purpose of research or private study only and not for distribution or further reproduction or any other purpose.
3. The reader agrees to indemnify and hold the University harmless from and against any loss, damage, cost, liability or expenses arising from copyright infringement or unauthorized usage.

IMPORTANT

If you have reasons to believe that any materials in this thesis are deemed not suitable to be distributed in this form, or a copyright owner having difficulty with the material being included in our database, please contact lbsys@polyu.edu.hk providing details. The Library will look into your claim and consider taking remedial action upon receipt of the written requests.

Pao Yue-kong Library, The Hong Kong Polytechnic University, Hung Hom, Kowloon, Hong Kong

<http://www.lib.polyu.edu.hk>

The Hong Kong Polytechnic University

Department of Industrial and Systems Engineering

**Effect of Electropulsing Treatment on Microstructure
and Machinability in Ultra-precision Machining of
Mg-9Al-1Zn Alloy**

Zhang Duo

A thesis submitted in partial fulfillment of the
requirements for the degree of Master of Philosophy

November 2010

Certification of Originality

I hereby declare that this thesis is my own work and that, to the best of my knowledge and belief, it reproduces no material previously published or written, nor material that has been accepted for the award of any other degree or diploma, except where due acknowledgement has been made in the text.

_____ (Signed)

Zhang Duo (Name of student)

Abstract

Abstract of thesis entitled: Effect of Electropulsing Treatment on Microstructure and Machinability in Ultra-precision Machining of Mg-9Al-1Zn Alloy

Submitted by: ZHANG Duo

For the degree of: Master of Philosophy

At The Hong Kong Polytechnic University in November 2010.

The machinability of metals and alloys is well-known for being affected by the cutting conditions, cutting tools and material properties. A high quality surface finish can be obtained by the use of advanced machine tools based on single point diamond turning (SPDT). However, no matter how accurate the machining system is, the limit of performance is determined by the tool/workpiece interaction during the chip removal process at the micro- and nano-scale levels. In particular, the dimensional accuracy and stability of the machined surface depend on the metallurgical properties of the surface before and after machining, such as the plastic deformation, microstructural changes, phase transformations, etc. Good surface finish and low cutting force are associated with a high shear angle, which is characterized by continuous chip formation and is intimately related to the properties of the workpiece materials. The chip formation process involving the dynamic interaction of the cutting tool and microstructural state of the workpiece is decisive in determining the surface quality and integrity of an ultra-precision machined surface. However, little attention has been paid to studying the effect of material properties on the machined surface.

As an alternative to traditional thermal and mechanical processes, electropulsing treatment (EPT) has been widely applied to materials processing to improve the mechanical properties by means of inducing microstructural changes, refining grain size, and improving dislocation distributions, etc. In EPT, critical electric current pulses can be applied to pass through the materials with the high current density. The treatment can be done so efficiently that only one thousandth of the energy is needed and as little as one thousandth of the time is taken compared with a conventional furnace treatment. The electropulsing treated materials are expected to have better ductility and better machinability in terms of the achievable surface finish.

An attempt is made in this thesis to design an optimal EPT condition to obtain a work material with better machinability and a fine grain microstructure, which are also conducive to the high-quality surface finish by ultra-precision diamond turning. The thesis is divided into two parts. In the first part, microstructural evolution, phase decomposition and dislocation dynamics are investigated under various types of EPT. In the second part, the micro-cutting experiments on EPT treated work material Mg-9Al-1Zn alloy (AZ91) have been conducted by SPDT processing. The machinability of electropulsing treated materials under different cutting conditions is studied in ultra-precision diamond turning.

In the first part of the study, the effect of EPT on microstructural changes, phase transformations, and dislocation dynamics has been studied under static and dynamic EPTs. In the static EPT with cold-rolled specimens, decomposition and precipitation of the β phase are tremendously accelerated with increasing frequency of electropulsing, and both twins and the dislocation density are reduced in the process. For the

specimens under dynamic EPT, it is found that the β phase decomposition is considerably accelerated compared with the conventional thermal processing. The deformation twins disappear, the dislocation density decreases, and a homogenous structure with fine grains is achieved.

In the second part of the study, machinability of the EPT treated work materials is investigated under face turning and straight cutting experiments in SPDT. It is found that the cutting forces are significantly reduced and the surface roughness is improved with the increasing frequencies of EPT. The machinability changes are investigated from the point of view of dislocation dynamics. The serrated chip morphology with macroscopic shear bands is identified as one of the characteristics in micro-cutting, and the shear band projection length is extremely high compared with shear band thickness.

This research is multi-disciplinary and cuts across disciplines, from materials science to machining engineering. It aims at developing a framework to gain a better understanding of EPT and the diamond turning process, which in turn enables the control of the surface quality of the machined surface. The results of the study lead to the design of high quality materials suitable for ultra-precision diamond turning in a wide range of alloys through EPT. It also gives rise to the provision of practical guidelines and a data basis for creating high quality materials, which possess a fine grain structure and low residual stress for manufacturing precision components that demand ever-higher surface stability.

Publications Arising from this Study

Zhang, D., To, S., Cheung, C.F., Lee, W.B., and Jiang, Y.B., “Study on phase transformation and microstructural changes induced by electropulsing treatment and single point diamond turning of AZ 91 alloy”. Proceeding of the 3rd International Conference of Asian Society for Precision Engineering and Nano Technology (ASPEN 2009), Kitakyushu, Japan (11-13th Nov. 2009).

Zhang, D., To, S., Zhu, Y.H., Wang, H., and Tang, G.Y., “Electropulsing induced phase transformations and their effects on the single point diamond turning of a tempered alloy AZ91 sheet”, *Materials Transaction JIM* (under revision).

Zhang, D., To, S., Zhu, Y.H., Wang, H., and Tang, G.Y., “Static electropulsing induced microstructural changes and their effect on the ultra-precision machining of cold-rolled AZ91 alloy”, *Metallurgical and Materials Transactions A* (accepted for publication).

Zhang, D., To, S., Zhu, Y.H., Wang, H., and Tang, G.Y., “Dynamic electropulsing induced phase transformations and their effects on single point diamond turning of AZ91 alloy”, submitted to *Journal of Surface Engineered Materials and Advanced Technology*.

Acknowledgements

The author would like to express his sincere appreciation to his chief supervisor, Dr. Sandy To, Associate Professor of the Department of Industrial and Systems Engineering of The Hong Kong Polytechnic University, for her invaluable guidance, suggestions and support throughout the project. Special thanks are also for my co-supervisors, Professor W.B. Lee, and Professor G.Y. Tang of Tsinghua University, for their constant guidance and helpful advice on the project. Special thanks go to Professor Y.H. Zhu for his helpful discussions and interest in the project.

Special thanks are given to the staff in the Advanced Optics Manufacturing Centre (AOMC) for their continuous support in the experiments. Thanks for the hands-on assistance on experiment equipment from Mr. M.N. Yeung in Materials Research Centre (MRC) and Dr. X.M. Liu for carrying out the transmission electron microscopy. Thanks for the guidance on the materials preparation from Mr. S.Y. Lau in the Materials Engineering laboratory.

Many thanks are also due to colleagues in the department of Industrial and Systems Engineering for their kindly help on the usage of analysis software in processing the experiment data. Special thanks go to Ms. S.J. Wang and Mr. H. Wang for their continuous support and help on how to process data values.

Finally, the author would like to express his gratitude to his family and friends for their kind encouragement and continuous support during the course of the work.

Table of Contents

Abstract	i
Publications Arising from this Study	iv
Acknowledgements	v
Table of Contents	vi
List of Figures	x
List of Tables	xv
Chapter 1 Introduction	1
1.1 Motivation	1
1.2 The Research Problem	3
1.3 Objectives of Study	4
1.4 Organization of Thesis	5
Chapter 2 Literature Review	6
2.1 Overview of Electropulsing Treatment	6
2.1.1 Theories of EPT	7
2.1.2 Development of EPT	8
2.1.3 Effect of EPT on Microstructural Changes	10
2.2 Overview of Ultra-precision Machining Technology	15
2.2.1 Characteristics of Single Point Diamond Turning	17
2.2.2 Work Materials	18
2.2.3 Machine Tools	21
2.2.4 Mechanics of Machining at the Micro-scale	23
2.2.5 Cutting Force in SPDT	24

2.3	Surface Quality in SPDT	26
2.4	Plastic Deformation in Chip Formation	31
2.5	Summary	35
Chapter 3	Characterization and Measurement Techniques	36
3.1	Electropulsing Treatment	36
3.2	Characterization of Microstructure	38
3.2.1	X-ray Diffraction	38
3.2.2	Scanning Electron Microscopy	39
3.2.3	Transmission Electron Microscopy	40
3.2.4	Metallurgical Microscopy	41
3.3	Single Point Diamond Turning	42
3.3.1	Measurement of Surface Roughness	44
3.3.2	Measurement of Cutting Force	47
3.4	Summary	50
Chapter 4	Effect of Electropulsing Treatment on Microstructural Changes	51
4.1	Introduction	51
4.2	Material Preparation and Experimental Procedures	52
4.2.1	Static EPT on As-tempered Specimens	52
4.2.2	Static EPT on Cold-rolled Specimens	54
4.2.3	Dynamic EPT on Rolling Specimens	56
4.3	Results and Discussion	58
4.3.1	Static EPT induced Phase Transformations and Microstructural Changes on As-tempered Specimens	58
4.3.2	Static EPT induced Phase Transformations and Microstructural Changes on Cold-rolled Specimens	65

4.3.3	Dynamic EPT Induced Phase Transformations and Microstructural Changes on Rolling Specimens	69
4.3.4	Dislocation Identity	75
4.3.5	Driving Force in the Phase Transformations	76
4.3.6	Electropulsing Kinetics	78
4.4	Summary	80
Chapter 5	Machinability in Single Point Diamond Turning after Electropulsing Treatment	82
5.1	Introduction	82
5.2	Experimental Design	82
5.2.1	Specimens Preparation	82
5.2.2	Face Turning Experiments	84
5.2.3	Straight Cutting Experiments	88
5.3	Results and Discussion	90
5.3.1	Cutting Force Changes under Various Frequencies of EPT	90
5.3.2	Surface Roughness under Various Frequencies of EPT	92
5.3.3	Microstructural Changes on the Machined Surface of Specimens	96
5.3.4	Chips Morphology	99
5.4	Summary	104
Chapter 6	Conclusions and Suggestions for Future Work	106
6.1	Overall Conclusions	106
6.2	Suggestions for Further Work	110

References		113	
Appendixes	Appendix 1	List of Abbreviations	127
	Appendix 2	Specification of Wyko NT8000	129
	Appendix 3	Specification of Talysurf PGI 1240	130

List of Figures

Fig. 2.1	Surface morphology of as drawn wire deformed (a) without and (b) with electric current treatment. (after Yao et al., 2001)	12
Fig. 2.2	SEM micrograph of annealed sample (a) without current and (b) current density 10.5 kA/mm^2 , under pulse duration for $130\mu\text{s}$ (after Zhou et al., 2002)	13
Fig. 2.3	Diamond cutting tools	23
Fig. 2.4	Mechanics of machining at the micro-scale (after Cheung et al., 2003)	24
Fig. 2.5	Geometry of chip formation and the deformation zone	33
Fig. 2.6	Schematic illustration of built up edge (BUE)	35
Fig. 3.1	Self-made electropulsing generator (Shenzhen Tsinghua Graduate School)	36
Fig. 3.2	Contact thermocouple	37
Fig. 3.3	Hall effect sensor (HDC3000H)	37
Fig. 3.4	Oscilloscope (Tekronix-TDS 1002)	37
Fig. 3.5	XRD (Bruker D8 Discover, Materials Research Centre, The Hong Kong Polytechnic University)	38
Fig. 3.6	XRD (Bruker D8 Advance, Materials Research Centre, The Hong Kong Polytechnic University)	38
Fig. 3.7	Scanning electron microscopy (JSM-6490 JEOL)	39
Fig. 3.8	Ultra-high resolution field emission scanning electron microscopy (Hitachi-S4800)	39
Fig. 3.9	Transmission electron microscopy (JEOL 2010F field emission)	40
Fig. 3.10	Precision ion polishing system (Gatan 691)	41
Fig. 3.11	Metallurgical Microscopy (Olympus GX 51, Shenzhen Tsinghua Graduate School)	42
Fig. 3.12	SPDT machine (OptoForm 30, Advanced Optics Manufacturing Center, The Hong Kong Polytechnic University)	43

Fig. 3.13	Schematic illustration of the OptoForm 30 SPDT machine	43
Fig. 3.14	Description of arithmetic average roughness Ra	45
Fig. 3.15	Non-contact interferometric measurement system (WYKO NT8000, Advanced Optics Manufacturing Center, The Hong Kong Polytechnic University)	46
Fig. 3.16	Contact stylus type measurement system (Taylor Surf PGI 1230, Advanced Optics Manufacturing Center, The Hong Kong Polytechnic University)	47
Fig. 3.17	Piezoelectric force transducer (Kristler type 9252A)	48
Fig. 3.18	Schematic illustration of the signal flow in cutting force	48
Fig. 3.19	Cutting force measurement system in single point diamond turning machine (Advanced Optics Manufacturing Center, The Hong Kong Polytechnic University)	49
Fig. 3.20	Schematic diagram of cutting force calibration process	49
Fig. 4.1	Schematic illustration of the static EPT system for as-tempered specimens	53
Fig. 4.2	A schematic view of the cold-rolling process	55
Fig. 4.3	A schematic illustration of static EPT process	55
Fig. 4.4	A schematic illustration of dynamic EPT process	57
Fig. 4.5	XRD patterns for as-tempered specimens under various frequencies of EPT	59
Fig. 4.6	SEM micrographs of the specimens under (a) non-EPT, (b) 120 Hz frequency of EPT, (c) 183 Hz frequency of EPT, (d) 252 Hz frequency of EPT	60
Fig. 4.7	TEM images of non-EPT (a) bright field image; (b2) dark field image of $(\bar{1}10\bar{1})$ reflection together with (b1) diffraction pattern from $B=[\bar{1}21\bar{3}]$ of the α phase; (c2) dark field image of $(3\bar{3}0)$ reflection together with (c1) diffraction pattern from $B=[001]$ of the β phase	62

Fig.4.8	TEM images of 252 Hz-EPT (a) bright field image; (b2) dark field image of $(\bar{1}0\bar{1}0)$ reflection together with (b1) diffraction pattern from $B=[0001]$ of the α phase; (c2) dark field image of $(3\bar{2}\bar{3})$ reflection together with (c1) diffraction pattern from $B=[335]$ of the β phase	63
Fig. 4.9	TEM bright field images of (a) non-EPT, (b) 120 Hz frequency of EPT, (c) 183 Hz frequency of EPT and (d) 252 Hz frequency of EPT	64
Fig. 4.10	XRD patterns for cold-rolled specimens under various frequencies of EPT	65
Fig. 4.11	BSEM images of (a1) non-EPT, (a2) 151 Hz-EPT, (a3) 294 Hz-EPT and TEM bright field images of (b1) non-EPT, (b2) 151 Hz-EPT, (b3) 294 Hz-EPT, showing β phase precipitates changes with various frequencies of EPT	67
Fig. 4.12	Optical micrographs of (a) non-EPT (b) 209 Hz-EPT (c) 253 Hz-EPT and (d) 294 Hz-EPT	68
Fig. 4.13	XRD patterns for the specimens under various frequencies of dynamic EPT	69
Fig. 4.14	BSEM images of (a1) non-EPT (a2) 204 Hz-EPT (a3) 309 Hz-EPT and TEM bright field images of (b1) non-EPT (b2) 204 Hz-EPT (b3) 309 Hz-EPT, showing β phase precipitates changes with various frequency of EPT	71
Fig. 4.15	TEM images of 204 Hz-EPT (a) bright field image; (b2) dark field image of $(10\bar{1}0)$ reflection together with (b1) diffraction pattern from $B=[\bar{1}2\bar{1}3]$ of the α phase; (c2) dark field image of (110) reflection together with (c1) diffraction pattern from $B=[\bar{1}11]$ of the β phase	72
Fig. 4.16	Optical micrographs of (a) non-EPT (b) 126 Hz-EPT (c) 204 Hz-EPT and (d) 265 Hz-EPT (e) 309 Hz-EPT	74
Fig. 4.17	TEM bright field images of as-tempered specimens (a) non-EPT (b) 120 Hz-EPT (c) 183 Hz-EPT and (d) 252 Hz- EPT	75
Fig. 5.1	Low speed saw	83
Fig. 5.2	Specimens with the length of 12 mm were fixed on the plate	83
Fig. 5.3	Single point diamond turning machine	84

Fig. 5.4	Schematic illustration of the diamond turning system	85
Fig. 5.5	Schematic illustration of cutting force measurement system	86
Fig. 5.6	Schematic illustration of different sectors of the specimen	87
Fig. 5.7	Schematic illustration of straight cutting process	89
Fig. 5.8	Schematic illustration of chip formation in straight cutting process	89
Fig.5.9	Mean cutting force of the as-tempered specimens under various frequencies of static EPT (depth of cut of 20 μm)	90
Fig. 5.10	Mean cutting force of the cold-rolled specimens under various frequencies of static EPT (depth of cut of 20 μm)	91
Fig. 5.11	Mean cutting force of the rolling specimens under various frequencies of dynamic EPT (depth of cut of 20 μm)	91
Fig. 5.12	Ra and Rq changes of as-tempered specimens under various frequencies of static EPT (depth of cut of 20 μm)	94
Fig. 5.13	Correlation between mean cutting force and surface roughness of as-tempered specimens under various static EPT frequencies	94
Fig. 5.14	Surface roughness of cold-rolled specimens under various frequencies of static EPT (depth of cut of 20 μm)	95
Fig. 5.15	Surface roughness of rolling specimens under various frequencies of dynamic EPT (depth of cut of 20 μm)	95
Fig. 5.16	SEM micrographs of the as-tempered specimen under 5 μm depth of cut with (a) non-EPT and (b) 252 Hz-EPT, in different cutting speed (1) $v_1=837$ mm/s (2) $v_2=2512$ mm/s (3) $v_3=4187$ mm/s	97
Fig.5.17	SEM micrographs of the 252 Hz-EPT with depth of cut (a) 5 μm (b) 10 μm (c) 20 μm (d) 40 μm	99
Fig. 5.18	SEM micrographs of free surface of chips in face turning experiment under (a) non-EPT (b) 120 Hz-EPT (c) 183 Hz-EPT (d) 252 Hz-EPT	100
Fig. 5.19	SEM micrographs of side face of chips in the straight cutting experiments under (a) non-EPT (b) 120 Hz-EPT (c) 183 Hz-EPT (d) 252 Hz-EPT	101

Fig. 5.20	Segmented chip geometry (after Cotterell and Byrne 2008)	102
Fig. 5.21	Side view of chip morphology and principle of straight cutting	103
Fig. 5.22	SEM micrographs of tool-contact face of chips in straight cutting experiments under (a) non-EPT (b) 120 Hz-EPT (c) 183 Hz-EPT (d) 252 Hz-EPT	104

List of Tables

Table 2.1	Comparison between conventional and ultra-precision machining (after Cheung, 2003)	17
Table 2.2	Work materials in SPDT	21
Table 2.3	Factors influencing surface quality in SPDT	27
Table 3.1	Specification of single point diamond turning machine (Optoform 30)	44
Table 4.1	Experimental parameters of as-tempered specimens under static EPT	54
Table 4.2	Experimental parameters of cold-rolled specimens under static EPT	56
Table 4.3	Experimental parameters of dynamic EPT	57
Table 5.1	Cutting conditions of Group-A for specimens with different types of EPT	87
Table 5.2	Cutting conditions of Group-B for as-tempered specimens with static EPT	87
Table 5.3	Cutting conditions of Group-C for as-tempered specimens with static EPT	88
Table 5.4	Cutting conditions of straight cutting process	89
Table 5.5	Surface profiles of specimens under various frequencies of EPT	93

Chapter 1 Introduction

1.1 Motivation

Single point diamond turning (SPDT) is one of the most effective cutting techniques to produce optical quality components in ultra-precision machining technology (Ikawa, 1991). As the demands for high tolerance optics products increase rapidly with manufacturing technology, the quality of the machined surface becomes much more crucial. The difference between conventional and ultra-precision diamond turning, lies not only on the factors such as cutting conditions, cutting tools and machine tools which affect the surface finish in machining, but also on the material behavior such as deformation behavior, ductility, residual stress, swelling of material at sub-micro depths of cut (Ueda et al., 1991; Inanura et al., 1990; Zhang, 1986). It was reported that the dimensional accuracy and stability of the machined surface depends on the metallurgical properties of the surface before and after machining (Lee et al., 2000), such as plastic deformation, residual stress, material swelling and phase transformation. In order to achieve good surface finish, low cutting force and a high shear angle should be expected in the ductile mode of continuous chip formation (Furukawa et al., 1988). The dynamic interaction of the cutting tool and the microstructural state of the workpiece at the surface during the chip formation process are very complicated, and together they play an important role in determining the quality and integrity of the ultra-precision machined surface. Moreover, as the inherent

materials factors which would affect surface finish, including material swelling, anisotropy and crystallographic orientation, cannot be eliminated or minimized by the optimization of the process parameters and machine design, the surface roughness is restricted in the machining system. To enhance the precision of the machined surface, residual stress and swelling should be decreased from the aspect of material properties. As shown in previous research (Yang et al., 2001), the electropulsing effect can reduce the residual stress of the processed materials, which would be a feasible method to improve the quality of the machined surface in the micro-cutting process.

As an alternative to traditional thermal and mechanical processes, electropulsing treatment (EPT) has been widely used in material processing to improve the mechanical properties, including the healing effect of cracks and flaws, the refining of grain size, and the improvement of elongation ratio, which is the ratio of the materials elongation length to its original length. It was firstly discovered in the 1960s (Troitskii et al., 1973) that with the application of high-density current pulses, the residual stress in work material could be reduced. Thereafter, extensive studies have also been carried out to examine its effect on recrystallization, phase transformation and dislocation movements in electropulsing treated materials (Conrad et al., 2001). Although the EPT process can reduce the deformation resistance and improve the surface integrity of the material, the pre-machining treatment has not been implemented in ultra-precision machining technology, which can produce optical quality components with submicron form accuracy and surface roughness within a few or tens of nanometres

In this research, the effect of EPT is studied from the viewpoint of microstructural changes, and focuses on phase transformations, grain structure changes and dislocation movements. On the basis of study of EPT, the advantages of pre-machining EPT treated work materials are investigated in single point diamond turning, focusing on the consequential microstructural changes, cutting force variations and the improvements on surface roughness of the machined surface.

1.2 The Research Problem

In the past decades, the majority of research focused on the mechanism of ultra-precision machining, such as optimizing cutting parameters (Born and Goodman, 2001), and conducting computer simulation to study the cutting mechanics at the micro-scale (Ueda et al., 1992). Considerable attention has also been devoted to the modeling and simulation of the topography of the machined surface (Akedo, 1993). Unfortunately, little research has been conducted on the influence of materials properties on the surface quality in single point diamond turning. Moreover, few studies consider developing an appropriate material for achieving high surface quality in ultra-precision machining. Thus the research concerning the micro-scale rather than the macro-scale study, such as microstructure of the machined surface and phase transformation, has made little progress. A surface finish with high form accuracy and surface roughness still relies on the experiences and skills of the machine operators. The materials factors, including microstructure and phase stability of the machined surface in SPDT, have drawn even less attention in this area. Therefore, a thorough investigation on the

influence of these materials factors on the surface quality in SPDT is of urgent and paramount importance for practical applications.

This thesis is dedicated to introducing EPT into the field of ultra-precision machining with a set of machining experiments on SPDT. The project can be divided into two parts. In the first stage, the effects of electropulsing in static and dynamic states are investigated on AZ91 alloy, which focus on the microstructural changes, phase transformations and dislocation movements; in the second stage, the materials after electropulsing treatment are machined by SPDT. Changes in surface roughness and cutting force are studied and compared with specimens without EPT, and the chip morphology during the turning process is also investigated.

1.3 Objectives of Study

The main goal of the study is to gain a better understanding of the effect of EPT on the microstructural changes and phase transformations of AZ91 alloy. An optimal EPT process is designed to obtain high quality work materials suitable for ultra-precision diamond turning. The objectives of the study are:

- (i) To study the effect of static and dynamic EPT on the microstructural changes and phase transformations of AZ91 alloy;
- (ii) To investigate the machinability of electropulsing treated materials under different cutting conditions by ultra-precision diamond turning; and

(iii) To explore an ideal material by EPT in order to improve the surface quality in ultra-precision machining.

To achieve these goals, AZ91 alloy is electropulsing treated under various EPT parameters, and then facing and straight cutting are conducted by SPDT. With an insight on the microstructural changes and phase transformations induced by EPT, the machinability in SPDT is investigated focusing on the cutting force variations, the surface roughness and chips morphology.

1.4 Organization of the Thesis

The thesis is divided into six chapters as follows:

In the first Chapter, the background of the study is introduced, the research problem is discussed and the objectives of the study are stated. In Chapter 2, a literature review on the theories of electropulsing treatment, the effect of EPT on microstructure, an overview of ultra-precision machining, and the development of the SPDT process are addressed. The experimental set-up and measurement methods for investigating materials properties are introduced in Chapter 3. The effect of both static and dynamic electropulsing treatment on microstructural changes of AZ91 alloy under various conditions of EPT are studied in Chapter 4, focusing on the EPT induced phase transformations and dislocation changes. In Chapter 5, surface roughness and cutting force of materials by single point diamond turning after various electropulsing treatment parameters are investigated in detail, and the chip morphology is also discussed. Final conclusions and recommendations for further studies are given in Chapter 6.

Chapter 2 Literature Review

2.1 Overview of Electropulsing Treatment

The electropulsing effect is a phenomenon in which the properties of materials, including various metal materials, ceramic materials, superconductor materials and metallurgic powder products, are transnured by the application of a high-density current pulse. The drawing force and the ultimate tensile strength decrease, and the plasticity and the elongation ratio improve significantly. As an alternative to traditional thermal and mechanical processes, EPT has been recognized for its high efficiency and low cost. In recent years, the influence of an electric current on the following solid state transformations in metals are considered to be the crucial parts of the study: (1) interfacial reactions leading to intermetallic compound formation, (2) precipitation (ageeing) of substitutional and interstitial solutes, (3) crystallization of amorphous alloys and (4) recrystallization and grain growth following cold work (Conrad, 2000).

The phenomenon was first found in the 1960s by a Russian scientist in experiments in drawing a Zn single crystal with radiations of electrons. It was found that with the radiation of the electrons, the drawing stress was decreased (Troitskii, 1963). It later became a subject of greater interest. Okazaki (1962) reported that under constant-strain-rate conditions, stainless steel wires subjected to current pulses varying in intensity between zero and 8000 A/mm^2 experienced stress relaxation during the pulses. Since then, the applications of EPT are booming in the materials science and

engineering fields, such as electroplasticity (Yang et al., 2001), electromigration (Lloyd et al., 1999), enhanced powder densification (Mishra, 2000), recrystallization (Xiao et al., 2002), and healing crack and damages (Zhou et al., 2000). In recent years, more work has been conducted in this field, and simultaneously many more problems have been confronted. Research on the effect of electropulsing treatment on material properties in ultra-precision machining is an area full of challenges and is of great significance.

2.1.1 Theories of Electropulsing Effect

Since the Russian scientist Troitskii (1963) studied in drawing a single Zn crystal, and Conrad (1989) experimented on the recrystallization of copper, numerous research have been carried out on the electropulsing effect (EPE) mechanism, from different aspects of the respective theoretical basis.

(i) Electric wind force

In drawing a Zn single crystal with radiation of electrons, it was found that the drawing stress was decreased. Troitskii (1984) claimed that when the electrons were introduced into the wire drawing process, the electrons gave a force to the dislocations, which led to the movement of the dislocations and their homogeneous distribution. The explanation was that with the introduction of current pulses, the electrons would exert a force named “electro wind force” on the dislocations and enhance their movement so as to scatter the tangles of dislocations, thus leading to an increase in the plasticity of the material.

(ii) Magnetic field effect

When current pulses were introduced into a metal wire drawing process, the motion of dislocations was hindered by a pinning center of paramagnetic character, and the diffusion rate was strongly affected by the magnetic field induced by the current. Such a model was established on the assumption that the principal cause of the electroplastic effect was the increase in the length of the free dislocation segments in the current-induced magnetic field, and the paramagnetic character of the pinning centers was another important assumption.

2.1.2 Development of Electropulsing Treatment

Electropulsing treatment is the key technique in the manufacture of high quality metal parts. Currently, many experiments have been done on drawing Zinc, Copper single crystal, dual-phase austenite and martensite, and stainless steel wires. Since the EPE was found, the phenomenon has been used in machining many hard to work materials: Tang (1998) investigated the application of electroplastic processing technology for the cold-drawing of steel wires, mainly focusing on the properties of Cr₁₇Ni₆Mn₃ and 4J42 alloys in the process. It was found that the drawing stress decreased by about 20–50% with the application of electric current pulses. For Cr₁₈Ni₉, the drawing stress decreased to about 50% compared with the conventional wire-drawing process. Simultaneously, the plasticity of the material is significantly improved. Due to the application of electric current pulses, a better surface quality than that drawn by the conventional process is expected. When a density of approximately 10³ A/mm² for about 20 μs current pulse is applied to the drawing process of Cr₁₇Ni₆Mn₃ and 4J42, the drawing force and the ultimate tensile strength decreased, the

plasticity of the wire and the elongation ratio improved significantly. Moreover, there was an increased velocity of the steel from 9 m/min to 60 m/min, which is the velocity used in the actual production process in the factory.

At present, the main fields of international research include: research on paramagnetic or ferromagnetic metals; dual phase crystals or single crystals; superconductive materials; application on producing accurate parts for the aero fields. The influence of an electric current on the following solid-state transformations in metals is considered to be the crucial parts of the study:

- (1) Inter-metallic compound formation and growth in diffusion couples;
- (2) Precipitation;
- (3) Crystallization of amorphous alloys; and
- (4) Recrystallization and grain growth of cold worked metals.

The formation and growth of inter-metallic compounds are in qualitative accord with electro-migration theory. Regarding precipitation, an electric current can either enhance or retard the precipitation rate, depending on the alloy, the current density and its frequency. Although electromigration plays a major role in the phase transformation process, many factors including the quenched-in vacancies to various sinks and the local internal stress are also important considerations. Both a continuous direct current (DC) and high current density electropulsing enhances the crystallization rate of amorphous alloys. The effects of EPT are greater than the simple electro-migration theory, and it suggests the cooperative motion of a larger number of atoms. Electropulsing enhances the recrystallization rate of cold worked metals, but retards subsequent grain growth (Conrad, 2000).

Research on microstructures under electropulsing was also conducted on amorphous materials. It was reported that amorphous $\text{Fe}_{78}\text{Si}_9\text{B}_{13}$ ribbons were nano-crystallized by using high current density electropulsing instead of the usual annealing (Teng et al., 1995). Crystallization under electropulsing suggested that a resonant collective motion of many atoms and modification of the thermodynamic parameters in amorphous alloys would occur (Mizubayashi et al., 2001). The maximum stress impedance ratio of 350% was obtained in amorphous $\text{Fe}_{73.5}\text{Cu}_1\text{Nb}_3\text{Si}_{13.5}\text{B}_9$ ribbons in optimal conditions of current annealing (Li et al., 2002). Electropulsing would also induce many factors which would cause nanostructure transitions, such as high-rate heating, rapid cooling, thermal stress, reduced thermodynamic energy barrier, high-rate electron impacting, and accompanying phase transformation (Zhang et al., 2003). The dominant factor determining the microstructural changes depends on the material and experimental conditions.

2.1.3 Effect of Electropulsing on Microstructural Changes

As an alternative to traditional thermal and mechanical processes, EPT has been recognized for its high efficiency and low cost. Extensive studies have been carried out in the areas of precipitation diffusion, recrystallization and dislocation movements, crack healing, nucleation rate changes, nano-structure formation and electro plastic effects.

Campbell (1984) reported that with precise frequency control it was possible to completely suppress the carbon precipitation in the quench aging process of low carbon

steel. By applying electropulsing treatment of 1000 A/cm^2 current at 100 Hz, the age hardening behavior could also be reduced. This phenomenon is attributed to the fact that when the frequency of the pulsed current matches the carbon atom jump frequency towards a vacancy, precipitate nucleation in the iron would be under scrutiny. Li et al. (1998) also reported that the electric current would help the segregation of impurity atoms at the grain boundaries. In 2004, it was found that electric current improved long range diffusion of the β phase precipitation in Cu-Zn alloys (Zhou et al., 2004). Classical electromigration theory failed to explain the order of the increased diffusion rate needed for supporting the formation of the microstructure. The assumption of the dramatic increment in the diffusion coefficient and the decrease in the activation energy is raised to explain the phenomena.

The effects of electropulsing on dislocation movement and recrystallization were first reported by Conrad (1983). It was found that the application of direct current electropulsing on cold worked copper would result in a refined microstructure. Short treating time, high heating rate, accelerated nucleation and lower final dislocation density under electropulsing conditions might cause this phenomenon. Dislocation structure in an electropulsed specimen was also found to be vastly different from that of a thermally treated one. It was proposed that the movement of dislocation enhancement by electropulsing treatment was caused by (1) electron wind effect (2) localized atomic scale heating (3) increment of the dislocation vibration frequency and (4) improvement of the sub-grain coalescence. It was also found that a recrystallized nucleus would form in the lower dislocation density region, while boundaries would form in the higher dislocation density region when the dislocation density gradient accumulated to a

certain level. The nucleation rate in recrystallization under electropulsing treatment was reported to be 10^4 times higher than in the conventional treatment methods.

The crack healing effect by electropulsing treatment was firstly reported by Conrad (1991). The voids or cavities of 7475 aluminum alloy were healed by using electropulsing treatment. Tang and Yao (2000; 2001) also reported the improvement of surface finishing, scratches healing and micro cracks healing by using an electric current. Qin (2001) developed a rigorous theory towards understanding the healing effect of EPT. The thermodynamic driving force for healing cracks was calculated, and was found to be proportional to the square of current density. For better crack healing, the electropulsing treatment should be controlled considering following factors: (1) the temperature rise by joule heating should be lower than the structural transformation temperature in the bulk material, but higher than the melting temperature at the crack region (2) the electric current should be above certain value ($30\text{-}60\text{ A/cm}^2$) depending on the material.

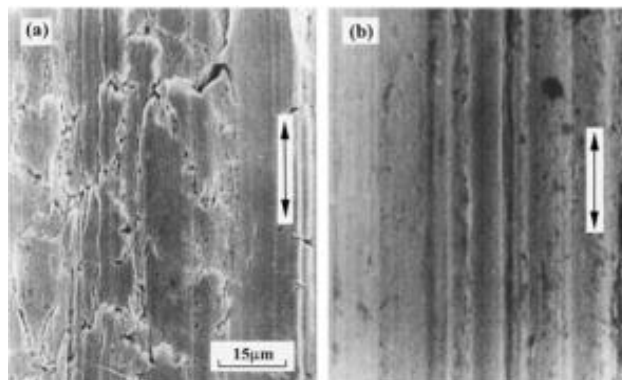


Fig. 2.1 Surface morphology of as drawn wire deformed (a) without and (b) with electric current treatment (after Yao et al., 2001)

The effect of electropulsing on the nucleation rate has drawn attention ever

since the 1980s. Conrad (1984) reported that the colony size of the cast tin lead alloy under electropulsing was reduced significantly under electropulsing treatment. Qin (1998) developed a quantitative relationship between nucleation rate and applied electropulsing parameters. The excess free energy for a spherical nucleus under electropulsing was calculated, and it was found the application of a low electric pulse of about 10^3 A/cm^2 would decrease the grain size. However, the influence of the pinch force and joule heating was ignored in the theory, which could play an important role in a high current density situation. High current density electropulsing experiments with 10.5 KA/mm^2 and of $130 \mu\text{s}$ duration were made on low carbon steel, and the results showed dramatic changes in the microstructure. Application of electropulsing with current density up to 10^{10} A/m^2 was used on some metallic alloys too. For cold worked H52 Cu-Zn alloy, the randomly oriented grains were of three orders of magnitude smaller than the original size.

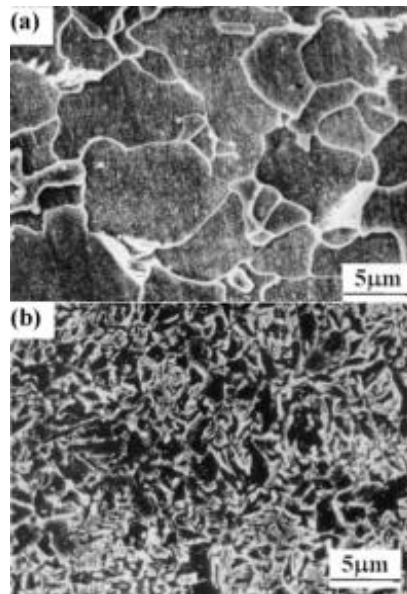


Fig. 2.2 SEM micrographs of annealed sample (a) without current and (b) current density 10.5 kA/mm^2 , under pulse duration for $130 \mu\text{s}$ (after Zhou et al., 2002)

The electro plastic effect is the application of electric current on metals that reduce deformation resistance and strain hardening, while increasing the materials' plasticity. Li (1998) reported softening behavior of Zn 5wt%-Al alloy with reduced flow stress, decreased creep rate, increased strain hardening rate and a strengthening property by using a 3.2 KV/cm electric current. Cao (1990) also reported high electric current would improve the hardening ability of 4030 steel during quench casting, and at the same time reduce defects and micro twins in the material. For $Cr_{18}Ni_9$ austenitic steel, decreases of ultimate tensile strength and increases of elongation were found by using electropulsing treatment (Tang et al., 2000). It was assumed that the excess energy in the electropulsing process provided activation energy for the dislocations to overcome obstacles and thus reduce internal friction resistance. Livesey (2001) conducted electropulsing experiments in silicon steel, and found the hardness decreased linearly with increasing current density. Noticing that an optimal frequency existed for the phenomena, Tang (2003) suggested that when the frequency of the input pulses approached the substance wave in the material, an intensive elastic vibration of waves with the same frequency would occur, thus enabling the movement of the dislocations in the material along the flow direction at a high speed. This hypothesis was later proven to be deficient, as the atomic vibration frequency is of much higher order than the pulse frequency.

Although the EPT process can reduce the deformation resistance and improve the surface quality of materials, it has not been widely implemented in ultra-precision machining technology. This is one of the most used cutting techniques for producing

optical quality components with submicron form accuracy and surface roughness within tens of nanometres.

2.2 Overview of Ultra-precision Machining

The rapid development of advanced science and technology has given rise to advanced manufacturing technology. Ultra-precision machining technology was firstly established in the 1960's using the precision machine tools available at that time for the production of dedicated mechanical or optical parts of a particular advanced system (Ikawa, 1991). In the 1970's, the technique was applied for the production of a variety of optical components, such as the production of mirrors for the inertial confinement fusion reactor, due to its high precision, versatility and lower overall manufacturing cost. Through the 1980's, the technique, with the development of highly advanced machine tools with sophisticated metrology and control, has resulted in extended industrial use for the manufacturing of aluminum scanner mirrors, aluminum substrate drums in photo copying machines and aluminum substrates for computer memory disks (McKeown, 1987). To meet the rapidly increasing demands for high quality optic components in the field of advanced science and technology, including computer, electronics and defense industries, and the operation of ultra-precision machining process is widely used and has further evolved in the past few decades (Wilks, 1980; Shimada, 1989).

Ultra-precision machining is defined as a cutting technique, which produces optical quality components with sub-micron meter form accuracy and surface

roughness within a few tens of nanometers. The technique is based on a high degree of tool profiles duplication and relative tool work motions (Taniguchi, 1983). It makes use of a mono-crystalline diamond cutting tool which possesses nano-metric edge sharpness, form reproducibility in a sub-micrometer range and wear resistance. The machining process is widely used to produce high quality molds, optical surfaces, engineered surfaces, and its main field of application is the production of micro-parts. A comparison of conventional and ultra-precision machining is listed in Table 2.1 (after Cheung, 2003). It can be seen that the machining accuracy of ultra-precision machining is about 100 times better than that of conventional machining, and the surface roughness is about 1000 times smaller. The ultra-precision machining can be classified into five divisions: single point diamond turning (SPDT), ultra-precision grinding (UPG), two-axis milling, ultra-precision raster milling and ultra-precision raster grinding. The ultra-precision single point diamond turning (SPDT) is an advanced machining process known for its comprehensive features including its capability to produce optical components with form accuracy of sub-micrometer range, and its capability of producing components to the required accuracy at just one cutting.

Meanwhile, most research carried out mainly focused on the effects of materials properties on ultra-precision machining, such as the cutting behavior and mechanism of materials removal and chip formation (Yuan et al., 1992; Paul et al., 1996). Considerable attention has also been devoted to modeling and simulation topography (Chiu, 1997; Ueda et al., 1980). Unfortunately, few studies have been conducted on the effect of materials properties on ultra-precision machining.

Table 2.1 Comparison between conventional and ultra-precision machining (after Cheung, 2003)

Type of process		Conventional machining		Ultra-precision machining	
		Rough cut	Finish cut	Rough cut	Finish cut
Cutting conditions	Feed rate (mm/rev)	0.1-1	0.01-0.05	0.01-0.05	0.005-0.001
	Spindle speed(r/min)	100-300	200-300	1000-2000	2000-3000
	Depth of cut	0.1 mm-1 mm	0.01 mm-0.1 mm	10 μm -50 μm	1 μm -5 μm
	Tooling	High speed steel tool Carbide tool Ceramic tool Industrial diamond tool		Single crystal diamond tool Industrial diamond tool	
Machining part	Roughness	10 μm -100 μm	1 μm -10 μm	0.02 μm -0.03 μm (20 nm-30 nm)	Less than 0.01 μm (10 nm)
Machining quality	Form accuracy	1 mm-0.5 mm	0.01 mm-0.05 mm	1 μm -2 μm	0.3 μm -0.5 μm

2.2.1 Characteristics of Single Point Diamond Turning (SPDT)

SPDT is an advanced ultra-precision manufacturing technology, it employs a mono-crystalline diamond cutting tool, and possesses a nanometric edge radius, form reproducibility and wear resistance; SPDT can cut a workpiece with an extremely high precision in a controlled machining environment. It is an important technology for the fabrication of high precision components, such as optical, mechanical and electronic products. The depth of cut being used in SPDT is in the order of a micrometer or less;

as a result, micrometer to sub-micrometer form accuracy and surface roughness in the nanometer range for the machined components can be achieved.

Firstly introduced in 1960's, SPDT was developed to produce computers and electronic components with simple cylindrical or flat shapes, such as disks for computer memory systems (Ikawa et al., 1991). Owing to the military's need for optical components and the lack of industrial suppliers, this advanced manufacturing technology began to transfer to industry in the 1970's. The pioneering work by Bryan (1979) was carried out for its application in producing optical components of complex forms. Known for its high precision, versatility and low overall manufacturing cost, SPDT made its way into industrial use for manufacturing aluminum scanner mirrors, aluminum substrate drums in photo copying machines and aluminum substrates for computer memory disks, all of which possess the surface finish in nanometers range and micrometer sub-micrometer form accuracy. The extensive usage of SPDT has in turn resulted in the fast development of highly advanced machine tools with sophisticated metrology and control of diamond tools of reliable quality. Applications are now used in the manufacturing of inserts for injection-molded plastic camera lenses, and other optical parts with complex forms, like aspheric surfaces.

2.2.2 Work Materials

The selection of work materials plays an important role in the material removal process, and the desired nanometric surface finish can only be achieved in some specific work materials with good machinability (Evans, 1991; Fukukawa, 1988;

Okuda, 1989). Machinability is used to rate ease of machining a material relative to tool life, or surface finish produced. The basic machinability of a material is the function of its chemistry, structure and compatibility with tool material. The basic machining characteristics of iron, aluminum, titanium, nickel, copper and their alloys are quite different due to the difference in chemical and physical properties of the base metal.

The materials that can be machined by a diamond tool are those where the wear rate is low enough so that reasonable surface areas can be produced economically. They generally include most face centered cubic (FCC) elements, fundamentally non-ferrous alloys such as aluminum, copper, nickel, gold, brass and bronze. Typical work materials used in diamond turning can be classified into four main types:

- (1) Ductile materials like copper and aluminum;
- (2) Brittle materials like silicon and germanium;
- (3) Single crystal materials like KDP; and
- (4) Amorphous materials like electroless nickel and PMMA.

Although relevant research has also been conducted in the machinability of special materials like SiCw/Al composites and Al/SiCp composites (Yuan, 1993; Chan, 2000; Cheung, 2000), these materials are not commonly used in industry.

Ductile materials, such as aluminum, copper and nickel copper, which are widely used in the mold and die industries, would suffer from the low specific stiffness, the high thermal coefficient of expansion and the high oxidation when machined by

conventional machining technique. However, the optical quality together with damage-free surfaces on these brittle materials can be achieved by SPDT using fewer manufacturing steps, comparing with the traditional grinding and polishing methods. The theoretical basis for the diamond turning of ductile materials is better established than that for the other types of materials, and the machinability of these materials has been fully investigated a lot in the past decades (Okuda, 1989; Masuda, 1989). Sugano (1987) carried out an investigation of the residual stress in diamond turning on aluminum alloys and found that the effect of the slip in crystals on surface roughness must be considered in the cutting process; the magnitude of the residual stress on the work surface was also dependent on the nose radius of the cutting tools and the feed rate. Black (1972) conducted research in large strain plastic deformation processes and reported that the shear front-lamellar structures at the top of the chip were correlated with grain orientations.

Brittle materials, including glass and silicon, are widely used for a variety of devices that are incorporated into electronic, optical and laser optical products. The cutting of brittle materials is performed by brittle fracture, and plastic chip formation is only feasible at an extremely small depth of cut, which means that when an extremely small amount of materials is removed, the material removal mechanism may change from brittle fracture to plastic deformation. Nakasuji (1990) reported that the brittle-ductile transition was dependent on the material properties, the magnitude of the applied force and the volume of material to be removed. Meanwhile, the crystallographic orientation in single crystals also played an important role in the

transition, because the resolved stresses on the cleavage plane and on the slip plane varied with their orientations (Kim, 1998; Yoshuda, 1990).

In addition, it is found that diamond cutting is well suited to cutting crystal materials such as germanium, silicon, zinc sulfide, as well as polymers such as polymethylmethacrylate (PMMA), polystyrene, and polycarbonate (Yuan, 1993; Ikawa, 1991; Lin, 1998). Ferrous materials cannot be machined by diamond tools as the diffusion of carbon from the diamond tool to the workpiece leads to rapid tool wear, and as the carbon is absorbed by the metal from the tool, the cutting mechanism becomes very complex. Materials available for diamond turning are listed in Table 2.2.

Table 2.2 Work Materials in SPDT

Semiconductors	Metals	Plastics
cadmium telluride	aluminum and alloys	acrylic
gallium arsenide	magnesium and alloys	fluoroplastics
germanium	copper and alloys	nylon
lithium niobate	electroless nickel	polycarbonate
silicon	gold	PMMA
zinc selenide	silver	propylene
zinc sulphide	zinc	styrene

2.2.3 Machine Tools

The cutting tools used in SPDT differ from those in traditional turning. Improvements in surface finish and form accuracy in diamond turning have depended

mainly upon advances in their design (Chiu, 1997). Initially, hydrostatic bearings with either gas or fluid for machine tool spindles were widely used through their ability to operate at submicron rotational accuracy (Bryan, 1979; Donaldson, 1982). In the 1960's, air-bearing spindles enjoyed fast development and most significantly affected progress in machining process (Kobayashi, 1978). Thereafter, with the introduction of machine tools with high stiffness, laser position feedback, hydrostatic slide ways, materials with high thermal stability and techniques to characterize machine tool errors have also improved the diamond turning process (Kanai, 1983). The general requirements for cutting tools in diamond turning are stable cutting in the submicron or nanometer region, nanometric edge sharpness, form reproducibility and wear resistance. The hardness is four times that of carbide, permitting the sharpness of its edge is the range of 0.3 nm to 0.5 nm, about the level of the diamond's atomic spacing, and the sharper the cutting edge the tool possesses, the smaller the minimum depth of cut, and consequently the amount of surface roughness the workpiece will suffer is reduced (Ikawa et al., 1987; Zhang et al., 1986). The rounded cutting edge radius of diamond tools can reach up to 0.01 μm , and the critical edge radius was calculated to be about 2 nm based on the energy balance between the surface and elastic strain energies at the cutting edge. Besides, a diamond tool also has a very high thermal conductivity, low thermal expansion and a low rate of compression, giving it the capability of conducting heat away from the cutting edge while maintaining its geometry. Samples of diamond cutting tools are shown in Fig. 2.3.



Fig. 2.3 Diamond Cutting Tools

2.2.4 Mechanics of Machining at the Micro-scale

The mechanics in ultra-precision diamond turning are very different from the conventional machining process in the following aspects: the chips from diamond turning are usually continuous and stable when being cut with a thickness of a few nanometers. The feasibility of a nanometric chip removal suggests that an atomistic approach to the removal process is appropriate; the force during the turning is also very small, usually in the range of sub-newton level. Though it is difficult to measure, due to its small magnitude, the force is influenced by size effect and the high ratio of the normal to the tangential component of the cutting force, especially at very small depth of cut. The cutting model of diamond turning depends on the interaction of the fine depth of cut, finite edge radius of the tool, low ratio of depth of cut to edge radius, quality of the cutting edge and minute amounts of wear on the clearance face of the tool. The accurate cutting model can only be determined by the spatial extent of the zones of

plastic deformation and the sliding contact lengths at the tool-chip and tool-workpiece interfaces. The diamond tools damage are always in the form of cutting edge chipping, when the stress level in a tool edge exceeds the strength of diamond at a specific location, and in wear. They are also subject to thermo-chemical wear due to oxidation, graphitization, diffusion and carbide formation. The surface finish of a diamond turned part depends largely on the smoothness of the tool motion and the tool geometry. The schematic illustration of the mechanics of machining at the micro-scale is shown in Fig. 2.4.

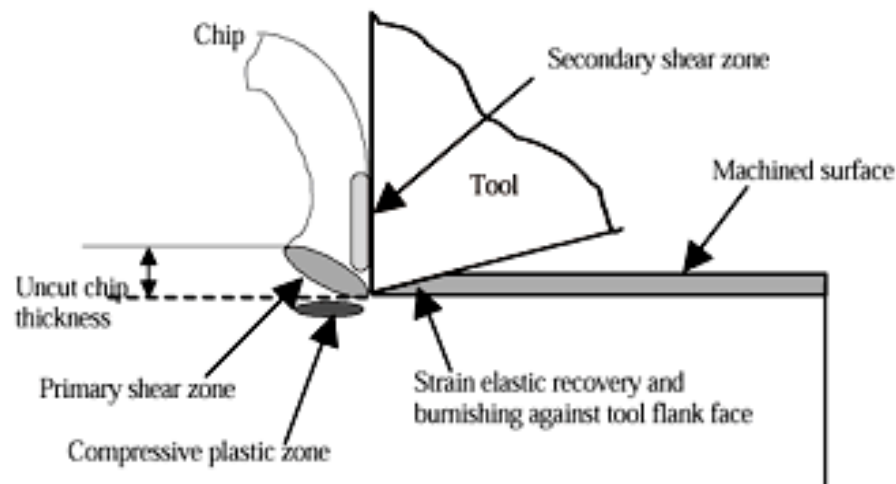


Fig. 2.4 Mechanics of machining at the micro-scale (after Cheung et al., 2003)

2.2.5 Cutting Forces in the SPDT

Cutting force is a parameter widely used to study the cutting mechanism in the machining process. In single point diamond turning, crystallographic orientation has been reported to have a significant influence on the cutting force (Lee et al., 1993).

Sugano et al. (1987) reported that the cutting force increased with the cutting distance, and a non-linear increase in the value of F_t (thrust force) indicated tool wear. Lucca et al. (1991) conducted research on the influence of the depth of cut to the cutting force and showed that a significant fraction of mechanical energy was contributed by the plastic work of the work material source when the cutting force increased with the decreasing depth of cut. When the depth of cut becomes of the same order as the tool edge radius, the effect on the overall force system by changes in the effective tool rake angle and resultant plowing is very significant. It is called the “size effect” by Furukawa and Moronuki (1988). Inamura (1993) reported that, a significant fraction of the mechanical energy expended in the diamond turning process of copper is not associated with material removal, but related to the redundant plastic work caused by the plowing of the edge of the tools as well as the sliding of the flank face elastically loaded at the machined surface. Lucca (1993) also reported that the redundant work resulted in energy dissipation and the amount of dissipation depended on the tool edge geometry.

There was also some research conducted on the cutting force model. Predictive cutting force models for flat-end and ball-end milling operations have been developed by DeVor (1982). These models generalize the empirical relationship between the instantaneous cutting forces and the chip load distribution for the range of cutting conditions being investigated. They can also be used to predict the cutting forces when the cut geometries are known. Due to the large number of empirical coefficients to be determined for each combination of machining conditions before the force prediction can be actually conducted, these models are not suitable for use in milling simulation and optimization. Drescher et al. (1990) proposed a tool force model in diamond

turning with the work material of oxygen-free high thermal conductivity (OFHC) copper and aluminum alloy 6061-T6. It suggested that the tool geometry and material hardness had a large influence on the tool force. Arcona (1988) concluded that shear angle did not change much with the depth of cut but varied according to the material used; the shear angle decreased as the ratio of tool edge radius to depth of cut increased. However, these models did not consider the effect of crystallographic orientation of the work material. Lee et al. (1999) developed a microplasticity model to predict the effect of crystallographic orientation on the shear angle and on the chip formation, as well as on the variation of micro-cutting force. This model is the basis for studying material induced vibration and its effects on surface quality. Milfelner and Cus (2003) developed a simulation system to determine the cutting forces in the ball-end milling process. This model considered many factors, such as tool geometry, work material, and cutting parameters. However, optimization of cutting parameters cannot be determined using this method.

2.3 Surface Quality in SPDT

In SPDT, the quality of a machined surface plays a very important role in the functional performance of a product, especially in optical applications. A lot of research has been conducted on the factors that contribute to surface quality. Sata et al. (1985) found that the quality of the machined surface is influenced by tool geometry, feed rate, material properties, spindle rotational errors and relative tool-work vibration. Mitsui and Sato (1978) reported that the surface roughness affected by the relative tool-

work vibration was almost equal to the whole amplitude of the vibration. This argument, however, was undermined by experimental evidence provided by Tai (1980) in that a surface finish better than the whole amplitude is often obtained in single-point diamond turning. In general, these factors can be categorized into process factors and the microstructures of the materials as listed in Table 2.3.

Table 2.3 Factors influencing surface quality in SPDT

Process factors	Controllable	Cutting geometry	Cutting conditions (spindle speed, feed rate) Tool geometry
		Dynamic characteristics of a cutting system	Relative tool-work vibration
Material microstructures	Uncontrollable	Crystal defects, grain boundaries	
		Nature of each phase	
		Crystallographic orientation	

Process factors include cutting conditions such as spindle speed, feed rate, tool geometry and relative vibration between the tool and the work material. These factors are closely related to the cutting geometry and the dynamic characteristics of the cutting system, and can be minimized or even eliminated through a proper selection of operational settings and better control of the dynamic characteristics of the machine system. According to Cheung et al. (2003), the peak-to-valley height and arithmetic roughness would decrease as a higher spindle speed is used in the cutting system. The material microstructures include crystal defects and grain boundaries and the geometry, shape, size and crystallographic orientation distributions of various phases, and the nature of each phase. These factors are the inherent properties of the material, thus

cannot be eliminated or even minimized by the optimization of process parameters and machine design.

In process factors, the effect of spindle speed plays an important role in the generation of machined surfaces. It is found that for aluminum and copper alloys, the maximum peak-to-valley height, R_t , and the arithmetic roughness, R_a decreases with increasing spindle speed (Cheung et al., 2003), and the surface roughness parameters increase with increasing feed rate. It is also found that R_a decreases with increasing tool nose radius for a small radius but increases at large radius. There is no systematic relationship found between the depth of cut, the maximum peak-to-valley height and the arithmetic roughness: as the depth of cut increases, the surface roughness is found to vary unsystematically. For the tool geometry, tools having large negative rake angles are generally preferred since a diamond tool with a negative rake angle will have stronger edge strength to protect the tool from damage when brittle materials are machined. However, the compressive stress on the work material yields plastic deformation of the workpiece (Cheung et al., 2002). The appropriate negative rake angle in the diamond turning of brittle materials exerts a high compressive stress on the workpiece that inhibits the occurrence of extensive tensile cracking (Leung et al., 1998). Relative tool-work vibration also plays an essential role in a machined surface. It includes face error motion, axial spindle error motion, vibration of the machine and foundations, and material induced vibration (Lee et al., 1999). These vibrations induce surface modulation or waviness which is formed in both the cutting and the tool feed directions as vibration occurs during machining and thus modifies the surface roughness profile, significantly increasing the surface roughness. The high spindle

speed and fine feed rate mentioned above also result in tool interference, a phenomenon in which the chip is intended to be removed in the succeeding movement of the tool but has been cut away by some of the preceding tool movements.

Since the depth of cut in SPDT is often less than the grain size (10 μm -100 μm), material factors weigh heavily in the surface generation. It was found that continuous chip formation of a lamella structure was formed under various depths of cut from 1 μm to 10 μm , which indicated that there was a highly inhomogeneous strain distribution in the chip (To et al., 1997). It was also found that the effect of the crystallographic orientation on the cutting force played a significant role when the depth of cut was above 1 μm , however, when the depth of cut was below 1 μm , a “size effect” was dominant in the cutting process. When the depth of cut is much less than the average grain size, the nature of the cutting becomes similar to that in the cutting of a single crystal. The cutting behavior, the mechanism of chip formation and the generation of surface roughness are considered to be dependent on crystallographic factors such as the orientation, the slip system and the dislocation of grains that occurs (Ueda & Iwata, 1980).

Other factors influencing surface generation include the cutting friction, flood coolant, etc. Cheung et al. (2003) conducted research on the effect of cutting friction on the surface properties in diamond turning brittle single crystals. As the results showed, anisotropy of surface roughness occurs in diamond turning when the cutting direction relative to the crystallographic orientation varies successively. Moreover, the anisotropy of surface roughness decreases while the mean arithmetic roughness increases as the cutting friction increases. Kishawy et al. (2005) conducted research on

the influence of flood coolant and dry cutting on tool wear, surface roughness and cutting forces. Chen et al. (2003) studied the effect of the cutting temperature in high-speed milling and presented an inverse heat-transfer model considering three-dimensional transient heat conduction to calculate the heat flux and the temperature distribution on the tool-workpiece interface in the high speed milling process.

The measurement of surfaces, the nature of surface roughness and surface characterization have a close relationship with each other. Different measurement methods and characterization techniques may give different data and information about the surface topography. Surface roughness includes the tool traverse feed marks such as those found in turning and grinding, and it is generally examined in a plane view with the aid of optical or electron microscopy, in cross-sections normal to the surface with stylus instruments and in oblique cross-sections with optical interference methods. The profile measurement based on these methods evaluates the roughness parameters for the test length that is treated as a specimen randomly selected from the surface. Surface characterization can be regarded as the breakdown of the surface geometry into basic components based on functional requirements, including various shapes, scales of size, distribution in space and a multiplicity of boundaries in height and position (Cheung et al., 2003).

The methodology for the characterization of surface roughness has drawn much theoretical and practical attention. Traditional surface characterization methods relied on surface roughness data in one cross section of the workpiece only, thus undoubtedly inadequate to represent the vibration of the characteristics of the surface quality at different regions of the surface (Whitehouse, 1994). The stylus method of measurement

had been proven to be more useful because of its convenient output, ease of use and robustness. However, strong experimental evidence has been raised that there is localized variation of surface roughness due to the crystallographic orientation and plastic anisotropy of the work material, thus making a single profile approach for the surface roughness characterization inaccurate. Amplitude probability density function (APDF), autocorrelation function (ACF) and 2D Fourier analysis for the characterization of surface roughness are used as they are related to the whole surface rather than to individual profiles, however the complexity inherent in these methods makes them inconvenient for evaluation and specification purposes in practical applications. Swelling ratio (SR) and coefficient of anisotropy (COA), which are defined based on the power spectral density of the feed components in the surface roughness spectrum, are also used to characterize the properties of swelling and plastic anisotropy of single crystal materials (Cheung et al., 2003), and the degree of roughness anisotropy (DRA) was used to measure the extent of localized variations in surface roughness by Lee (2000).

2.4 Plastic Deformation in Chip Formation

The purpose of any milling and turning operation is to remove material in order to achieve the required dimensions of the finished part; therefore a basic understanding of the material removal process at the tip of the diamond cutting tool is very important.

Under different cutting conditions, such as varying depths of cut, workpiece material, rake angles, cutting speed and machine rigidity etc., different types of chip can be formed. The two basic types of chip are continuous and

discontinuous. Continuous chips are usually formed when cutting soft or ductile materials such as aluminum or copper, where there is less likelihood of chatter and surface finish is usually better than when discontinuous chips are formed. A disadvantage of continuous chips is the fact that they can become very long and become entangled in the machine or pose a safety hazard. Discontinuous chips are usually formed when cutting hard, brittle materials, partly because these materials cannot withstand high shear forces and therefore the chips formed shear cleanly away (<http://machine-tools.netfirms.com>).

In conventional machining, various chip formation models have been proposed. Albrecht (1961) firstly developed analytical models for the chip formation process based on the combined effect of shear and bending stresses in the shear zone, and investigated the periodic patterns in segmented chips. Ostafiev et al. (1994) proposed a trapezium shaped lamellar structure formation process, which took into account both the plastic and elastic chip deformations in the contact length and contact load distribution. Recently, the finite element analysis (FEA) method is used to model and simulate chip formation and shear localization phenomena in the metal cutting process (Wang, 2010).

In ultra-precision diamond turning, the chip formation can be classified into two groups. The first one is caused by the plastic deformation on the slip planes, and the second one is due to fracture on the cleavage plane. In the cutting process, the work material under the shear zone is subject to a large compression deformation exerted by the cutting tool, which leads to the distortion of the atomic arrangement and the distribution of defects in the metal. A primary shearing process is triggered by the fine

cracks produced near the vicinity of the tool tip, and due to the compression loading ahead of the tool, many dislocations are moved towards the free surface. As the cutting tool advances, the material is compressed in the cutting direction and a shear band joining the tool to the surface of the work material is developed, which forms the chip. Specifically, when a diamond cutting tool with zero rake angle penetrates into the work material, it creates pressure at the contact surface and stress localization at the tool nose area, which makes the material deform elastically (Lee et al., 2001). When the dislocation is concentrated at the tool nose area above the yield point, plastic deformation occurs by dislocation slip, twinning or shear banding. The multiplication of defects occurring at the tool tip area and imperfections in the work material leads to inhomogeneous strain. The detailed geometry of chip formation is shown in Fig. 2.5.

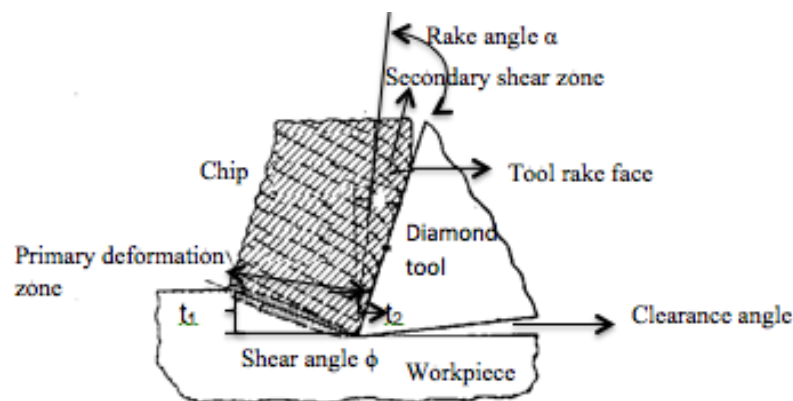


Fig. 2.5 Geometry of chip formation and the deformation zone

In practical tests, the mean chip thickness can be obtained by measuring the length l , and the weight W of a piece of chip. The mean thickness t_2 can be described as:

$$t_2 = \frac{W}{\rho w l} \quad (2.1)$$

in which ρ is the density of the material and w is the width of the chip. The deformation coefficient ξ can be defined as the chip thickness ratio between the undeformed chip thickness t_1 to the deformed chip thickness t_2 . The chip thickness is related to the tool rake angle (α) and shear angle (Φ). Assuming the work material is incompressible and no side spread occurs, from the geometry of the cut it can be shown that

$$\frac{t_1}{\sin \phi} = \frac{t_2}{\cos \phi \cos \alpha + \sin \phi \sin \alpha} \quad (2.2)$$

$$\tan \phi = \frac{\xi \cos \alpha}{1 - \xi \sin \alpha} \quad \tan \phi = \frac{\xi \cos \alpha}{1 - \xi \sin \alpha} \quad (2.3)$$

Based on the above equations, the shear angles formed in the cutting process can be estimated for different depths of cut (Cotterell et al., 2008).

One important effect that is not considered in the model above is the built up edge. When particles of the workpiece material weld to the rake face of the tool during cutting, a built up edge (BUE) can be formed as shown in Fig. 2.6. By accumulating material against the rake face, and reducing the contact area between the chip and the cutting tool, a large BUE would lead to excessive work hardening at the surface of the workpiece, poor surface finish and a reduction in the dimensional control of the process. However, a thin and stable BUE is generally considered desirable, as this can tend to reduce frictional wear on the rake face of the tool.

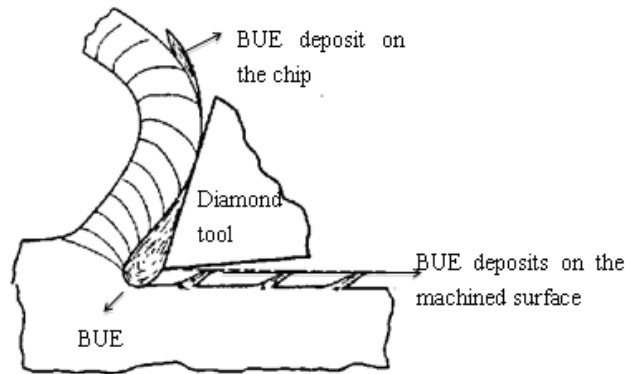


Fig. 2.6 Schematic illustration of built up edge (BUE)

2.5 Summary

In this chapter, a review on both the electropulsing treatment and ultra-precision single point diamond turning is presented. The theories and experimental investigations on the effect of EPT in microstructural changes and physical property improvements are discussed in detail, and a thorough investigation on the ultra-precision machining cutting process at the micro and nano-scale is conducted. The characterization of surface roughness and research in cutting force and plastic deformation of chip formation are also reviewed in detail. As EPT can improve the materials properties and induce microstructural changes, it provides a feasible way to change the machinability in the SPDT process. In this thesis, the effect of EPT on microstructural changes and phase transformation are studied in Chapter 4, and on its basis, the machinability and microstructural changes in SPDT after EPT of AZ91 are also reported in Chapter 5.

Chapter 3 Characterization and Measurement Techniques

Techniques

3.1 Electropulsing Treatment

The series of electropulsing treatment experiments are carried out in this research. A self-made alternating current (AC) generator is used to provide high frequency electropulsing during the experiments, as shown in Fig. 3.1. The current frequency and voltage values can be acquired from the monitor of the power generator.



Fig.3.1 Self-made electropulsing generator (Shenzhen Tsinghua Graduate School)

The room temperature of the tensile test is 300 K, and the surface temperature of the specimens during the electropulsing process is measured by using a contact thermocouple as shown in Fig. 3.2. Accurate electropulsing parameters are acquired by

using a Hall effect sensor (HDC3000H) as shown in Fig. 3.3 connected to an oscilloscope (Tektronix-TDS 1002) as shown in Fig. 3.4. When the measured current passes through the sensor, according to the Hall effect in electromagnetic theory, the current is transferred into the Hall electric potential immediately, and the oscilloscope measures this electric potential value. By monitoring the wave pattern and its peak and trough, accurate frequency, amplitude and the root mean square (RMS) values of the electropulsing current can also be acquired.



Fig. 3.2 Contact thermocouple



Fig. 3.3 Hall effect sensor (HDC3000H)

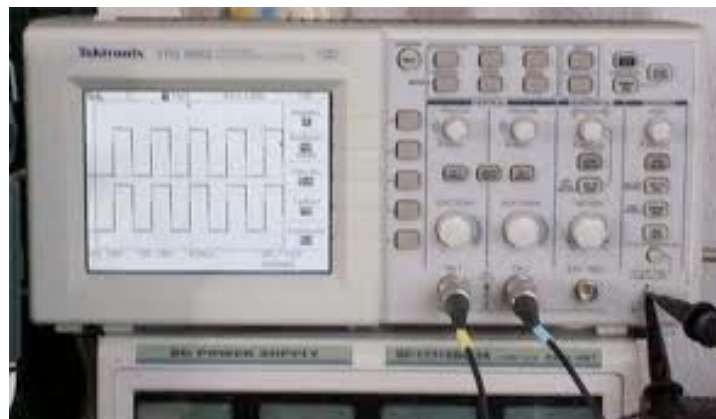


Fig. 3.4 Oscilloscope (Tektronix-TDS 1002)

3.2 Characterization of Microstructure

3.2.1 X-ray Diffraction

The phases of the specimens are identified by a Bruker D8 Discover X-ray diffractometer and a Bruker D8 Advance X-ray diffractometer, which are shown in Fig. 3.5 and Fig. 3.6 respectively. The XRD examination is carried out on the X-ray diffractometer with nickel-filtered Cu K_{α} radiation. A range of diffraction is selected, and the scanning speed is 1 degree/min, with increments of 0.03.



Fig. 3.5 XRD (Bruker D8 Discover, Materials Research Centre, The Hong Kong Polytechnic University)



Fig. 3.6 XRD (Bruker D8 Advance, Materials Research Centre, The Hong Kong Polytechnic University)

3.2.2 Scanning Electron Microscopy

Microstructures and phases of the specimens are observed by a scanning electron microscopy (JSM-6490 JEOL SEM), and a field emission scanning electron microscopy (Hitachi-S4800 ultra-high resolution SEM), which are shown in Fig. 3.7 and Fig. 3.8. In order to produce a medium resolution of atomic contrast among the various phases involved, specimens after electropulsing treatment should be polished before they are examined using SEM; however, for specimens with SPDT, no mechanical polishing is needed because the specimens already have the surface roughness at the nanometer scale.



Fig. 3.7 Scanning electron microscopy (JSM-6490 JEOL)



Fig. 3.8 Ultra-high resolution field emission scanning electron microscopy (Hitachi-S4800)

3.2.3 Transmission Electron Microscopy

Examination of conventional transmission electron microscopy (TEM) is carried out using JEOL 2010F field emission transmission electron microscopy (Fig. 3.9). In order to make electrons pass through the specimen, it must be very thin (usually less than 100 nanometers thick). To obtain the thin foil specimens suitable for TEM observation, the Gatan 691 precision ion polishing system (PIPS) is used in the preparation stage. In PIPS, two miniature penning ion guns are adjusted to thin the specimen. The rough thinning is carried out at a milling angle of 8° for a time dependent on the particular material, and then a low angle of 4° , where the slow milling layers protect the fast milling layers from the ion beam, is selected. To prevent the preferential thinning that occurs when the ion beam passes along the cross-section interface, the beam intensity during specimen rotation is modulated during the thinning process, and the rotation of the specimen is kept at 3.5 rpm, as shown in Fig. 3.10.



Fig. 3.9 Transmission electron microscopy (JEOL 2010F field emission)



Fig. 3.10 Precision ion polishing system (Gatan 691)

3.2.4 Metallurgical Microscopy

To obtain the optical metallograph of the electropulsed specimens, the specimens are polished to gain a smooth surface without scratches, and then etched with a solution of picric acid (6 g), acetic acid (20 ml), ethanol (50 ml) and distilled water (20 ml). Metallurgical micrographs are observed by Olympus GX 51 microscopy (Fig. 3.11) and HiROX KH-7700 digital microscopy. The straight-line intercept procedure in multi-directions is used to measure the average grain size, in order to prevent the departure from equiaxed or non-equiaxed grain shapes of the specimens in any local portion. According to the “standard test methods for determining average grain size” (ASTM E112–96), five vertical lines and five horizontal lines are drawn on the metallographs, and when the test line intercepts with the grain boundary, one count is measured; when the test line penetrates into a grain at the end, half a count is measured.



Fig. 3.11 Metallurgical Microscopy (Olympus GX 51, Shenzhen Tsinghua Graduate School)

3.3 Single Point Diamond Turning

A two-axis computer numerically controlled (CNC) precision contouring lathe is used for the ultra-precision cutting process, as shown in Fig. 3.12 and Fig. 3.13. The machine incorporates a precision air-bearing spindle and contacting type linear bearing slides, which provide ultra smooth, low friction motion of the critical moving components. Total slide travel is 150 mm on the X-axis and 100 mm on the Z-axis. The slide feed is bi-directional and infinitely variable up to 5,000 mm/min. The spindle speed is infinitely variable from 3,000 to 10,000 rpm. The spindle is air cooled and is driven by an integral AC drive motor, which allows acceleration and deceleration in less than five seconds (<http://www.sterlingint.com>). The property parameters of the turning machine are listed in Table 3.1.



Fig. 3.12 SPDT machine (OptoForm 30, Advanced Optics Manufacturing Center, The Hong Kong Polytechnic University)

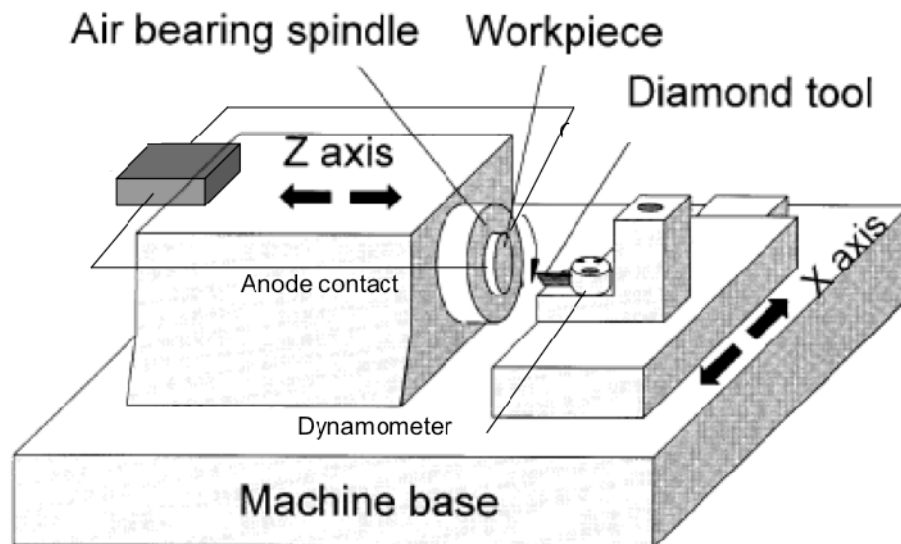


Fig. 3.13 Schematic illustration of the OptoForm 30 SPDT machine (Advanced Optics Manufacturing Center, The Hong Kong Polytechnic University)

Table 3.1 Specification of single point diamond turning machine (Optoform 30)

Work spindle	Design	Air bearing
	Speed range	3000 rpm-10000 rpm
	Acceleration time	<5 s
Slide ways	Design	Precision contacting way
	X Travel	150 mm
	Z travel	100 mm
	Velocity	0.25 mm/min-1500 mm/min
Feedback system	Linear glass scales	
Feedback resolution	0.02 μm	
Form accuracy	0.5 μm	

3.3.1 Measurement of Surface Roughness

The roughness of a surface can be measured in different ways, which are classified into three basic categories (<http://www.zeus.plmsc.psu.edu>):

(1) Statistical descriptors that give the average value of the surface height. It includes arithmetic roughness R_a ; the root mean square roughness R_q ; skewness S_k and kurtosis K ;

(2) Extreme value descriptors that depend on isolated events. Examples are the maximum peak height R_p , the maximum valley height R_v , and the maximum peak to valley height R_{max} ; and

(3) Texture descriptors that describe variations of the surface based on multiple events. An example for this descriptor is the correlation length.

Among these descriptors, the Ra and Rq measures are the most effective surface roughness measures commonly adopted in general engineering practice. They give a good general description of the height variations in the surface. Arithmetic average roughness Ra (Fig. 3.14) is obtained by measuring the mean deviation of the peaks from the centerline of a profile trace. Rq is the root mean square deviation (RMS) of the roughness profile ordinates. For a sine wave, Rq is 0.9 times the arithmetic average roughness Ra.

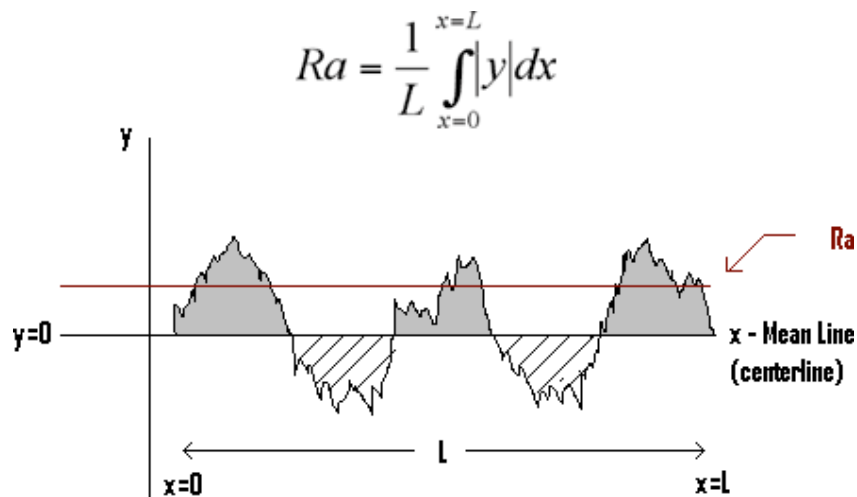


Fig. 3.14 Description of arithmetic average roughness Ra

The surface roughness of the specimens after completing SPDT process is measured by WYKO NT 8000 (Fig. 3.15) and Taylor Surf PGI1240 (Fig. 3.16). WYKO NT 8000 is a phase shifting interferometric instrument, and due to its noncontact measuring nature, the surface of the specimens will not be damaged during the testing process, and a three dimensional (3-D) surface topography of the machined

surface can also be acquired. The system consists of a phase shifting interferometer, an electronic interface unit and a computer. The phase shifting interferometer firstly acquires the optical data of the specimen surface, and the topography of the surface can be established on the basis of these data. In this process, both the paths of light reflecting off the workpiece surface and the path of light reflecting off the reference surface are combined inside the magnification head to produce fringes, which are digitized and processed to give a 3D surface topography. The Phase Shifting Interferometry (PSI) stitching mode is described for resolving the surface topography, along the cutting direction with an objective lens of 20.5x, in which the sampling area is $231\ \mu\text{m} \times 309\ \mu\text{m}$, the array size 640×480 , and the sampling size $482.85\ \text{nm}$.

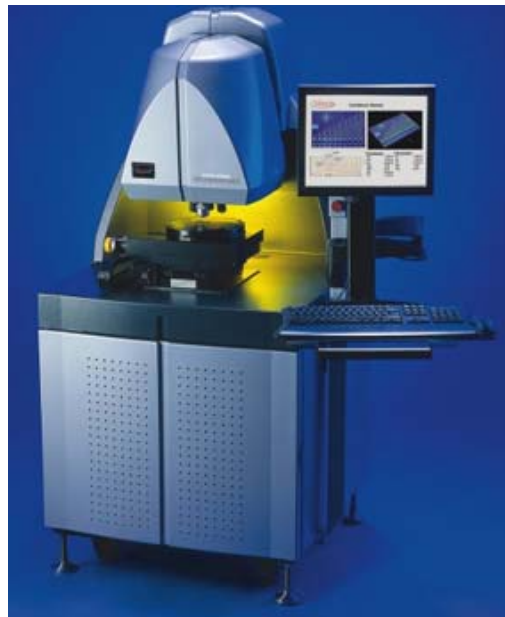


Fig. 3.15 Non-contact interferometric measurement system (WYKO NT8000, Advanced Optics Manufacturing Center, The Hong Kong Polytechnic University)

In order to get an unbiased view of the whole specimen, stylus type instrument Taylor Surf PGI 1240 is used after the test using WYKO NT 8000. It is a contact type measuring system used to measure the surface texture, waviness, dimensions and the form of a diamond turned surface with a resolution down to 10 nm. The surface profile of the specimen is measured by the automatic vertical movement of the stylus with a lateral resolution of 0.8 nm across the surface. This movement is then converted into an amplified electrical signal, which is filtered and analyzed by the computer.



Fig. 3.16 Contact stylus type measurement system (Taylor Surf PGI 1240, Advanced Optics Manufacturing Center, The Hong Kong Polytechnic University)

3.3.2 Measurement of Cutting Force

The cutting force during the turning process is collected and analyzed. Before each precise measurement, the specimens are cut for 6 times to achieve the same flatness. Firstly, the force is picked up by a load cell mounted underneath the tool, then these charges are fed into a piezoelectric force transducer (Kistler type 9252A) as shown in Fig. 3.17. The captured signal is amplified by a charge amplifier, which

transforms the signal into an analogue voltage output. These output voltage signals are collected by the Tektronix TDS744A digitizing oscilloscope, and transferred into the computer for further analysis. A schematic illustration of the signal flow in cutting force measurement is shown in Fig. 3.18, and a photo of the system is shown in Fig. 3.19.

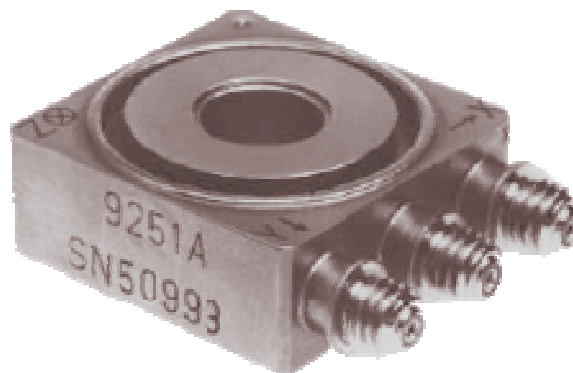


Fig. 3.17 Piezoelectric force transducer (Kistler type 9252A)

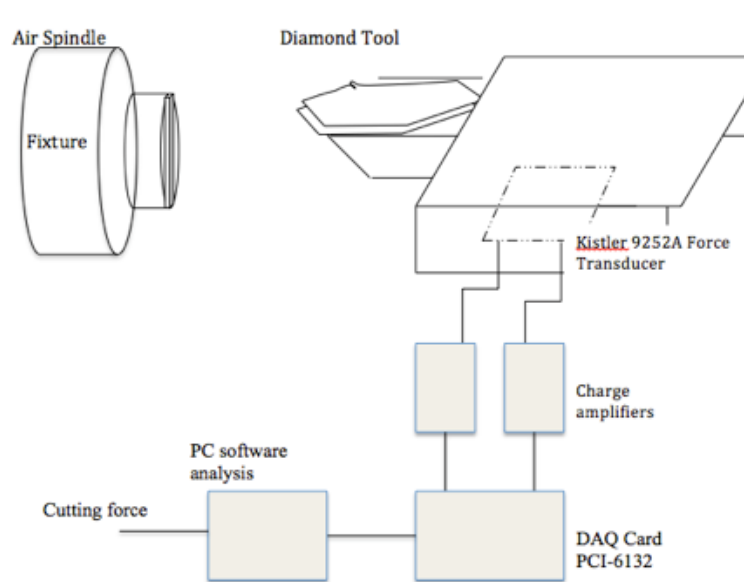


Fig. 3.18 Schematic illustration of the signal flow in cutting force measurement

The force transducer is calibrated by applying loads on the screw above the diamond cutting tool, and by analyzing the voltage signal of this load. A linear relationship can be established between the actual cutting force and the induced voltage signal. The calibration process is carried out six times to get an accurate value, as shown in Fig. 3.20.



Fig. 3.19 Cutting force measurement system in single point diamond turning machine (Advanced Optics Manufacturing Center, The Hong Kong Polytechnic University)

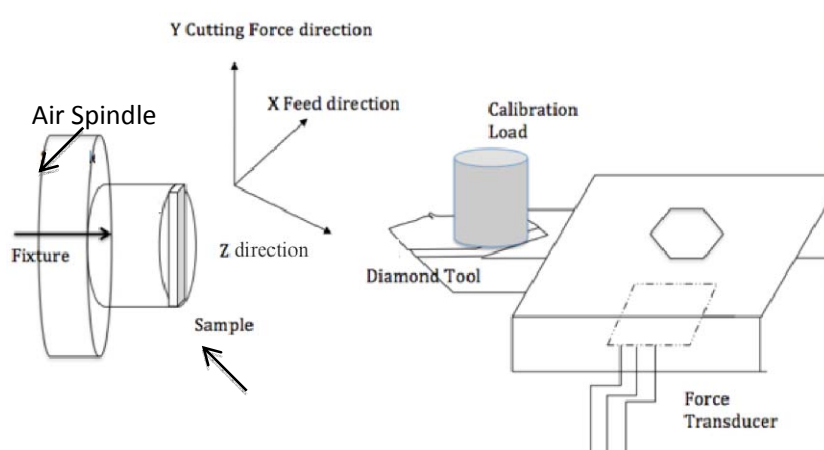


Fig. 3.20 Schematic diagram of cutting force calibration process

The data of sampling frequency is 100 Hz, in total 10000 dots are recorded for one record, and there are 120 records for each specimen throughout the whole cutting process. For better accuracy, each specimen is cut 6 times. In order to obtain accurate values, the commencement stage of cutting, which induces large vibration to the specimen and the diamond tool, is excluded from the measuring process.

3.4 Summary

In this chapter, the equipment of both electropulsing treatment and the SPDT machining process used in the experiments are introduced. The measurement methods of the microstructure and metallographs, including SEM, TEM, and XRD are stated. Especially, the measurement and characterization of the surface roughness and cutting force are discussed, and the data analysis process is also addressed in detail.

Chapter 4 Effect of Electropulsing Treatment on Microstructural Changes

4.1 Introduction

The electropulsing effect is a phenomenon in which the properties of materials (including various metal materials, ceramic materials, superconductor materials and metallurgic powder products) may be improved by the application of a high-density current pulse. As an alternative to traditional thermal and mechanical process, EPT has been recognized for its high efficiency and low cost. Most of the studies on the effect of EPT have already been carried out, including electroplasticity, recrystallization, crack healing, phase transformations and dislocation movements (Conrad, 1991; Tang and Yao, 2000; Qin, 2001; Li, 1998; Cao, 1990). There are two practical types of electropulsing: static electropulsing and dynamic electropulsing (Zhu, 2009). The former combines a thermal process and electropulsing. The latter is a complex thermal process, which simultaneously combines both electropulsing and plastic deformation.

Research and application of magnesium alloys is booming nowadays thanks to their excellent properties and flexible applications. The magnesium alloys were reported to be widely used due to their comprehensive properties, such as low density, high specific strength and stiffness, excellent machinability and good castability (Du, 2008). As one of the most widely and commercially used Mg alloy, AZ91 alloy with nominal composition Mg-9Al-1Zn, known for its low density, high specific strength

and stiffness, improved castability, is widely used as an ideal material for lightweight construction. It is one of the most popular of the cast magnesium alloys. Compared to conventional wrought magnesium alloys such as AZ31 and AZ61, the AZ91 alloy shows better combinations of castability, plasticity and cost (Jiang, 2009).

In this chapter, effects of static EPT and dynamic EPT on microstructural changes and phase transformations are described in detail for AZ91 Magnesium alloy, through SEM, XRD and TEM techniques.

4.2 Material Preparation and Experimental Procedures

A series of experiments are conducted on the commercial magnesium alloy AZ91 (9.1wt%Al, 0.9wt%Zn, 0.2wt%Mn, balance Mg). The material is homogenized at 693 K in a graphite crucible electric resistance furnace for 16 hours, and subsequently poured into a preheated iron mold at 593 K, which provides cuboid shaped specimens of thickness 1.9 mm and width 4 mm, and then subsequently extruded into a strip 2.90 mm width and 1.45 mm thickness. Differing in the preparation methods and electropulsing styles, the AZ91 alloy prepared for the present study can be divided into three groups: (1) as-tempered specimens for static EPT, (2) cold-rolled specimens with static EPT, and (3) rolling specimens with dynamic EPT.

4.2.1 Static EPT on As-tempered Specimens

For the as-tempered specimens, the strip is electropulsing-rolled to a thickness of 1.0 mm. Multiple positive electropulses are applied while the strip is moving at a speed

of 2 m/min over a distance of 225 mm between the two roller electrodes. The pressure between the electrodes and strips is adjusted to keep good electrical contact without causing deformation of the strip.

The rolled strip is tempered at 493 K for 12 hours, followed by natural cooling in air. The tempered strip is cut into pieces 80 mm long, and subjected to EPT. During the process, a jet-type oil cooling system is used to cool and protect the surface of the specimen. The duration time of electropulsing is controlled to 10 seconds. The current amplitude, root-mean-square value, frequency and duration time are monitored by an oscilloscope connected with a Hall effect sensor. A schematic illustration of the EPT system is presented in Fig. 4.1. Various electropulsing operational parameters, such as pulse frequency, root-mean-square value of current density, amplitude of current density and temperature are listed in Table 4.1.

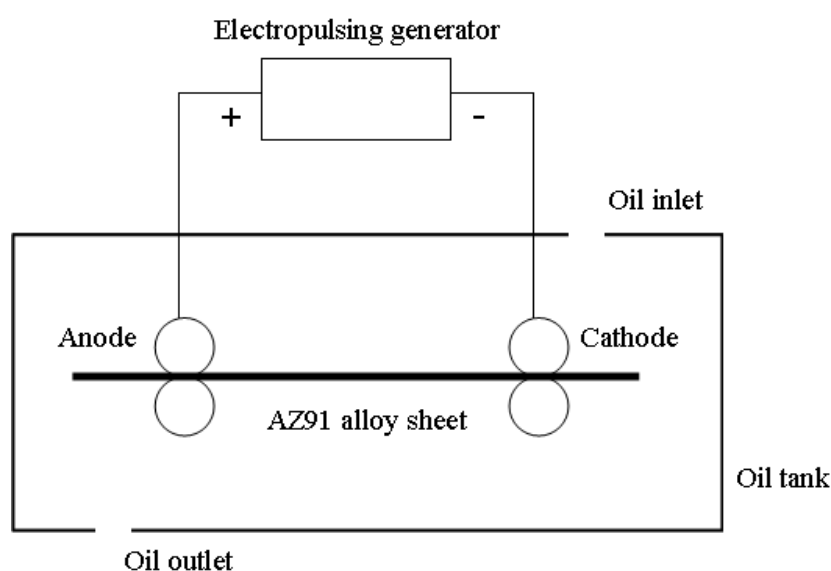


Fig. 4.1 The Schematic illustration of the static EPT system for as-tempered specimens

Table 4.1 Experimental parameters of as-tempered specimens under static EPT

Specimen No	Frequency (Hz)	RMS (A)	Amplitude (A/mm ²)	Temperature (K)
EPT 1	non-EPT	-	-	293
EPT 2	120	45.33	177.7	323
EPT 3	183	58.10	204.35	385
EPT 4	252	61.33	204.35	407

It is found that the temperature of the EPT specimen increases gradually with the frequency of electropulsing. The higher frequency contributes to larger RMS values of current density, which results in a larger Joule heating effect.

As introduced in Chapter 3, longitudinal cross-sections of the four specimens under various frequencies of EPT were polished and then examined using backscattered electron microscopy (JSM-6490 BSEM). These phases were also identified by an X-ray diffractometer (Bruker D8 Discover XRD). Examination of specimens is carried out using transmission electron microscopy (JEOL 2010 TEM).

4.2.2 Static EPT on Cold-rolled Specimens

In the second group, the extruded strip is cut to a 300 mm length, and then cold-rolled to 1.15 mm thick. During the rolling process, the strip is moving at the speed of 2 m/min. A schematic illustration of the cold-rolling system is shown in Fig. 4.2.

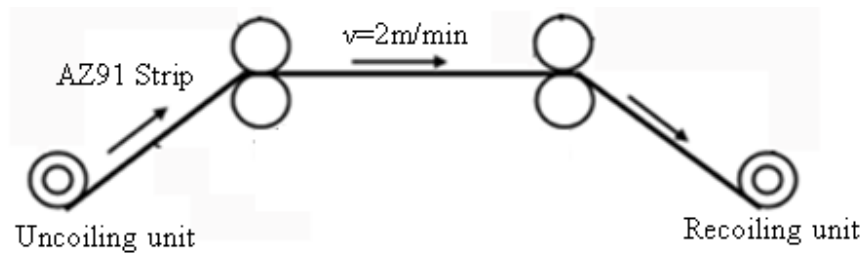


Fig. 4.2 A schematic view of the cold-rolling process

The middle parts of the cold-rolled strips with the length of 120 mm are selected to take static electropulsing treatments. A self-made electropulsing generator is applied to discharge positive direction multiple pulses with various current parameters for 10 seconds. Multiple electropulses are applied with two electrical contactors by the two sides of the strips. During the electropulsing process, the electropulsing parameters, including frequency, root-mean-square current (RMS), amplitude current and duration of the multiple pulses are monitored by an oscilloscope connected to a Hall effect sensor, as listed in Table 4.2. The EPT process is schematically shown in Fig. 4.3.

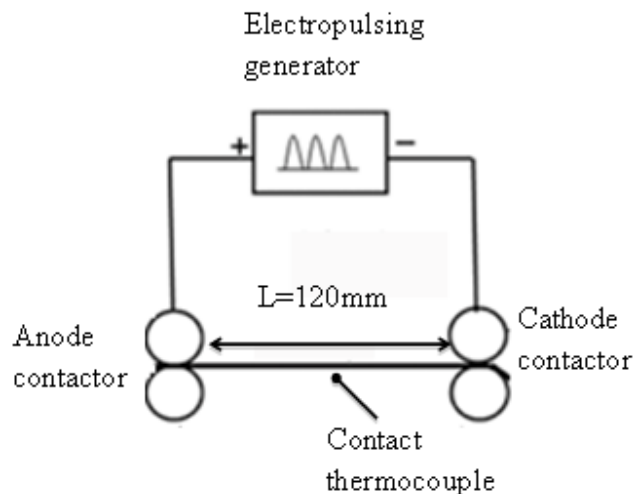


Fig. 4.3 A schematic illustration of static EPT process

Table 4.2 Experimental parameters of cold-rolled specimens under Static EPT

No.	Frequency (Hz)	RMS (A)	Amplitude (A/mm ²)	Temperature (K)
EPT 1	non-EPT	-	-	293
EPT 2	151	71.62	274.2	335
EPT 3	209	79.81	265.1	346
EPT 4	253	104.57	319.84	428
EPT 5	294	121.52	347.26	507

BSEM (Hitachi-S4800 ultra-high resolution field emission scanning electron microscopy) examination is carried out to observe the longitudinal cross-sections of the specimens under various frequencies of EPT. An X-ray diffractometer (Bruker D8 Advance) is used to identify the phases. The metallurgical structure is observed by an inverted microscopy (Olympus GX51). TEM examination is carried out using a transmission electron microscopy (JEOL 2010).

4.2.3 Dynamic EPT on Rolling Specimens

In the dynamic electropulsing process, the extruded strip is rolled under electropulsing. During the rolling, the strip is moving at a speed of 2 m/min between two electrodes spaced at a distance of 225 mm. A self-made electropulsing generator is continuously applied to discharge multiple positive pulses with various current parameters on the rolling material, and it takes about 10 seconds for the strip to pass the electrodes. The pressure between the electrodes and the strip is adjusted to keep good electrical contact without causing deformation of the strip. During the dynamic

electropulsing, the current parameters including frequency, root-mean-square current (RMS), amplitude current and duration of multiple pulses are monitored by an oscilloscope, and are listed in Table 4.3. A schematic illustration of the dynamic electropulsing system is shown in Fig. 4.4.

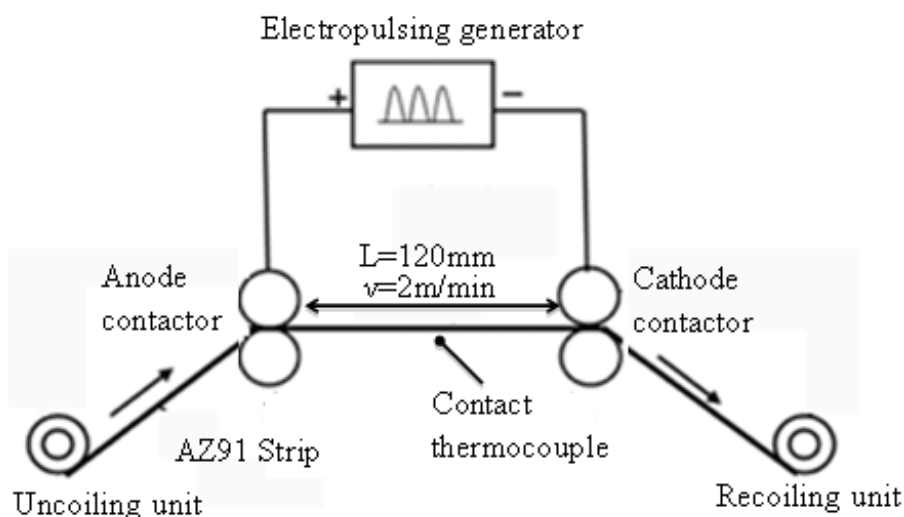


Fig. 4.4 A schematic illustration of dynamic EPT process

Table 4.3 Experimental parameters of dynamic EPT

No.	Frequency (Hz)	RMS (A)	Amplitude (A/mm ²)	Temperature (K)
EPT 1	non-EPT	-	-	293
EPT 2	126	52.00	211.2	316
EPT 3	204	63.05	237.6	349
EPT 4	265	89.53	256.5	359
EPT 5	309	100.19	271.6	390

The longitudinal cross-sections of the specimens under various frequencies of EPT are examined by a BSEM (Hitachi-S4800 ultra-high resolution field emission scanning electron microscopy). The phases are identified by an X-ray diffractometer (Bruker D8 Advance XRD), and a range of diffraction from 25° to 65° is selected. The scanning speed is 1 degree/min, with increments of 0.03. The metallurgical structure of the specimens is observed by an Inverted Microscopy (Olympus GX51), after the specimens are etched by using the customized solution introduced in Chapter 3. Examination of TEM is carried out using a TEM (JEOL 2010 transmission electron microscopy).

4.3 Results and Discussion

4.3.1 Static EPT Induced Phase Transformations and

Microstructural Changes on As-tempered Specimens

The phases in the specimen are identified by a Bruker D8 Discover X-ray diffractometer. The XRD patterns for the specimens under different parameters of EPT are shown in the Fig. 4.5, with a range of diffraction from 25° to 85° . The non-EPT specimen has typically a primary α -Mg phase matrix and a β -Mg₁₇Al₁₂ phase. As the frequency of the electropulsing treatment increases from 120 Hz to 183 Hz, the peaks of the β -Mg₁₇Al₁₂ phase increase, which implies that precipitation of the β phase has taken place; and as the frequency continues to increase from 183 Hz to 252 Hz, the peak of the β phase decreases, which implies that a reverse phase transformation occur.

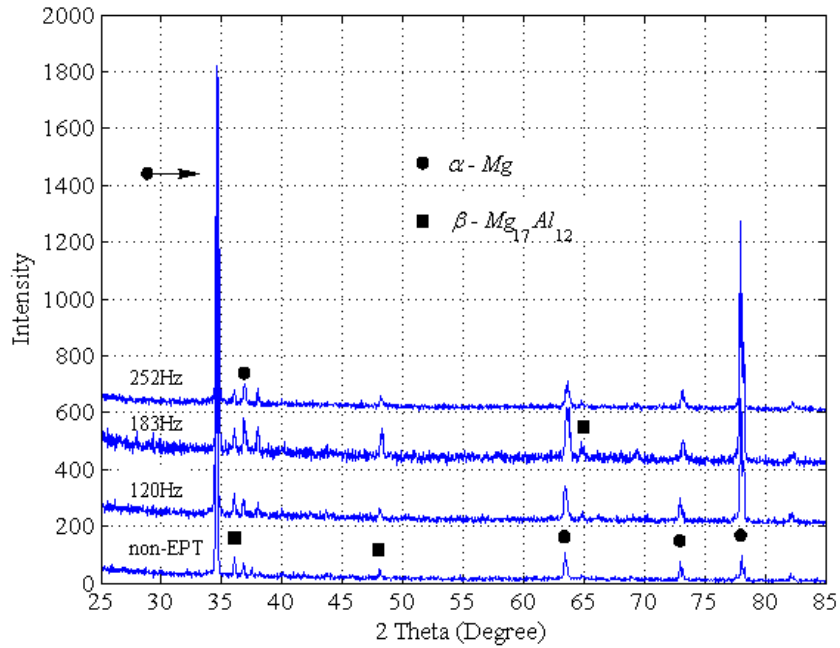


Fig. 4.5 XRD patterns for as-tempered specimens under various frequencies of static EPT

The microstructural changes were observed by BSEM. It is noticed that a phase transformation occurs in the specimens after EPT at various frequencies. The microstructure of the non-EPT specimen is shown in Fig. 4.6(a). The β -Mg₁₇Al₁₂ phase appeared as lamellar clusters shown in circles; when the frequency of EPT increases from non-EPT to 120 Hz and 183 Hz, the amounts of the β phase increase. The microstructures of specimens after EPT, with frequencies of 120 Hz and 183 Hz, are shown in Fig. 4.6(b) and (c). It is interesting to observe that the amounts of the β phase decrease after EPT with 252 Hz. This is in agreement with the XRD patterns shown in Fig. 4.5.

For the phase transformations taken place in EPT, the decomposition process of the β phase is defined as a way of up-quenching, and the precipitation process of the β phase is defined as a way of quenching.

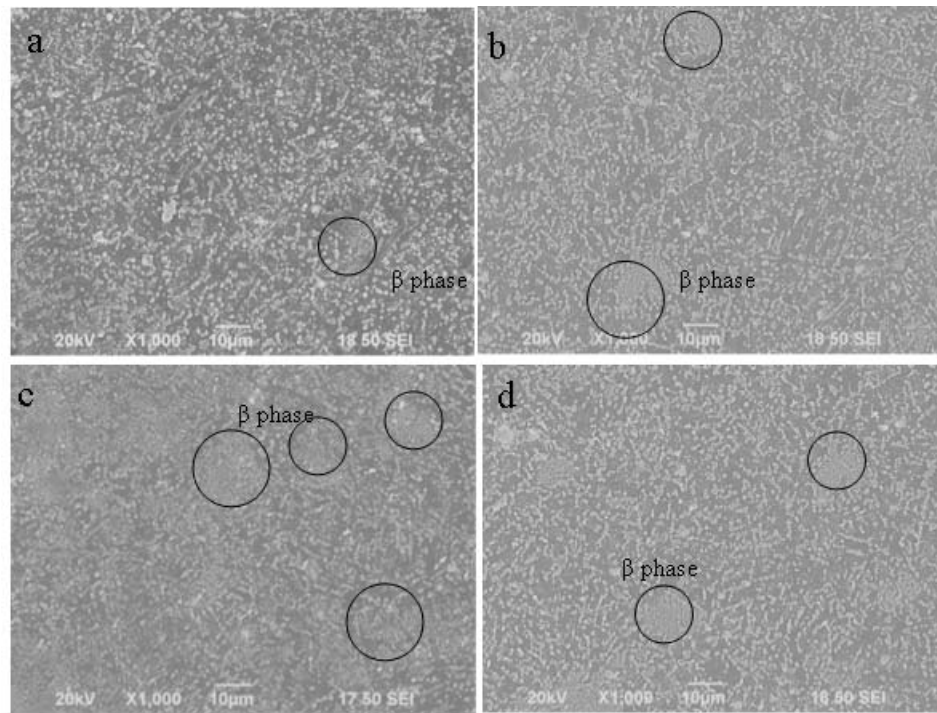


Fig.4.6 SEM micrographs of the as-tempered specimens under (a) non-EPT, (b) 120 Hz frequency of EPT, (c) 183 Hz frequency of EPT, (d) 252 Hz frequency of EPT

Further details of the phase transformations induced by the EPT are studied by TEM observation. The thin-foil specimens of non-EPT, 120 Hz frequency of EPT, 183 Hz frequency of EPT and 252 Hz frequency of EPT specimens are mechanically polished and produced using precision ion polishing system (PIPS), which is discussed in Chapter 3.

The TEM bright field of the non-EPT specimen is shown in Fig. 4.7 (a). Together with the indexed selected area diffraction pattern (SADPs) from $[\bar{1}2\bar{1}3]$ zone

of the hcp α phase and from [001] zone of the bcc β phase particle, the dark field images using $(\bar{1}10\bar{1})$ and $(\bar{3}\bar{3}0)$ reflections of these two phases are shown in Fig. 4.7(b2) and Fig. 4.7(c2) respectively. The lattice parameters of the α phase are $a=0.322$ nm, $c=0.523$ nm and $c/a=1.624$; the lattice parameters of the β phase is $a=1.0937$ nm. β phase particles are also examined inside the α lamella matrix in the 252 Hz-EPT specimen, as shown in Fig. 4.8. According to the identification, the β phase particle is about 520 nm in diameter. Both the α and β phases are marked in Fig. 4.8(a). The indexed diffraction patterns and the dark field images reflected from $[0001]$ $(\bar{1}010)$ of the α phase and $[001]$ $(\bar{3}\bar{3}0)$ of the β phase are shown in Fig. 4.8(b1), (b2) and Fig. 4.8(c1), (c2).

The evolution of the β phase particles can also be observed in the TEM micrographs. In Fig. 4.9(a), few precipitation of the β phase can be found in the TEM bright field of the non-EPT specimen, and as the frequency of EPT increases to 120 Hz, the amounts of the precipitates of the β phase increase (Fig. 4.9(b)). In Fig. 4.10(c), the bright field of the 183 Hz frequency of EPT, the amounts of β phase particles reach a high level. It is in agreement with the XRD results shown in Fig. 4.5 and the SEM results shown in Fig. 4.6, obviously, the precipitates of the β phase occur in a few seconds under electropulsing. In short, it is the phase transformation in a way of quenching in this first stage of EPT (To and Zhu, 2009).

Upon the frequency of EPT further increases to 252 Hz, the amounts of β phase particles decrease, as shown in Fig. 4.9(d). This means that dissolution of the β phase

occurs when further increasing the frequency of EPT. The decomposition of the β phase appears as a reverse transformation of the precipitate, in a way of up-quenching.

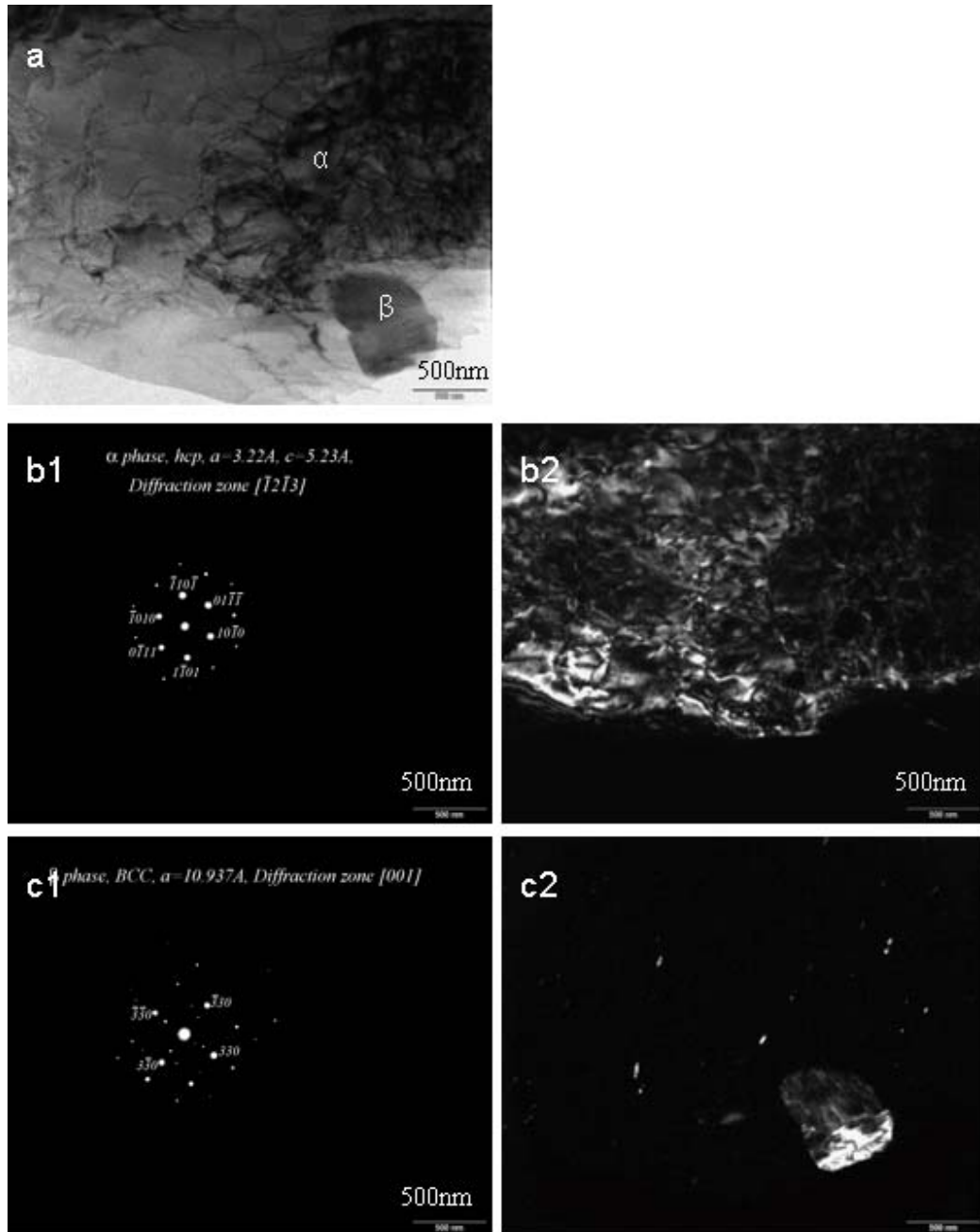


Fig.4.7 TEM images of non-EPT (a) bright field image; (b2) dark field image of $(110\bar{1})$ reflection together with (b1) diffraction pattern from $B=[12\bar{1}3]$ of the α

phase; (c2) dark field image of $(3\bar{3}0)$ reflection together with (c1) diffraction pattern from $B=[001]$ of the β phase

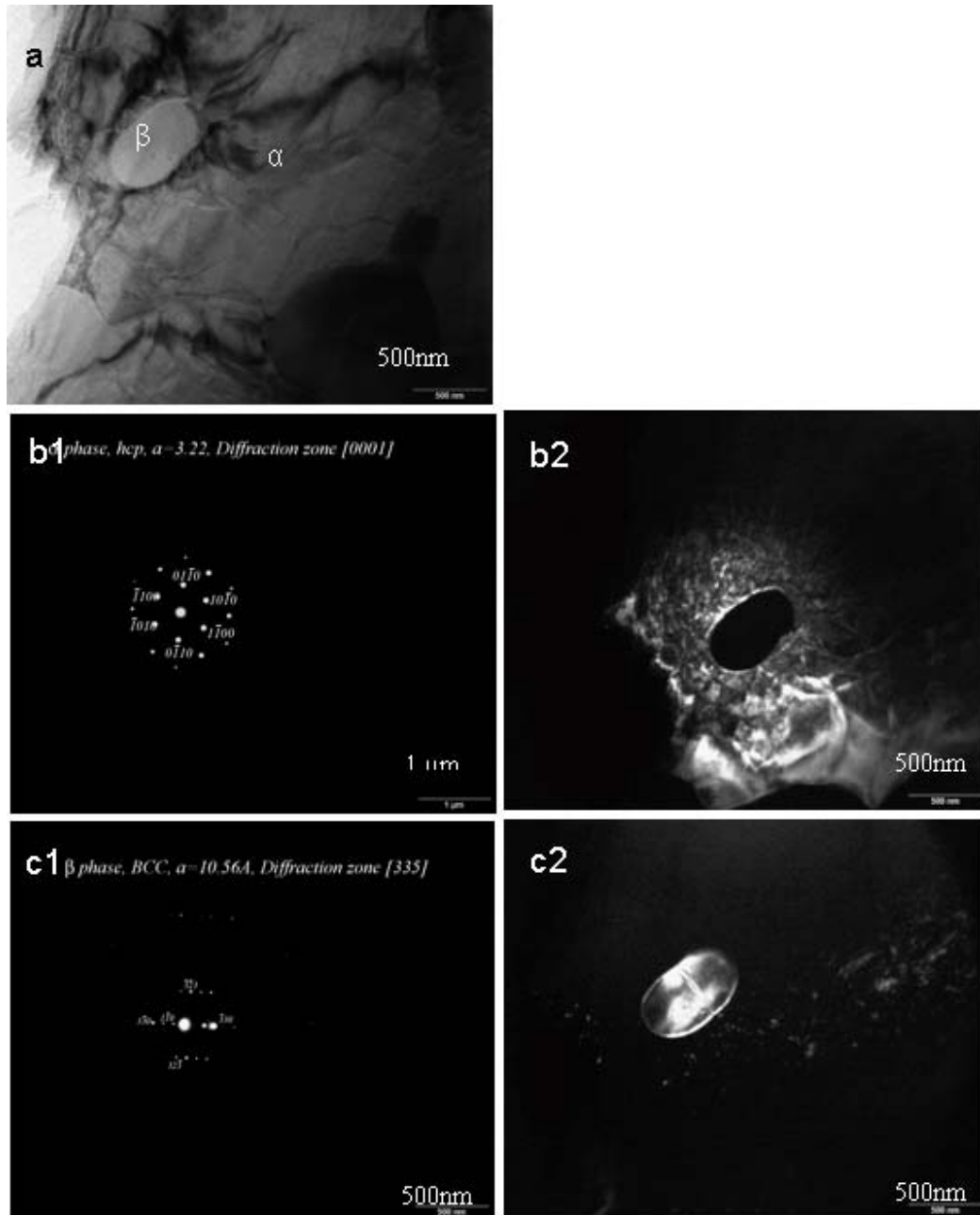


Fig.4.8 TEM images of 252 Hz-EPT (a) bright field image; (b2) dark field image of (1010) reflection together with (b1) diffraction pattern from $B=[0001]$ of the α phase; (c2) dark field image of $(3\bar{2}\bar{3})$ reflection together with (c1) diffraction pattern from $B=[335]$ of the β phase

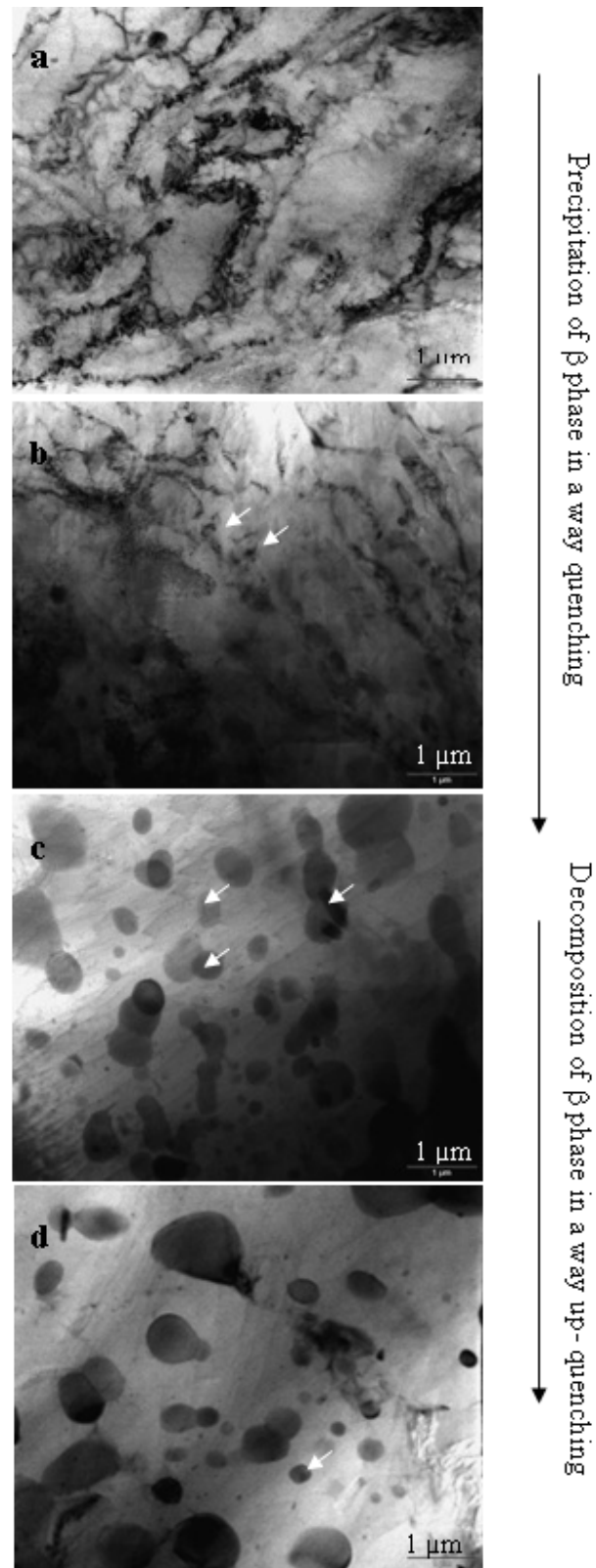


Fig. 4.9 TEM bright field images of (a) non-EPT, (b) 120 Hz frequency of EPT (c) 183 Hz frequency of EPT and (d) 252 Hz frequency of EPT

4.3.2 Static EPT Induced Phase Transformations and Microstructural Changes on Cold-rolled Specimens

The XRD patterns for the as-rolled specimen of non-EPT, the 151 Hz-EPT and 294 Hz-EPT specimens are shown in Fig. 4.10. The non-EPT specimen consists of mainly two phases, a α -Mg phase and a β phase ($\text{Mg}_{17}\text{Al}_{12}$). As the frequency of EPT increases to 151 Hz, the peaks of the β phase weaken, which implies that the amounts of the β phase decrease and transform. Upon increasing the frequency of electropulsing to 294 Hz, the peaks of the β phase increase, compared to that of 151 Hz-EPT. This means that precipitation of the β phase increases with increasing frequency of electropulsing.

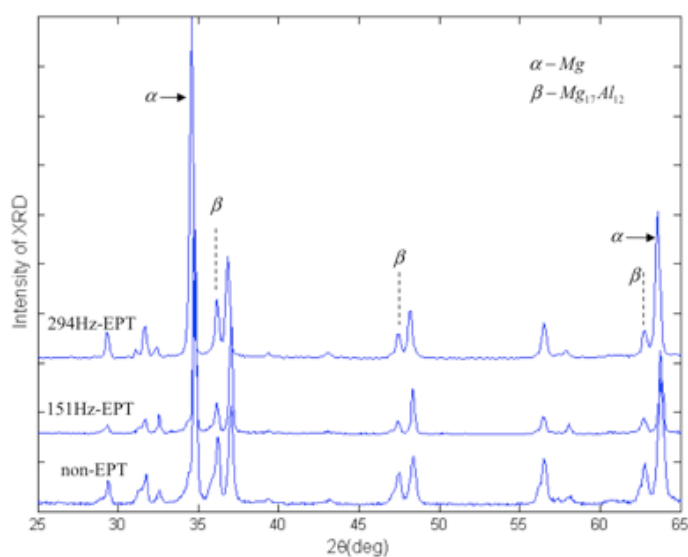


Fig. 4.10 XRD patterns for cold-rolled specimens under various frequencies of EPT

The BSEM images and TEM bright field images of the specimens at different frequencies of electropulsing are shown in Fig. 4.11. The microstructure of the non-EPT specimen mainly consists of the matrix α phase and precipitates of the β phase, as

shown in Fig. 4.11(a1). A large amount of β precipitates are observed in the cold-rolled specimen. After electropulsing with 151 Hz for 10 seconds, the amounts of the β phase precipitates decrease, as shown in Fig. 4.11(a2). It implies that the decomposition of the β phase is accelerated with increasing frequency of EPT. Previous studies reported that decomposition of the β phase occurred after 20 hours of ageing at 673-693 K (Jiang, 2009). It is obvious that under electropulsing the decomposition of the β phase is tremendously accelerated in a way of up quenching. Upon the frequency of electropulsing further increases to 294 Hz, the amount of the β phase increases in a way of quenching, as shown in Fig. 4.11(a3). TEM examination confirms the aforementioned phase transformations. The TEM bright field images of (b1) non-EPT, (b2) 151 Hz-EPT and (b3) 294 Hz-EPT are shown in Fig. 4.11. Both the SEM results and TEM observations are in good agreement with the XRD patterns.

Moreover, it is noticed in the TEM bright field images that the amounts of dislocation are influenced by electropulsing. For the non-EPT specimen, arrays and blocks of dislocation are observed, as shown in Fig. 4.11(b1). After 151 Hz-EPT for 10 seconds, the dislocation arrays decrease, as shown in Fig. 4.11(b2). When the frequency of electropulsing increases to 293 Hz, the amount of the dislocation is further reduced, as shown in Fig. 4.11(b3). It is assumed that under electropulsing, electron wind is formed and pushed the defects, including dislocations and vacancies, towards the grain boundaries, where accumulation and annihilation of the dislocation occur simultaneously. When the frequency of electropulsing increases, both the accumulation and the annihilation are enhanced and maintained an adequate balance, which result in decreasing of the dislocation density.

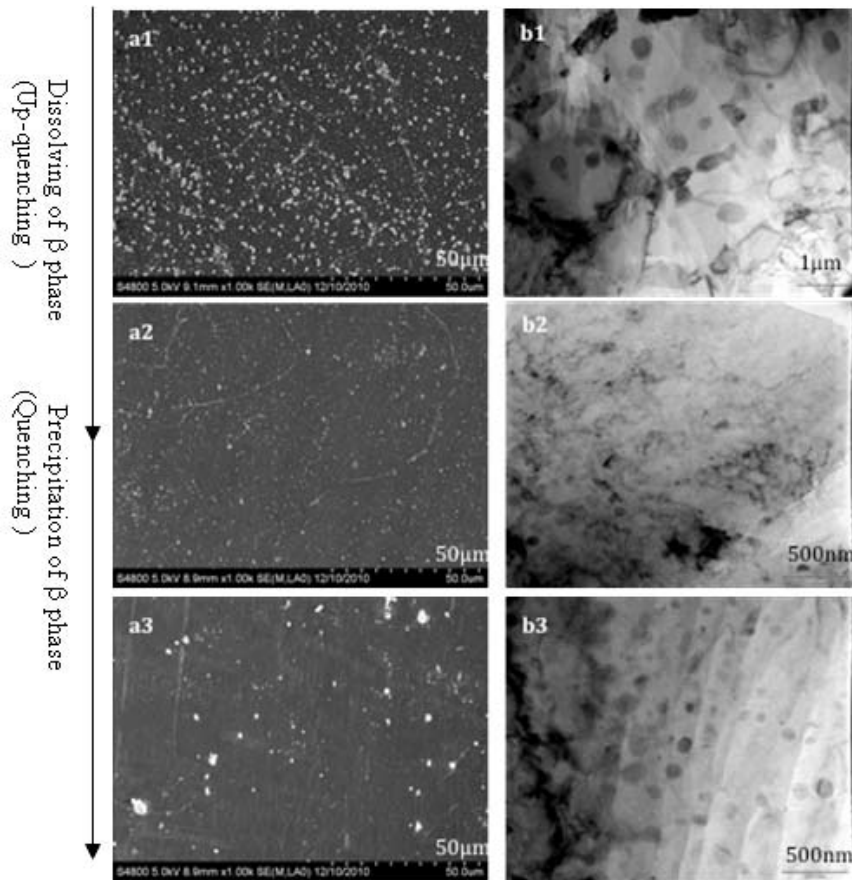


Fig. 4.11 BSEM images of (a1) non-EPT (a2) 151 Hz-EPT (a3) 294 Hz-EPT and TEM bright field images of (b1) non-EPT (b2) 151 Hz-EPT (b3) 294 Hz-EPT, showing β phase precipitates changes with various frequency of EPT

The optical micrographs of the non-EPT specimen and the EPT specimens with various frequencies of electropulsing are shown in Fig. 4.12. For the cold-rolled specimen (non-EPT specimen) in Fig. 4.12(a), plenty of deformation twins inside the grains are observed, and the average size of the grains is about 77 μm . With increasing the frequency of electropulsing, the amount of twins is decreased. The average grain size reduces from 68 μm , 63 μm to 35 μm in the 209 Hz, 253 Hz and 294 Hz EPT specimens, as shown in Fig. 4.12 (b), (c) and (d) respectively. A relatively homogeneous microstructure of equi-axed grains is observed after 294 Hz-EPT for 10

seconds, implying that electropulsing greatly accelerates recrystallization of the cold rolled alloy specimens.

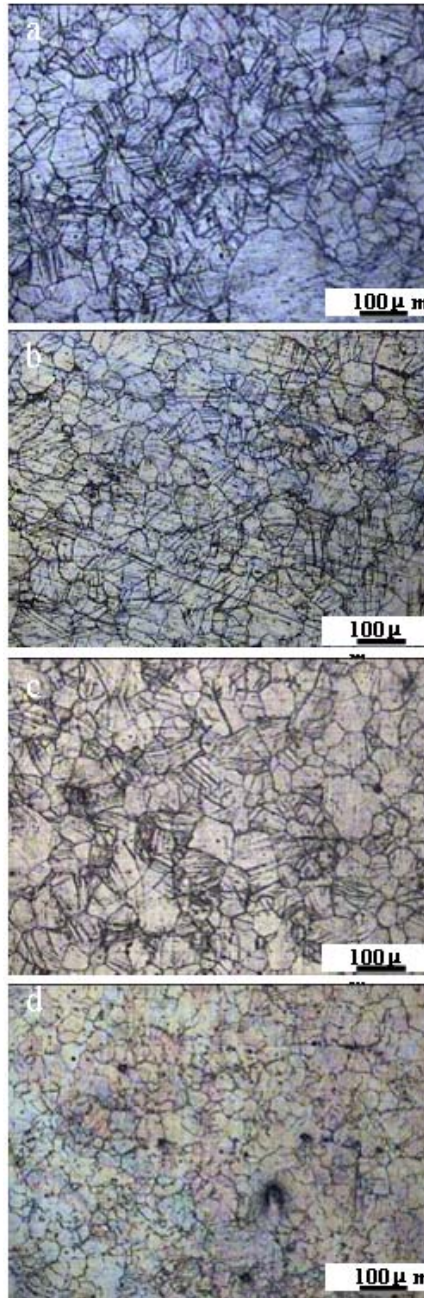


Fig. 4.12 Optical micrographs of (a) non-EPT (b) 209 Hz-EPT (c) 253 Hz-EPT and (d) 294 Hz-EPT

4.3.3 Dynamic EPT induced Phase Transformations and Microstructural Changes on Rolling Specimens

Fig. 4.13 shows the X-ray diffractograms of the as-rolled (non-EPT) specimen and the dynamic EPT specimens. The non-EPT specimen consists of mainly two phases, the α -Mg phase and the β phase ($Mg_{17}Al_{12}$). When the frequency of electropulsing increases to 204 Hz, the XRD intensity of the β phase reduces. Upon further increasing the frequency to 309 Hz, the XRD intensity of the β phase further reduces. This implies that the decomposition of the β phase is accelerated when the frequency of electropulsing increases during the dynamic electropulsing.

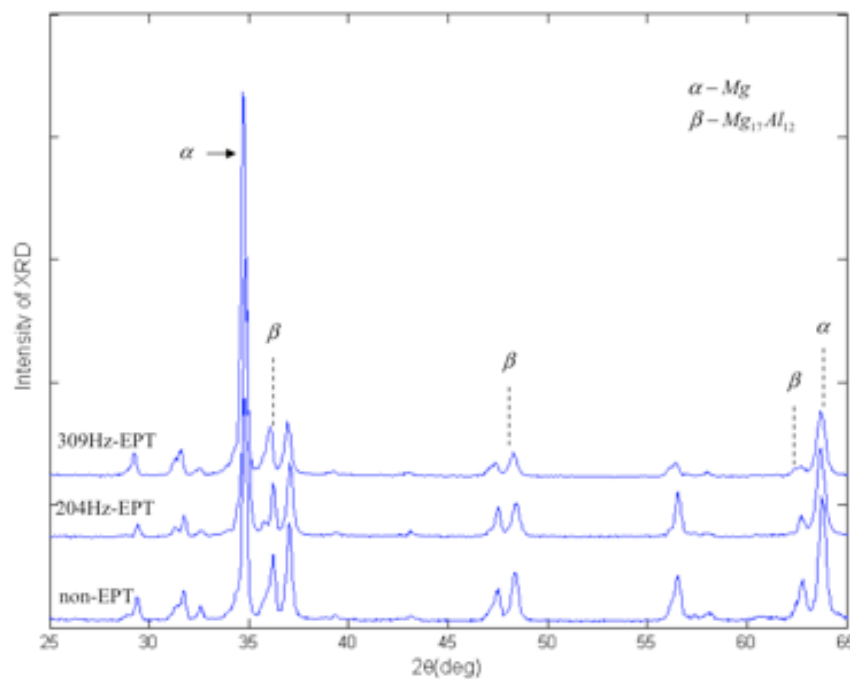


Fig. 4.13 XRD patterns for the specimens under various frequencies of dynamic EPT

The BSEM images and TEM bright field images of specimens under different frequencies of dynamic EPT are shown in Fig. 4.14. The matrix shows a α -Mg phase, while the precipitates are of β phase ($\text{Mg}_{17}\text{Al}_{12}$). For the as-rolled specimen, numerous β phase precipitates can be seen in Fig. 4.14 (a1); as the frequency of dynamic electropulsing increased to 204 Hz, the amounts of the β phase precipitates decrease as shown in Fig. 4.14 (a2); when the frequency of electropulsing increases to 309 Hz, even fewer precipitates could be observed in Fig. 4.14 (a3). TEM bright field images of these specimens confirmed the same microstructural changes as shown in Fig. 4.14 (b1), (b2) and (b3). As the frequency of electropulsing increases, the amounts of the precipitates marked by the white arrows decrease significantly, meaning that the decomposition of the β phase occur simultaneously in a way of up-quenching. Both the SEM results and TEM observations are in good agreement with the XRD patterns shown in Fig. 4.13.

To identify the phases during the process, the TEM examination of the dynamic electropulsing treated specimens is shown in Fig. 4.15. The bright field of the 204 Hz-EPT specimen is shown in Fig. 4.15 (a). Together with the indexed SADPs shown in Fig. 4.15(b1) and Fig. 4.15(c1), the dark field images reflected from $[\bar{1}2\bar{1}3](10\bar{1}0)$ of the hcp α phase, and $[\bar{1}11](110)$ of the bcc β phases are shown in Fig. 4.15 (b2) and Fig. 4.15 (c2), respectively. The lattice parameters of the α phase are $a=3.22 \text{ \AA}$, $c=5.23 \text{ \AA}$ and $c/a=1.624$; the lattice parameter of the β phase is $a=10.690 \text{ \AA}$.

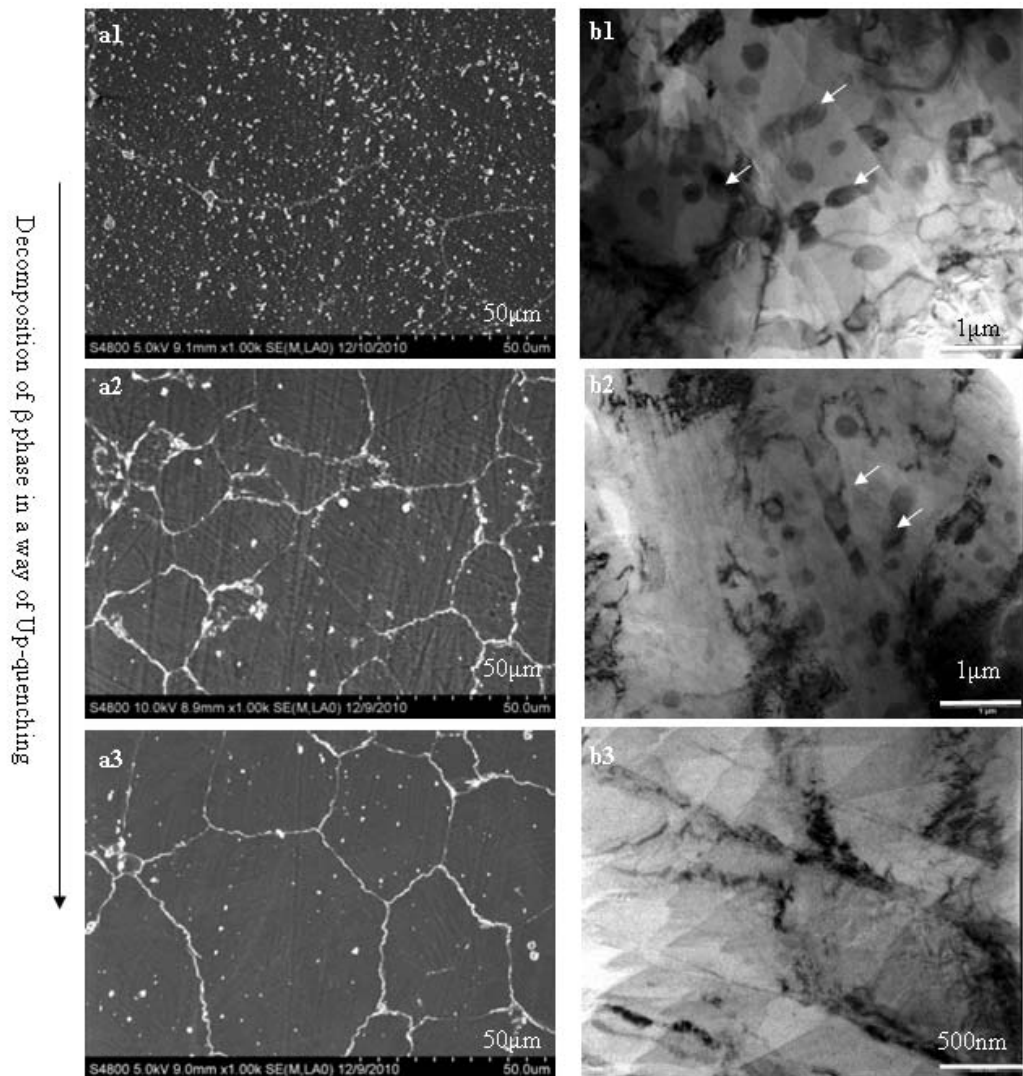


Fig.4.14 BSEM images of (a1) non-EPT (a2) 204 Hz-EPT (a3) 309 Hz-EPT and TEM bright field images of (b1) non-EPT (b2) 204 Hz-EPT (b3) 309 Hz-EPT, showing β phase precipitates changes with various frequency of EPT

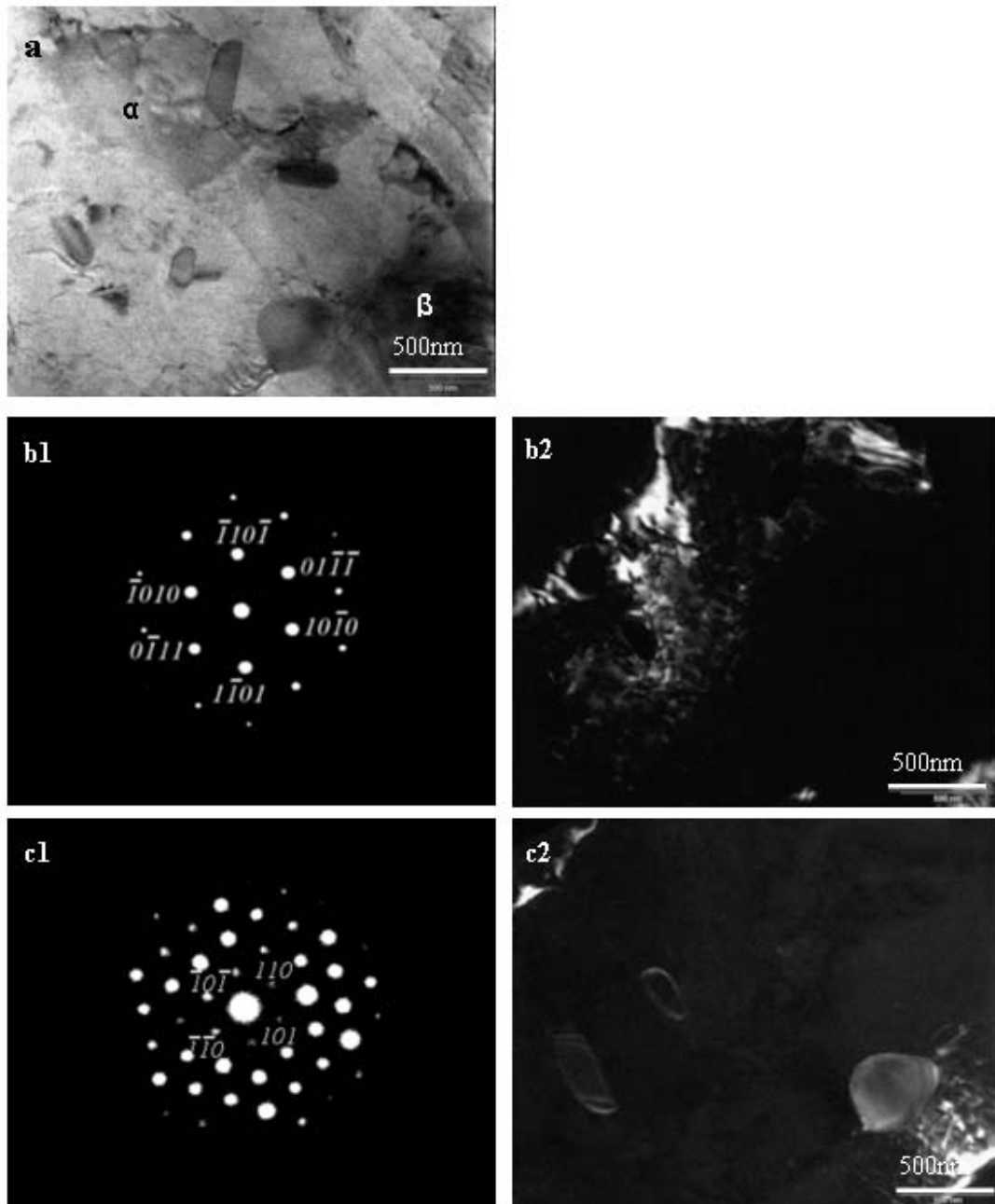


Fig.4.15 TEM images of 204 Hz-EPT (a) bright field image; (b2) dark field image of $(10\bar{1}0)$ reflection together with (b1) diffraction pattern from $B=[\bar{1}2\bar{1}3]$ of the α phase; (c2) dark field image of (110) reflection together with (c1) diffraction pattern from $B=[\bar{1}1\bar{1}]$ of the β phase

For comparison, the AZ91 strips are statically electropulsing-treated for various parameters. For the static EPT specimens, of which the BSEM images and TEM bright field images are previously shown in Fig. 4.11, it is found that with increasing frequency of electropulsing, decomposition and precipitation of the β phase are tremendously accelerated sequentially. While for the dynamic EPT specimens, only the decomposition of the β phase in a way of up-quenching occurs, as shown in Fig. 4.14. For the decomposition to be completed under the conventional thermal process of the AZ91 strips, about 10 hours of ageing in the range of 673-693 K is required (Jiang et al., 2009). This implies that electropulsing tremendously accelerates the phase transformations of the AZ91 alloy at a relatively lower temperature (349-390 K) within only a few seconds.

The optical micrographs of the non-EPT and the dynamic EPT specimens for various frequencies are shown in Fig. 4.16. For the non-EPT specimen, many deformation twins are observed inside the grains, as shown in Fig. 4.16 (a). When the frequency of the dynamic electropulsing increases to 126 Hz, the twins inside the grains are rarely observed, as shown in Fig. 4.16 (b). Upon further increasing the frequency to 309 Hz, a relatively homogeneous microstructure of equiaxed grains is obtained, as shown in Figs. 4.16 (c) to (e). This is because under the dynamic electropulsing, the external stress resulting from the plastic deformation is reduced simultaneously, and the twins quickly vanish. In comparison, for the static EPT specimens as shown in Fig. 4.12, the twins microstructure decrease gradually when the frequency increases from non-EPT to 209 Hz and 253 Hz, and disappear after 294 Hz-EPT.

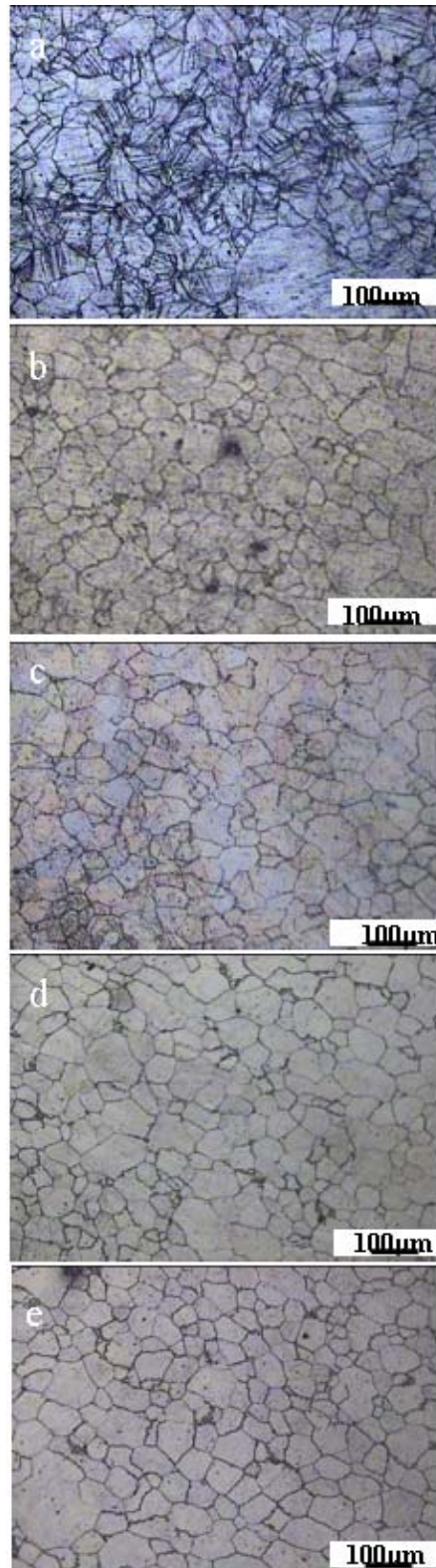


Fig. 4.16 Optical micrographs of (a) non-EPT (b) 126 Hz-EPT (c) 204 Hz-EPT and (d) 265 Hz-EPT (e) 309 Hz-EPT

4.3.4 Dislocation Identity

The dislocation evolution under various frequencies of EPT can be observed from the TEM images. TEM bright field images of the as-tempered specimens under various of frequencies of static EPT are shown in Fig. 4.17. In Fig. 4.17(a) non-EPT specimen, there are some dislocation arrays and nodes, introduced from the previously thermal and thermo-mechanical treatments.

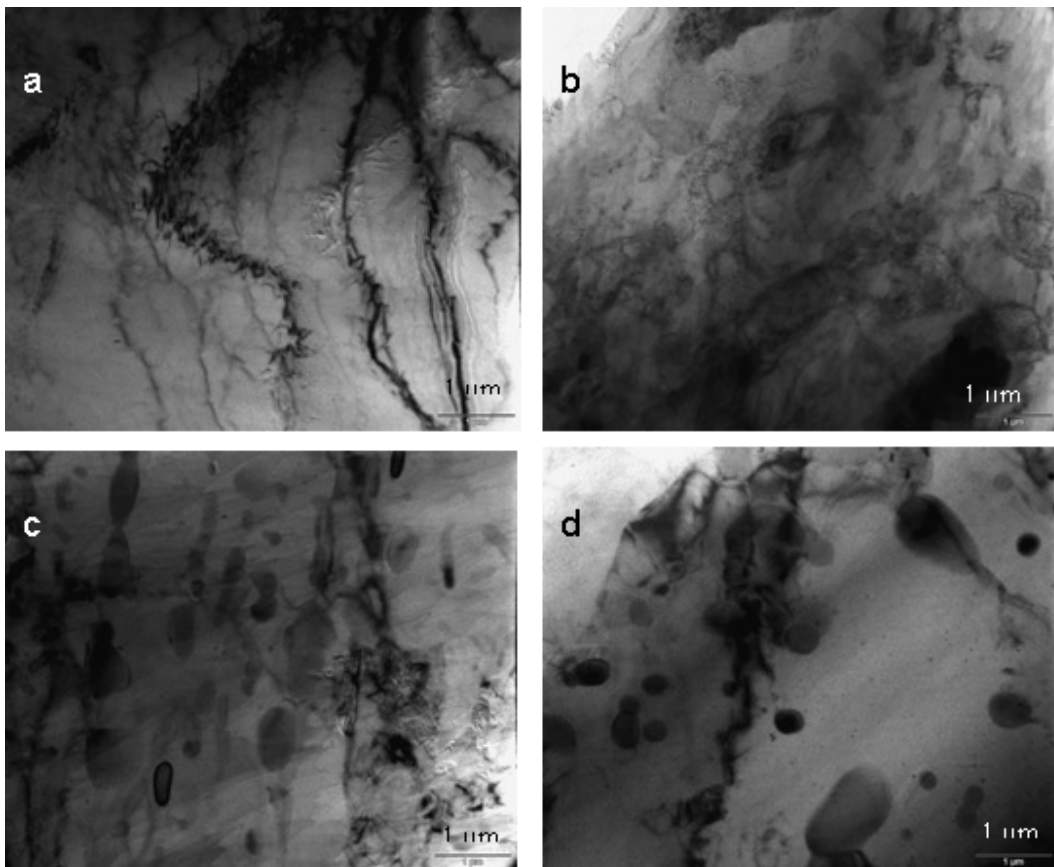


Fig. 4.17 TEM bright field images of as-tempered specimens (a) non-EPT, (b) 120 Hz-EPT, (c) 183 Hz-EPT and (d) 252 Hz-EPT

Due to the electron wind force factor introduced in Chapter 2, the defects in the specimen, such as dislocations and atomic vacancies are pushed towards the sub-grain boundaries by electropulsing. After 120 Hz-EPT, the dislocation arrays and nodes decrease as shown in the Fig. 4.17 (b). When the frequency of EPT increases to 183 Hz, the amounts of dislocations are significantly reduced, as shown in Fig. 4.17(c). It is proposed that under electropulsing, electron wind is formed and pushes the defects in the specimen, such as dislocations and atomic vacancies, towards the grain boundaries, where accumulation and annihilation of the dislocations occur at the same time (Zhu, 2009). With increasing frequency of electropulsing, both the accumulation and the annihilation of dislocation are enhanced, maintaining an adequate balance at the grain boundaries. Thus, the dislocation density decreases. After 252 Hz-EPT, the dislocation can rarely be observed, as shown in Fig. 4.17(d). The dislocation dynamics for the cold-rolled specimens under various frequencies of static EPT are shown in Fig. 4.11(b), and the specimens under various frequencies of dynamic EPT are shown in Fig. 4.14(b), and confirm the aforementioned theory.

4.3.5 Driving Force in the Phase Transformations

The driving force for phase decomposition consists of various factors, including chemical Gibbs free energy, surface energy, strain energy, crystal orientation Gibbs free energy and EPT induced Gibbs free energy. It is proposed that the free energy change for the phase transformations to occur can be shown as follows (Zhu, 2009):

$$\Delta G = \Delta G_{chem} + \Delta G_{surface} + \Delta G_{strain} + \Delta G_{orient} + \Delta G_{EPT} \quad (4.1)$$

The driving force of the as-tempered specimens under static EPT is discussed. In conventional thermodynamics, the chemical Gibbs free energy (ΔG_{chem}) is considered to be the dominant factor in determining phase transformations. The surface energy ($\Delta G_{surface}$) and preferred crystal orientation induced Gibbs free energy (ΔG_{orient}) are the main parts affecting phase transformations in the nano-phase of alloy films. The strain energy (ΔG_{strain}) includes the internal strain energies, such as thermal stress during solidification of melt, and external strain energies caused by tensile, creep, fatigue effect etc. For the AZ91 specimens used in this study, the major factors influencing phase transformations are ΔG_{chem} and ΔG_{EPT} , because no nanofilm and external strain exist in the experiments. The EPT accelerates the phase transformations in two stages:

- (1) When $\Delta G < 0$, with addition of EPT induced Gibbs free energy, the total Gibbs free energy of the specimen increases and is higher than that of the stable state. EPT accelerates the decomposition of the supersaturated α phase and more precipitation of β phase is generated, till the final stable state is reached, where $\Delta G = 0$;
- (2) When $\Delta G = 0$, further EPT would continue to increase the Gibbs free energy of the alloy, where $\Delta G > 0$. As a result, the stable phases reverse-decompose and precipitation of β phases decreases.

For the quenching process, both ΔG_{chem} and ΔG_{EPT} are negative:

$$\Delta G_{quench} = -\Delta G_{chem} - \Delta G_{EPT} \quad (4.2)$$

The chemical Gibbs free energy and the EPT induced Gibbs free energy together accelerate the phase transformation from the supersaturated state of the non-EPT specimen to the saturated state of 183 Hz-EPT specimen.

For the up-quenching process, the positive increment of ΔG_{EPT} induced by EPT is the only driving force for the phase transformations, and the specimen becomes unstable for reverse-transforms back to the initial state.

For the cold-rolled specimens under static EPT, the decomposition of the β phase occurred first when $\Delta G > 0$, subsequently followed by the precipitation of the β phase as $\Delta G < 0$.

For the specimens under dynamic EPT, only the decomposition of β phase occurred, reaching a stable state.

4.3.6 Electropulsing Kinetics

In EPT, due to the transient stress caused by electron wind, dislocation movements are very quick even at ultrasonic speeds. The electron wind is formed by the knock-on collision of high-rate electrons with atomic nuclei. The transfer of energy from electrons to the atoms is also much more effective than in the traditional thermal and thermo-mechanical processes. As shown in Fig. 4.10, Fig. 4.12 and Fig. 4.16, the sliding behavior of the dislocations and the phase transformations are significantly affected by the EPT, and electron migration induced by electric current might play an important role in the process. The effect of multiple electropulses through the

specimens can be described by the atomic diffusion flux, J in the Nernst-Einstein equation (Jiang, 2009; Zhu, 2009):

$$J = \frac{N_i \cdot D_i}{KT} \left(KT \cdot \frac{\partial \ln X_i}{\partial x} - \Omega \cdot \frac{\partial \sigma}{\partial x} + Z^* \cdot e \cdot \rho \cdot j \right) \quad (4.3)$$

In which N_i , stands for the density of the i th atom species, D_i is the pertinent diffusion coefficient, Z^* is the effective valence, e is the charge on an electron, ρ is the resistivity, j is the current density, X_i is the concentration of the i th solute, Ω is the atom volume, $\frac{\partial \sigma}{\partial x}$ is the stress gradient, K is the Boltzmann constant and T is the absolute temperature. The chemical gradient and composition gradient can be neglected under EPT because these effects are much weaker than that of electropulsing. The average atomic flux per second under EPT can be described as (Jiang, 2009):

$$J = J_t + J_a = \frac{2\pi D_l}{\Omega \ln \left(\frac{R'}{r_0} \right)} \cdot \left(l + \frac{\delta_c}{c_0} \right) + \frac{2N \cdot D_l \cdot Z^* \cdot e \cdot \rho \cdot f \cdot j_m \cdot \tau_p}{\pi KT} \quad (4.4)$$

In which $J_t = \frac{2\pi D_l}{\Omega \ln \left(\frac{R'}{r_0} \right)} \cdot \left(l + \frac{\delta_c}{c_0} \right)$ and $J_a = \frac{2N \cdot D_l \cdot Z^* \cdot e \cdot \rho \cdot f \cdot j_m \cdot \tau_p}{\pi KT}$.

The atomic flux in EPT consists of mainly two parts: the flux of diffusion atoms caused by the thermal effect J_t , and the flux of diffusion atoms caused by the athermal effect J_a . D_l is the lattice diffusion coefficient, c_0 is the average concentration of vacancies, δ_c is the super-saturation concentration of vacancies, r_0 , R' are the distances far from dislocation where the vacancy concentrations are c_0 and $c_0 + \delta_c$

respectively, j_m is the peak current density, f is the frequency and τ_p is the duration of each electropulsing of EPT.

Judging from Equation (4.4), in the electropulsing process where j_m , f and τ_p increase, the athermal effect J_a increases linearly. As these three parameters increase, the incremental athermal effect would provide sufficient energy to accelerate the diffusional phase transformations and dislocation movements. Meanwhile, during the EPT, the temperature also increases because of the Joule heating effect, thus the thermal effect in EPT would also increase.

4.4 Summary

The effect of both the static and dynamic EPT on the microstructural changes and phase transformations are investigated by the observations from optical microscopy, SEM, XRD and TEM.

For the as-tempered specimens under static EPT, it is found there are two stages of phase transformations in the EPT process:

- (1) Phase transformations in a way of quenching: from non-EPT to the specimens under 120 Hz and 183 Hz frequency of EPT, precipitation of the β phase increases; and
- (2) Reverse phase transformations in a way of up-quenching: 183 Hz to 252 Hz frequency of EPT, decrease of precipitation of the β phase occurs.

For the cold-rolled specimens under static EPT, it is found that:

- (1) With increasing frequency of electropulsing, the decomposition and precipitation of β phase are tremendously accelerated in the AZ91 alloy; and
- (2) Both twins and the dislocation density are reduced when the frequency of electropulsing increased.

For the specimens under dynamic EPT, it is found that:

- (1) The β phase decomposition is considerably accelerated in a way of up-quenching under dynamic electropulsing, compared with the conventional thermal processing; and
- (2) The deformation twins microstructure disappears, and a homogeneous fine grain structure is achieved under dynamic electropulsing.

In conclusion, as one of the driving forces for phase transformations, EPT is more powerful and effective than conventional thermal energy. Besides the phase transformations, the properties of the alloys and the mechanism of EPT, such as the interaction between electrons and lattice atoms, dislocation movements and annihilation are also discussed. The dislocation density and movements show a reverse relationship with the increasing frequency of EPT. The fine grain structure can also be obtained by the use of EPT. In order to study the machinability of the alloy after EPT, ultra-precision single point diamond turning is used to process these specimens and is discussed in the next chapter.

Chapter 5 Machinability and Microstructural Changes in Single Point Diamond Turning after Electropulsing Treatment

5.1 Introduction

In the previous chapter, microstructural changes of AZ91 strips under different electropulsing treatment parameters were discussed in detail. Phase transformations and dislocation movements were found in electropulsed materials.

This chapter describes the electropulsing treated work material AZ91 are employed in a series of microcutting experiments on single point diamond turning. Face turning and straight cutting methods have been conducted to study the machinability of the electropulsing treated specimens. Based on the prior experimental results and analysis on the microstructures and material properties investigated in Chapter 4, the effect of EPT on the improvement of surface finish is further studied.

5.2 The Experimental Design

5.2.1 Specimen Preparation

Specimens under various EPT parameters were prepared with the same methods discussed in Chapter 4, and were then cut with a low speed saw (Fig. 5.1) into rectangle

pieces of 12 mm length (Fig. 5.2), and prepared for diamond turning with different cutting parameters. A low speed saw is used to prevent the high temperature induced by high-speed cutting. The rectangle pieces are then affixed onto columnar plates. To make certain that each specimen have the same spindle speed during the cutting process, all the pieces are fixed on the plates with the same radius. These specimens are then machined by a single point diamond turning machine (Optoform[®] 30).



Fig. 5.1 Low speed saw

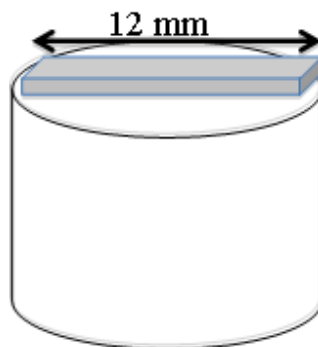


Fig. 5.2 Specimens with the length of 12 mm were fixed on the plate

5.2.2 Face Turning Experiments

Face turning experiments are conducted on all the three groups of electropulsed specimens, including (1) the as-tempered specimens with static EPT, (2) the cold-rolled specimens with static EPT and (3) the rolling specimens with dynamic EPT. The machinability changes of the specimens in SPDT are studied by observing the mean cutting force variations and surface roughness.

For the as-tempered specimens with static EPT, three groups of face turning are designed to study: (i) the effect of EPT on cutting force and surface roughness in Group-A, (ii) the effect of machining parameters on cutting force and surface roughness with electropulsing treatment in Group-B, and (iii) the effect of cutting speed on the microstructure evolution of machined surface in Group-C. The proposed design of the experiments is to reveal the relationship between machining, material and electropulsing treatment. A photo and a schematic illustration of the diamond turning process are shown in Fig. 5.3 and Fig. 5.4, respectively.

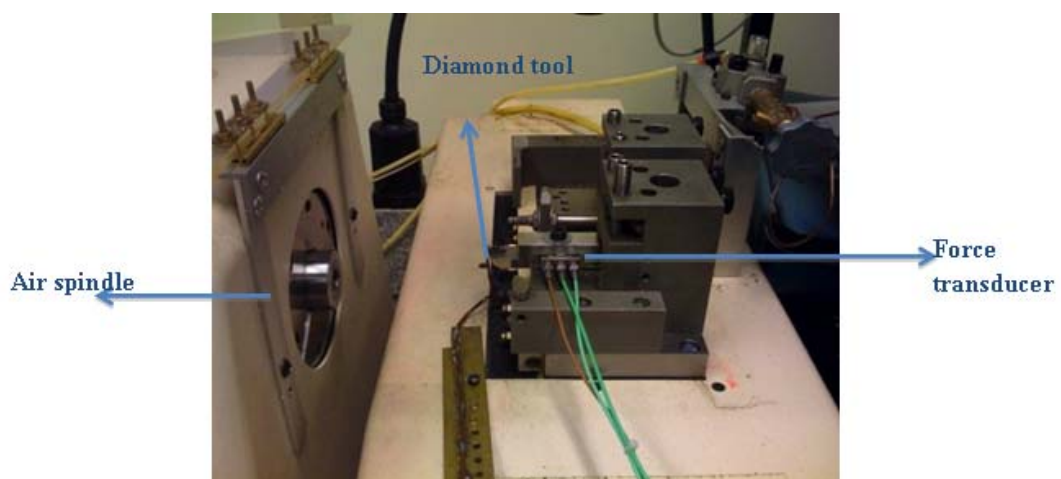


Fig. 5.3 Single point diamond turning machine

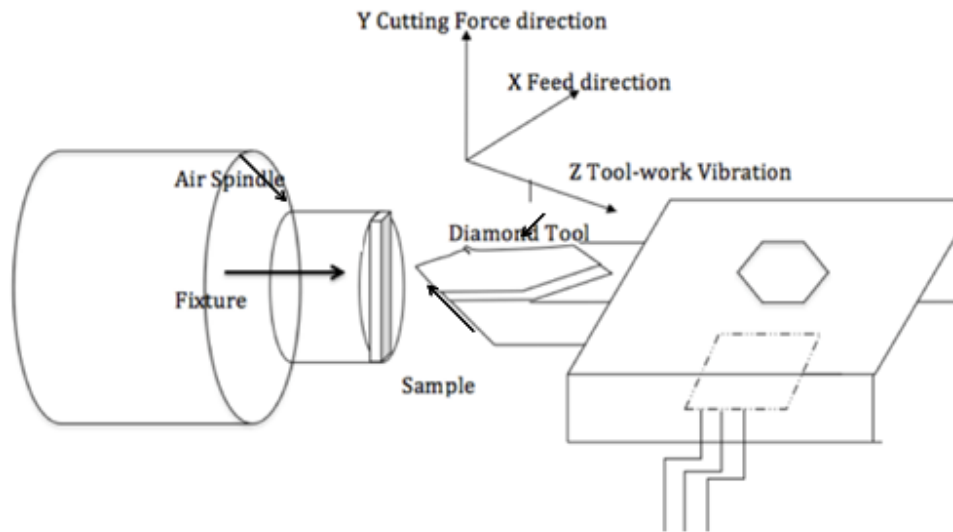


Fig. 5.4 Schematic illustration of single point diamond turning system

In Group-A, the AZ91 specimens after different types of EPT, including as-tempered specimens with static EPT, cold-rolled specimens with static EPT and rolling specimens with dynamic EPT, are cut with a slow speed saw into rectangular shapes (plate specimen) with length of 12 mm, width of 4 mm and height of 1.9 mm. These plate specimens are then glued to the surface of an aluminum-alloy cylinder with a radius of 12.7 mm, which would be chucked on spindle. The cutting parameters of Group-A are listed in the Table 5.1. The tool nose radius is 2.503 mm and the rake angle was 15° . A force transducer, Kistler 9252A, is mounted with a pre-loaded force under the tool shank. A 14-bit multifunctional data acquisition (DAQ) card PCI-6132 (National Instrument) is configured on a PC workstation to record the cutting force data (Fig. 5.5). The cutting forces during the cutting process for the specimens with various frequencies of EPT in the same group are compared, and the surface roughness is also discussed.

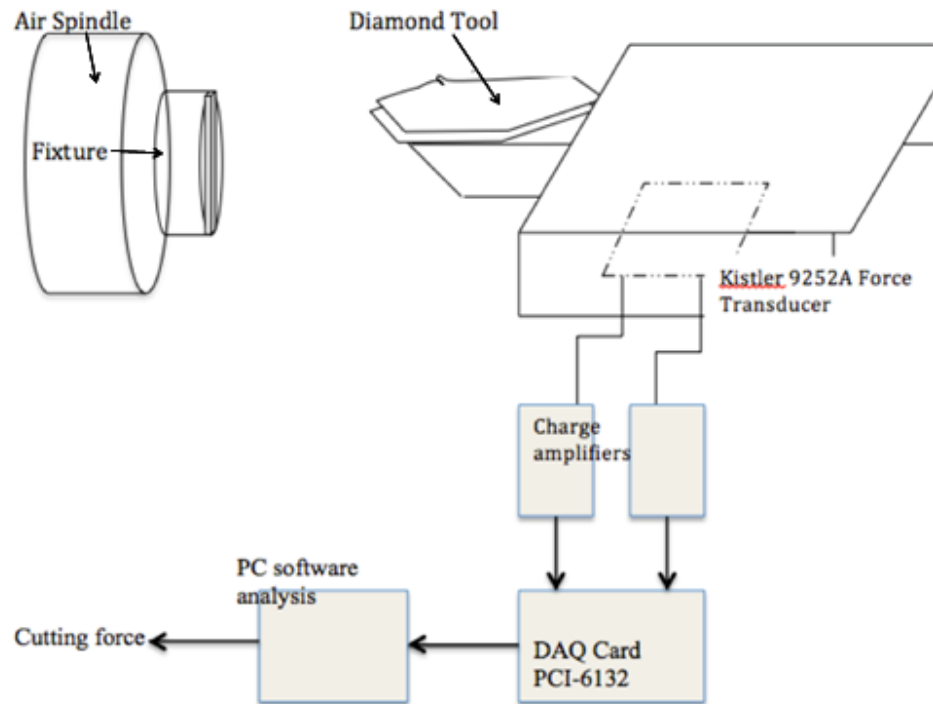


Fig. 5.5 Schematic illustration of cutting force measurement system

The microstructures of the as-tempered specimens after turning are obtained by using SEM, and the surface roughness are measured by both the Contact Taylor Surf PGI 1230 Stylus measurement system and the Noncontact WYKO NT8000 interferometric measurement system. The chips produced in each cutting experiment are collected and images of their free surfaces are taken using JSM-6490 JEOL scanning electron microscopy.

In Group-B, a fixed electropulsing parameter is selected for the as-tempered specimens to treat the work material before cutting. The depth of cut changes from 5 μm to 40 μm , while keeping other cutting parameters constant. The detailed cutting conditions are listed in Table 5.2.

In Group-C, the effect of cutting speed on the cutting force and microstructural changes of the specimen is investigated on the as-tempered specimens. As the distance from workpiece center changes from 1mm to 5 mm, the cutting speed changes from 837 mm/s to 4187 mm/s. The details of cutting condition are listed in Table 5.3.

Table 5.1 Cutting conditions of Group-A for specimens with different types of EPT

EPT Specimens	As-tempered with static EPT	Cold-rolled with static EPT	Rolling with dynamic EPT
Spindle speed (RPM)	8000	8000	8000
Feed (mm/min)	20	20	20
Depth of Cut (μm)	20	20	20

Table 5.2 Cutting conditions of Group-B for as-tempered specimens with static EPT

Depth of cut (μm)	5	10	20	40
Spindle speed (RPM)	8000			
Feed (mm/min)	20			
Passes	20	10	5	3
EPT Specimen	252 Hz			

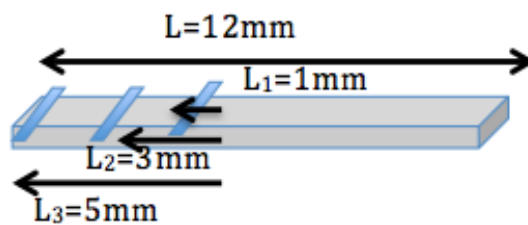


Fig.5.6 Schematic illustration of different sectors of the specimen

Table 5.3 Cutting conditions of Group-C for as-tempered specimens with static EPT

Cutting length (mm)	1	3	5
Cutting speed (mm/s)	837	2512	4187

Cutting speed $v = \omega \cdot R = 2\pi \cdot S/60 \cdot l_x$, in which R is the radius, S is the spindle speed and l_x is the distance from the workpiece centre.

5.2.3 Straight Cutting Experiments

For the as-tempered specimens with static EPT, four specimens pre-treated with various frequencies of EPT are cut with a slow speed saw into rectangular shapes with length of 12 mm, width of 4 mm and thickness of 1.9 mm. The AZ91 specimens are mounted on the customized fixture (Fig. 5.7) in order to minimize the vibration of the system during the high-speed cutting process. The diamond tool insert is mounted on a customized tool holder with the normal of the tool rake face parallel to the cutting direction. The parameters of straight cutting are listed in Table 5.4. The side face of specimen plates is polished to remove the oxidization layer and to ensure a straight cutting condition with a smaller thickness of about 1 mm. The chip formation geometry is shown in Fig. 5.8. These chips are collected after each cutting process and then observed by SEM to examine the morphology of the side face and the tool-contact face.

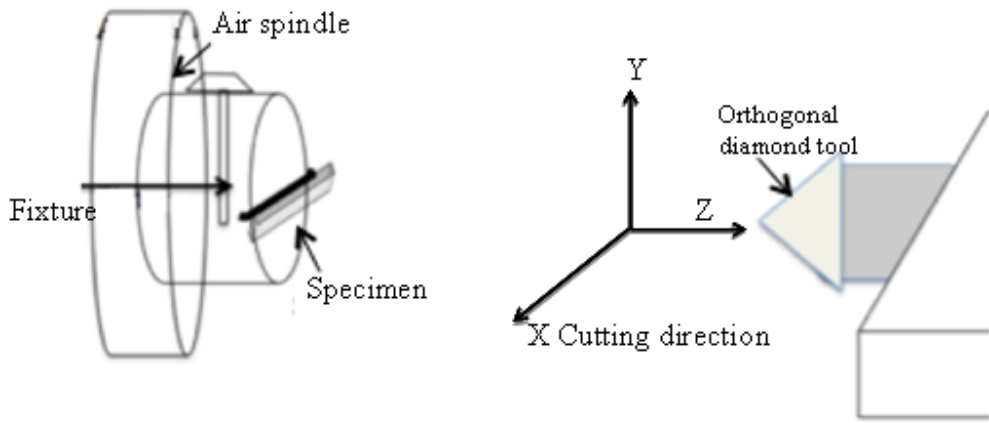


Fig. 5.7 Schematic illustration of straight cutting process

Table 5.4 Cutting conditions of straight cutting process

As-tempered specimens with various frequencies of static EPT (Hz)	non-EPT	120	183	252
Cutting speed (mm/min)	500			
Spindle speed (rpm)	0			
Depth of Cut (μm)	10			
Tool nose radius (mm)	2.503			

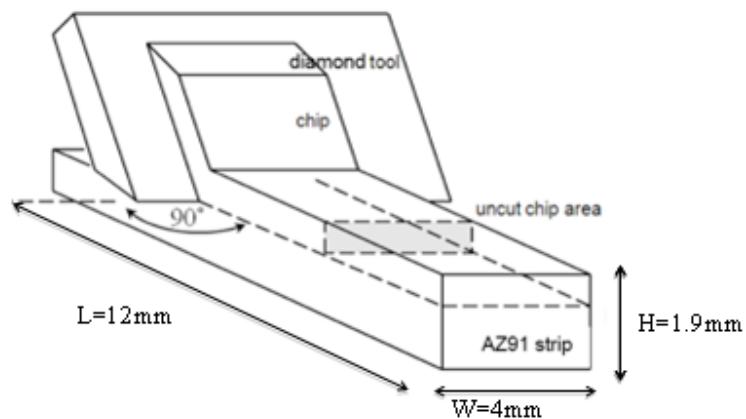


Fig. 5.8 Schematic illustration of chip formation in straight cutting process

5.3 Results and Discussion

5.3.1 Cutting Force Changes under Various frequencies of EPT

Cutting forces during the turning process are measured by the methods introduced in Chapter 3. By comparing the values of the cutting force, the effect of EPT on the machinability properties of the specimens are discussed in detail. For the as-tempered specimens with static EPT, it can be observed that when EPT frequencies increase, the cutting force under same cutting parameters decreases significantly, as shown in Fig. 5.9. With the non-EPT specimen, the mean cutting force is 70.72 mN, and when the frequency of EPT increases from 120 Hz to 183 Hz and 252 Hz, the mean cutting force decreases from 55.92 mN to 50.75 mN and finally 48.84 mN respectively.

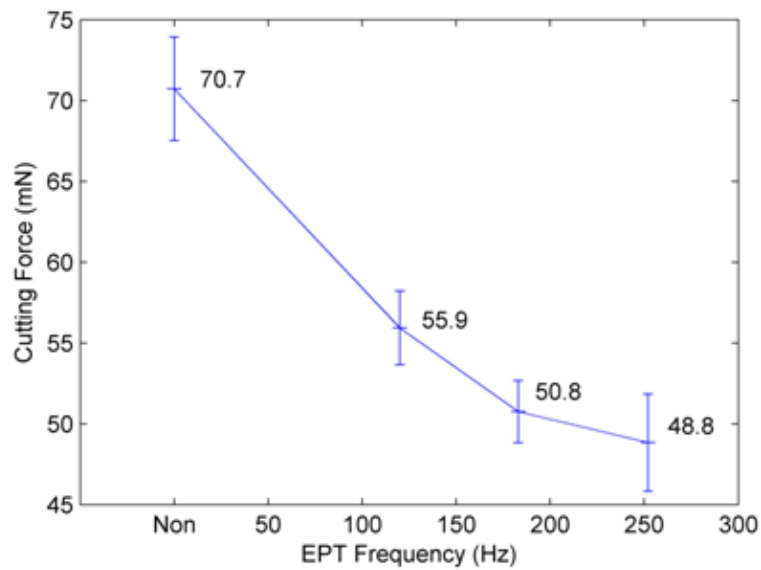


Fig.5.9 Mean cutting force of the as-tempered specimens under various frequencies of static EPT (depth of cut of 20 μm)

For the cold-rolled specimens with static EPT and the rolling specimens with dynamic EPT, it can also be observed that with increasing frequency of electropulsing, the cutting force decreases significantly, as shown in Fig. 5.10 and Fig. 5.11 respectively.

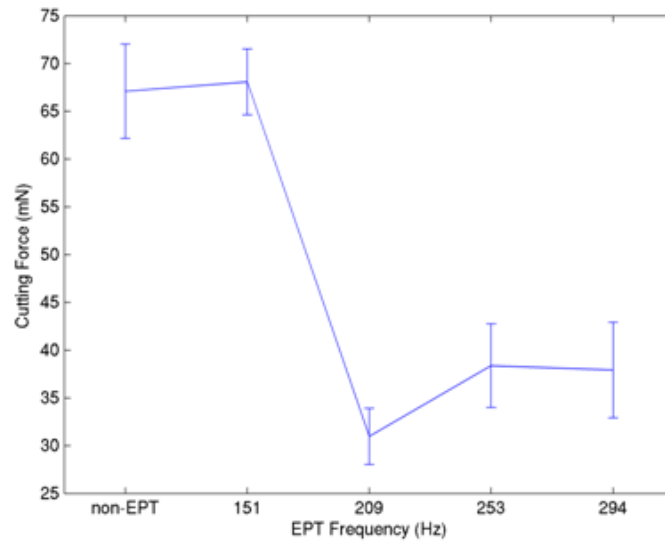


Fig. 5.10 Mean cutting force of the cold-rolled specimens under various frequencies of static EPT (depth of cut of 20 μm)

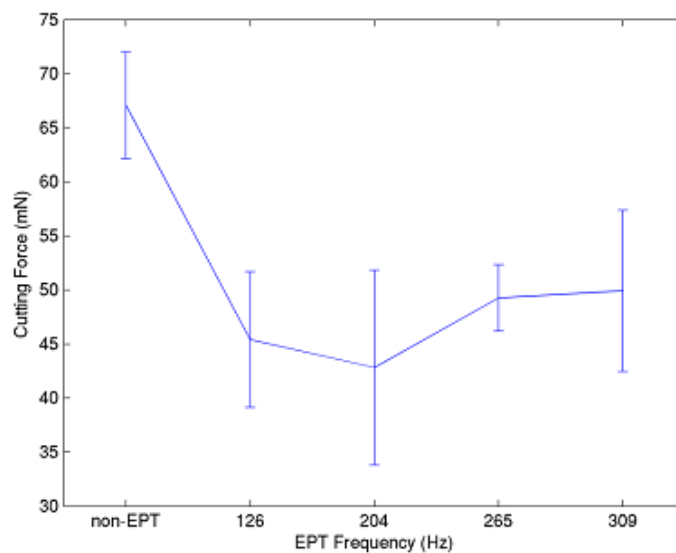


Fig. 5.11 Mean cutting force of the rolling specimens under various frequencies of dynamic EPT (depth of cut 20 μm)

5.3.2 Surface Roughness under Various Frequencies of EPT

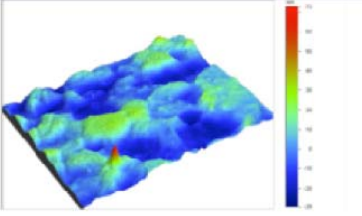
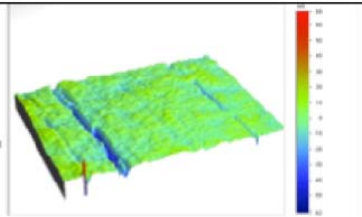
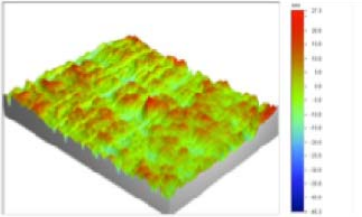
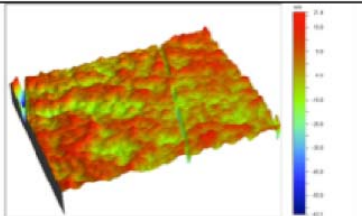
After the turning process, specimens in same depth of cut, with various frequencies of EPT, the surface roughness are measured. In order to get the surface profile data, the noncontact WYKO NT8000 is used for the reason that it would not damage the specimen surface while acquiring the profile image with sub-nanometer vertical resolution. In order to get an unbiased characterization of the whole surface of the specimens, contact form taylor surf PGI1240 equipment is used to measure the surface roughness. For each specimen, seven lines with the same length of 10 mm are set as the measurement parameters to get the surface roughness.

For the as-tempered specimens, the surface profiles of various frequencies with static EPT under the same cutting conditions are listed in Table 5.5. It can be seen that the specimens with higher frequencies of static EPT show better surface finish, compared with the non-EPT specimen. The arithmetic roughness of the non-EPT specimen is 9.78 nm, and as the frequency of EPT increases from 120 Hz to 183 Hz and 252 Hz, the arithmetic roughness changes from 5.31 nm, 5.48 nm and 5.17 nm, respectively. The mean roughness values measured by the contact system are shown in Fig. 5.12.

The correlation between the measured mean cutting force and the surface roughness for different pre-machining electropulsing treatments is plotted in Fig. 5.13. With the non-EPT specimen, the mean cutting force in the turning process is larger than those electropulsing treated specimens, and the surface roughness after turning also shows the same trends. For the electropulsed specimens, after the 120 Hz, 183 Hz

and 252 Hz frequency of EPT, it is noticed that as the frequency increases, the mean cutting force and the surface roughness decrease. To sum up the normalized trend as shown in Fig. 5.13, the effect of EPT results in a decrease of the mean cutting force as well as the surface roughness.

Table 5.5 Surface profiles of as-tempered specimens with various frequencies of static EPT

Non-EPT	<div style="display: flex; align-items: center;"> <div style="margin-right: 10px;"> <p>Surface State: Ra: 9.78 nm Rq: 11.84 nm Rz: 102.17 nm</p> <p>Measurement Info: Magnification: 20.70 Measurement Mode: PPS Sampling: 482.87 nm Array Size: 640 X 480</p> </div>  </div> <p style="text-align: center;">Ra=9.78nm Rq=11.84nm</p>
120Hz	<div style="display: flex; align-items: center;"> <div style="margin-right: 10px;"> <p>Surface State: Ra: 5.31 nm Rq: 8.36 nm Rz: 130.24 nm</p> <p>Measurement Info: Magnification: 20.70 Measurement Mode: PPS Sampling: 482.87 nm Array Size: 640 X 480</p> </div>  </div> <p style="text-align: center;">Ra=5.31nm Rq=8.36nm</p>
183Hz	<div style="display: flex; align-items: center;"> <div style="margin-right: 10px;"> <p>Surface State: Ra: 5.48 nm Rq: 7.42 nm Rz: 72.92 nm</p> <p>Measurement Info: Magnification: 20.70 Measurement Mode: PPS Sampling: 482.87 nm Array Size: 640 X 480</p> </div>  </div> <p style="text-align: center;">Ra=5.48 nm, Rq=7.42 nm</p>
252Hz	<div style="display: flex; align-items: center;"> <div style="margin-right: 10px;"> <p>Surface State: Ra: 5.17 nm Rq: 7.02 nm Rz: 84.47 nm</p> <p>Measurement Info: Magnification: 20.70 Measurement Mode: PPS Sampling: 482.87 nm Array Size: 640 X 480</p> </div>  </div> <p style="text-align: center;">Ra=5.17nm, Rq=7.02nm</p>

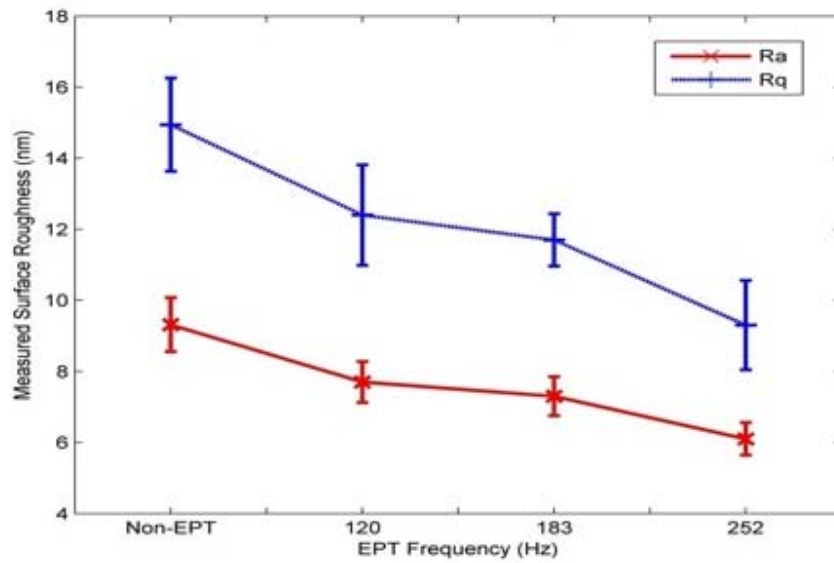


Fig. 5.12 Ra and Rq changes of as-tempered specimens under various frequencies of static EPT (depth of cut of 20 μm)

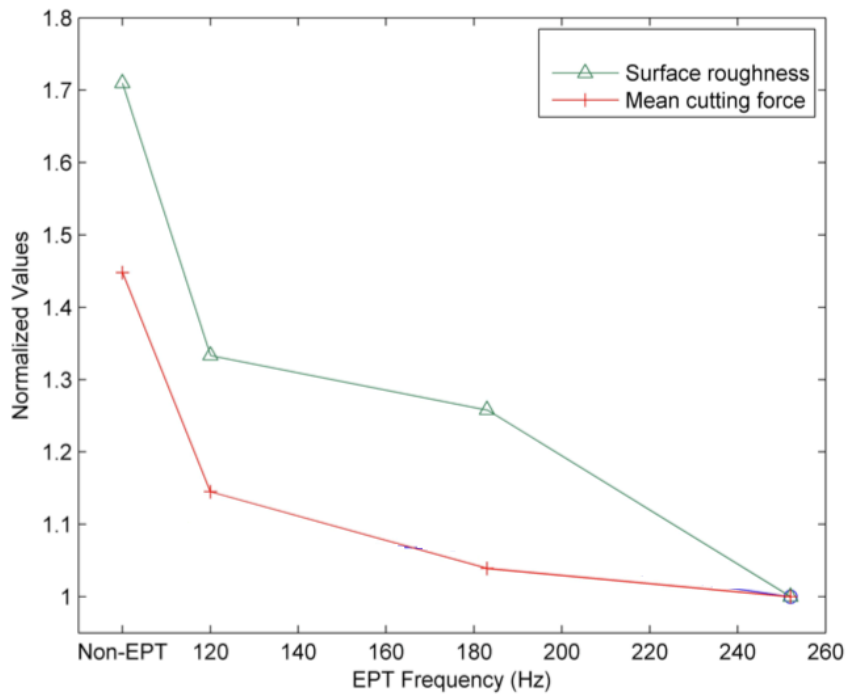


Fig.5.13 Correlation between mean cutting force and surface roughness of as-tempered specimens under various static EPT frequencies

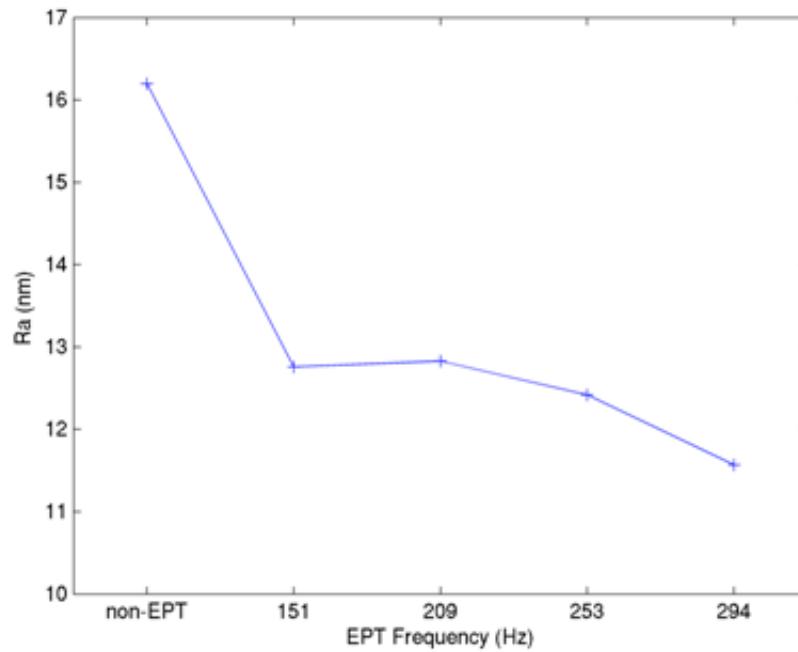


Fig. 5.14 Surface roughness of cold-rolled specimens under various frequencies of static EPT (depth of cut of 20 μm)

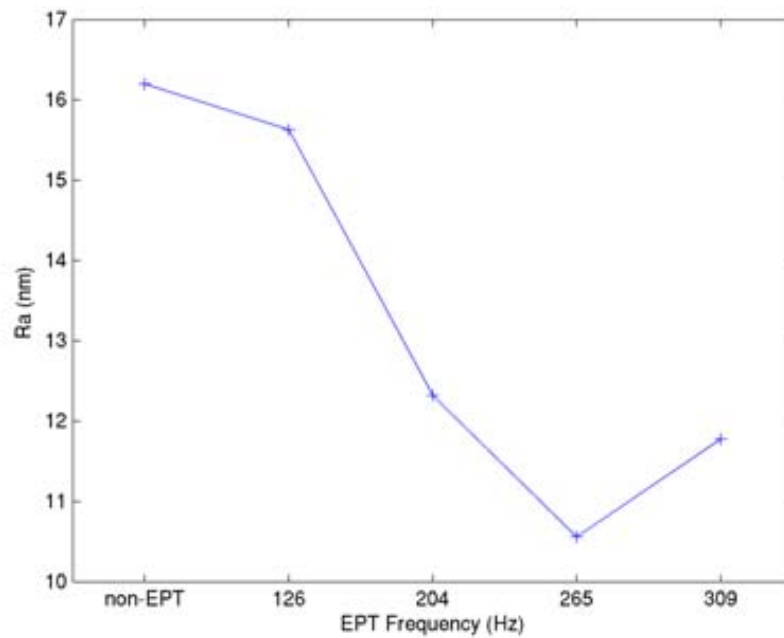


Fig. 5.15 Surface roughness of rolling specimens under various frequencies of dynamic EPT (depth of cut of 20 μm)

For the specimens after static EPT and the dynamic EPT, the surface roughness by SPDT decreases when the EPT frequencies increase, as shown in Fig. 5.14, Fig. 5.15 respectively. It can be observed that for the static EPT, the surface roughness decrease from 16.32 nm under non-EPT to 11.63 nm under 294 Hz-EPT; for the dynamic EPT, the surface roughness decrease from 16.28 nm under non-EPT to 11.82 nm under 309 Hz-EPT.

In conclusion, with increasing frequency of electropulsing, the cutting force decreases significantly (Fig. 5.9 to Fig. 5.11), meanwhile the surface roughness decreases (Fig. 5.12, Fig. 5.14 and Fig. 5.15). It is assumed that under electropulsing, large amounts of the deformation twins structure decrease, as the recrystallization is accelerated under electropulsing. The relatively homogeneous microstructure of the fine-equiaxed grain structure is formed (Fig. 4.12 and Fig. 4.16), and the decreasing amounts of dislocation (Fig. 4.11(b), Fig. 4.14(b) and Fig. 4.17) result in the decreasing cutting force and improving surface roughness for SPDT processing. The machinability of AZ91 alloy in SPDT is improved under EPT.

5.3.3 Microstructural Changes on the Machined Surface of Specimens

The as-tempered specimens without electropulsing treatment after turning process are measured by SEM. The strip can be divided into three parts with different distances from the center, ranging from 1mm, 3 mm to 5 mm. The cutting speed increases as the distance increases from 837 mm/s to 2512 mm/s and 4187 mm/s, respectively. It can be observed from the SEM micrographs (Fig. 5.16) that for

different distances from the center with different cutting speed and radius, the shapes and forms of the α phase show significant changes, both in the non-EPT and the 252 Hz-EPT conditions.

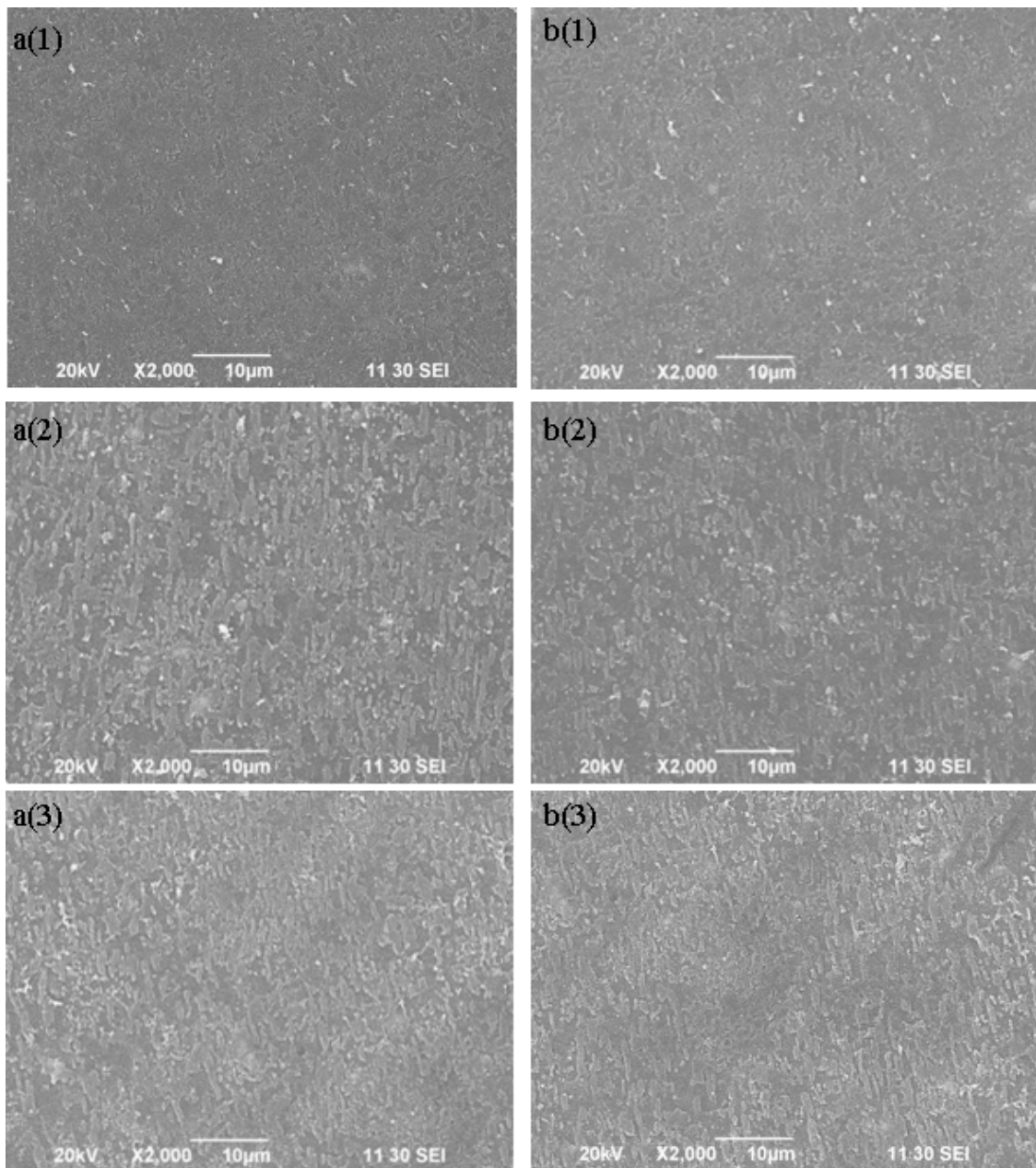


Fig. 5.16 SEM micrographs of the as-tempered specimen under 5 μm depth of cut with (a) non-EPT and (b) 252 Hz-EPT, in different cutting speeds (1) $v_1=837$ mm/s (2) $v_2=2512$ mm/s (3) $v_3=4187$ mm/s

As the cutting speed increases, the form of the α phase changes from a ball shaped mass into dispersed strips, and as the cutting speed continues to increase from sector L_2 to

L_3 , the strips become more dispersed, changing from long large ones into short small ones. The direction of these strips is the same as the cutting direction, therefore the elongated strips of the α phase can be used to study the effect of micro-cutting on the microstructure of a machined surface.

Apart from the microstructural changes induced by the cutting speed, the experimental results indicate that a similar microstructural change occurs with different depths of cut on the work material, with pre-machining EPT treatment at 252 Hz. When a small depth of cut is used (5 μm in Fig. 5.17a), the rubbing effect induced by the elastic deformation of the deformed layer is pronounced, which in turn increases the tool-work friction and heat generation. Therefore, as a complex result of the heating effect and imposed strain/stress, the elongation of the α phase along the cutting direction in Fig. 5.17(a) is more significant than that in Fig. 5.17(b), where a larger depth of cut of 10 μm is employed. At a depth of cut of 10 μm in Fig. 5.17(b), the α phase starts to change from a sphere to rod shape with one dimension elongated along the cutting direction. Most of the α phase spheres are transformed into rod shapes, as shown in Fig. 5.17(c) and (d), as the depth of cut increases to 15 μm and 20 μm respectively. This transformation is attributed to the imposed strain/stress field and heat generation by the friction force and plastic work induced by the micro-cutting process.

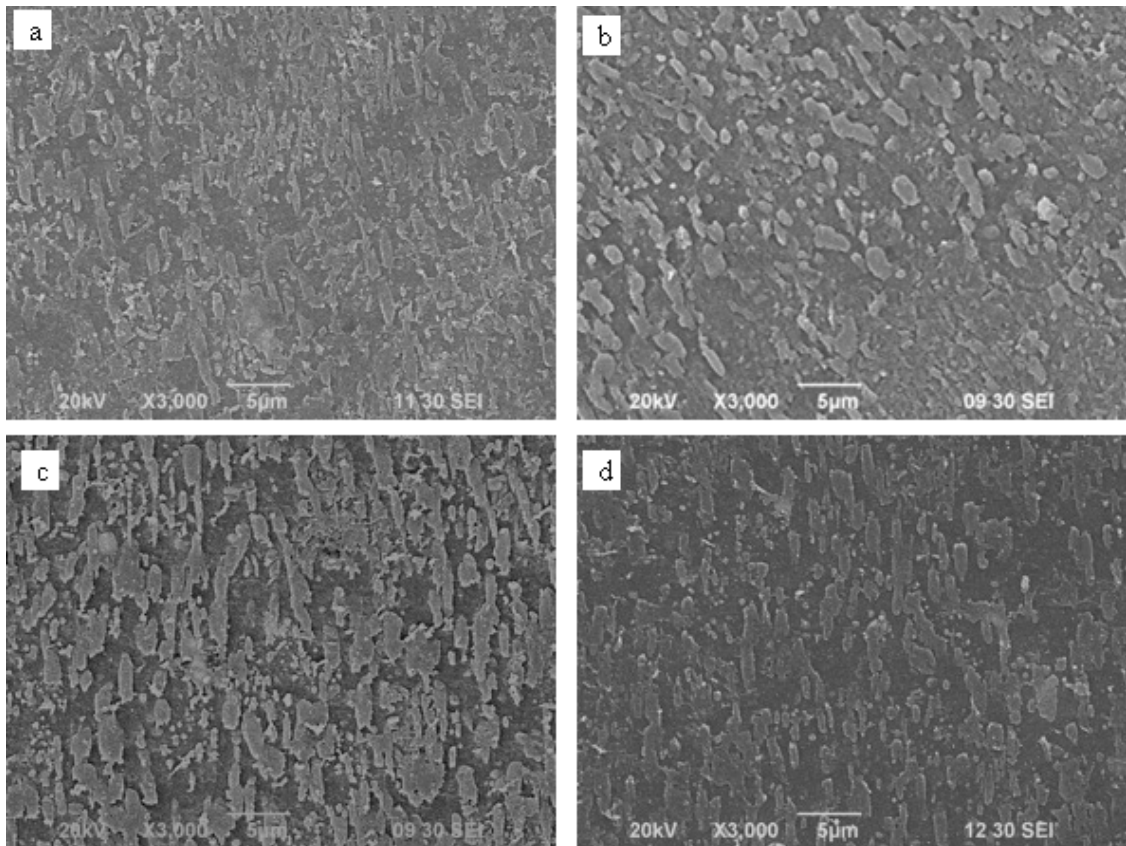


Fig.5.17 SEM micrographs of the 252 Hz-EPT with depth of cut (a) 5 μm , (b) 10 μm , (c) 20 μm , (d) 40 μm

5.3.4 Chips Morphology

The chips during the face turning process are collected by using a vacuum chamber with a filter paper on top of it. The micrographs of the free surface of chips are recorded by SEM, and are shown in Fig. 5.18. It is observed that the density of the lamella layers in the serrated chips increases with increasing of EPT frequency.

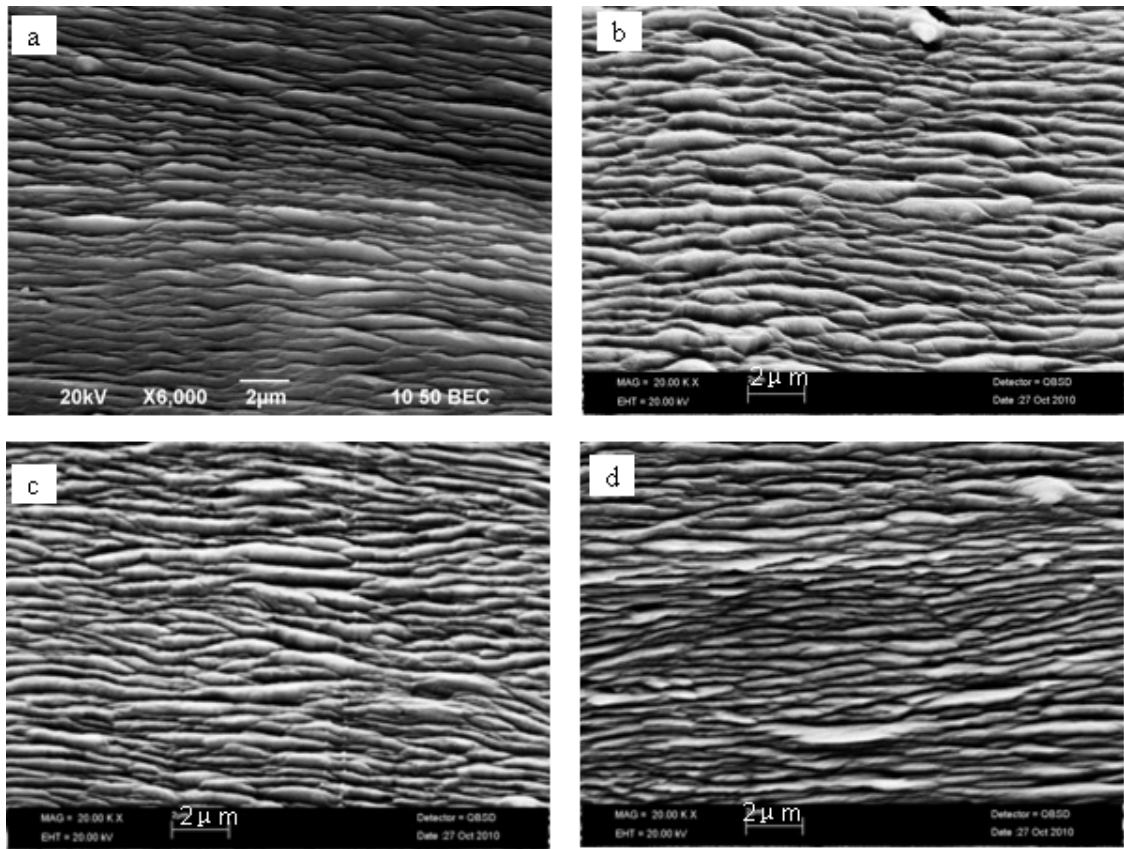


Fig. 5.18 SEM micrographs of free surface of chips in face turning experiment under (a) non-EPT (b) 120 Hz-EPT (c) 183 Hz-EPT (d) 252 Hz-EPT

Serrated chips with catastrophic shear bands are observed in the SEM micrograph of the side face of the chips produced in the straight cutting experiment, as shown in Fig. 5.19. The notation is adopted from the model proposed by Cotterell and Byrne (2008), where p_c is the distance between adjacent shear bands, and the catastrophic shear strain is expressed by $\varepsilon_c = p_{sb} / \delta_{sb}$, i.e. the ratio of shear band projection p_{sb} to shear band thickness δ_{sb} , as shown in Fig. 5.20.

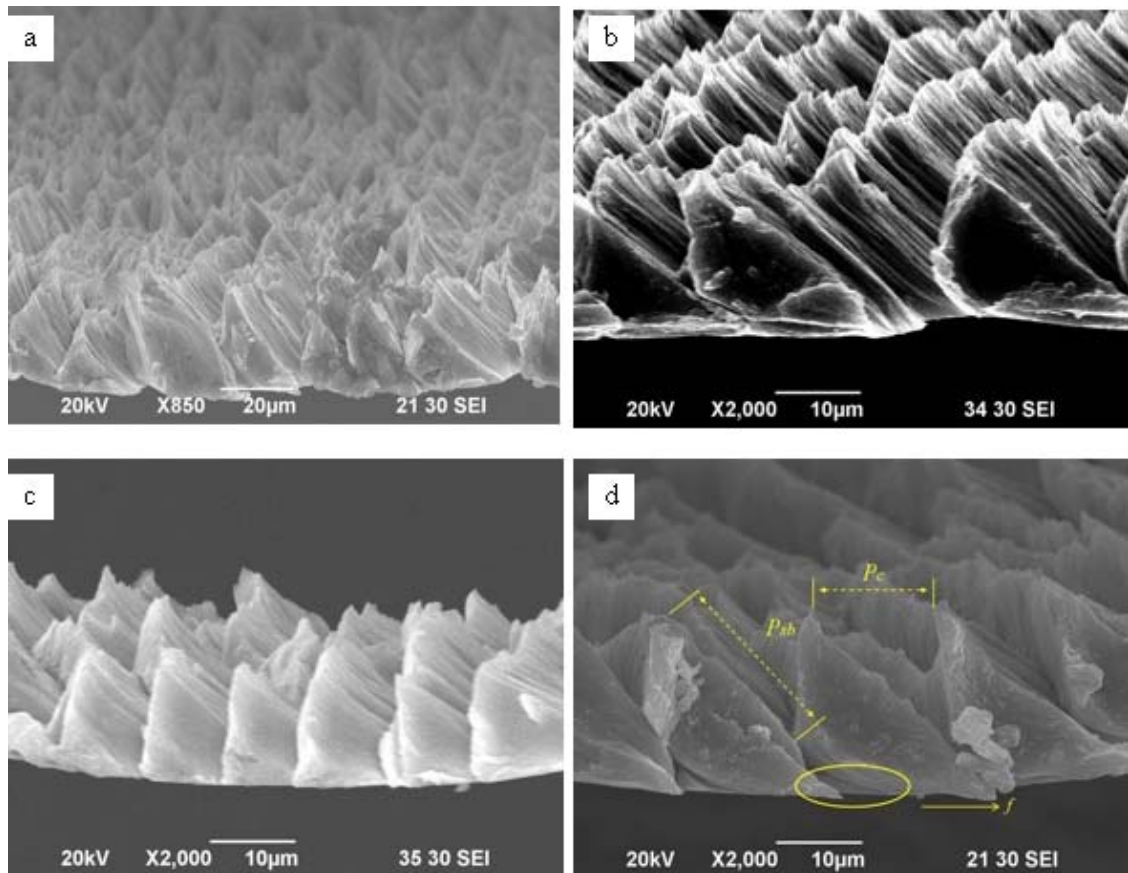
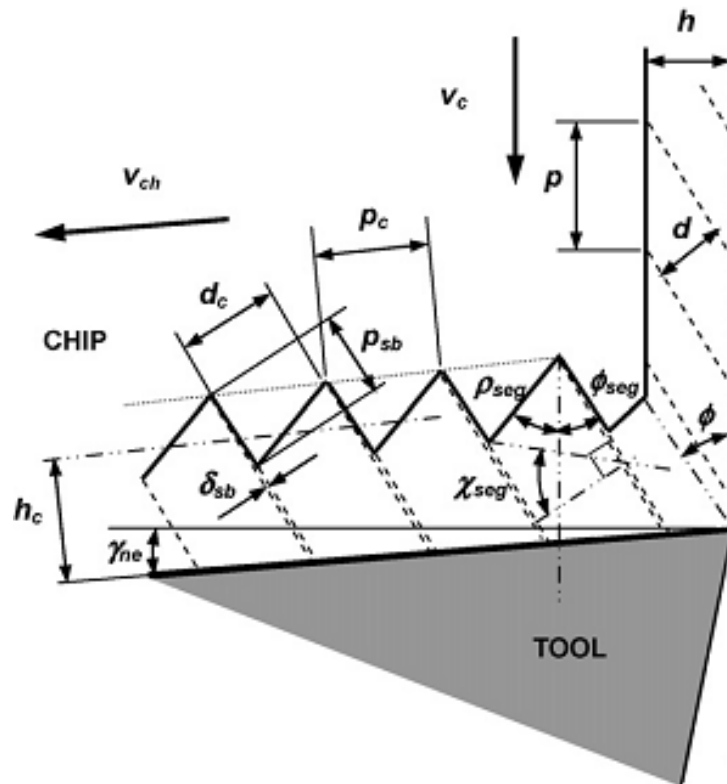


Fig. 5.19 SEM micrographs of side face of chips in the straight cutting experiments under (a) non-EPT (b) 120 Hz-EPT (c) 183 Hz-EPT (d) 252 Hz-EPT

The work material with pre-machining EPT treatment presents a better property of mechanical elongation, and is 82% longer than the as-received work material (Jiang et al., 2009). At the same time, the work-hardening of the EPT treated work material is less significant. Therefore, the seizing effect takes place on the tool-chip interface, leaving a stagnant region resulting from the frictional force, as indicated by the oval in Fig. 5.19. With a less work-hardening effect, unlike the cutting of steel, a build-up edge (BUE) on the cutting tool edge is not observable.

With a better elongation property, the stagnant region merely employs a relatively small volume of work material to (i) accommodate the large volume of elastic stress induced prior to the formation of the catastrophic shear band and (ii) deform and seize on the rake face of the cutting tool to provide the frictional force, which makes a very large shear band projection p_{sb} and total strain on the shear plane.



p_c : distance between adjacent shear bands, p_{sb} : shear band projection

δ_{sb} :shear band thickness, $\epsilon_c = p_{sb} / \delta_{sb}$: catastrophic shear strain

Fig. 5.20 Segmented chip geometry (after Cotterell and Byrne, 2008)

As shown in Fig. 5.21, the above procedure of stick-slip takes place in the secondary deformation zone. The frictional force can further be clearly examined in the

micrographs of tool-contact surface of chips in Fig. 5.22(b) and (c). From a physical point of view, the static friction coefficient between contact surfaces is larger than their kinetic friction coefficient. Therefore, the elastic strain builds up the larger static friction force in the location indicated by arrows in Fig. 5.22(b). Eventually the elastic strain induced force overcomes the static friction or the catastrophic shear bands takes place to reduce the stress capacity of the chip segment in contact with the tool rake face. Both phenomenon lead to an abrupt load drop on cutting tool where the “slip” occurs, as shown in the area between the arrows in Fig. 5.22(b). It can also be evidenced that the distance between adjacent static-friction marks (indicated by the arrows) is about 13 μm , which is consistent with the measured distance (as shown by p_c in Fig. 5.19(d)) between two neighboring shear bands in Fig. 5.19(b).

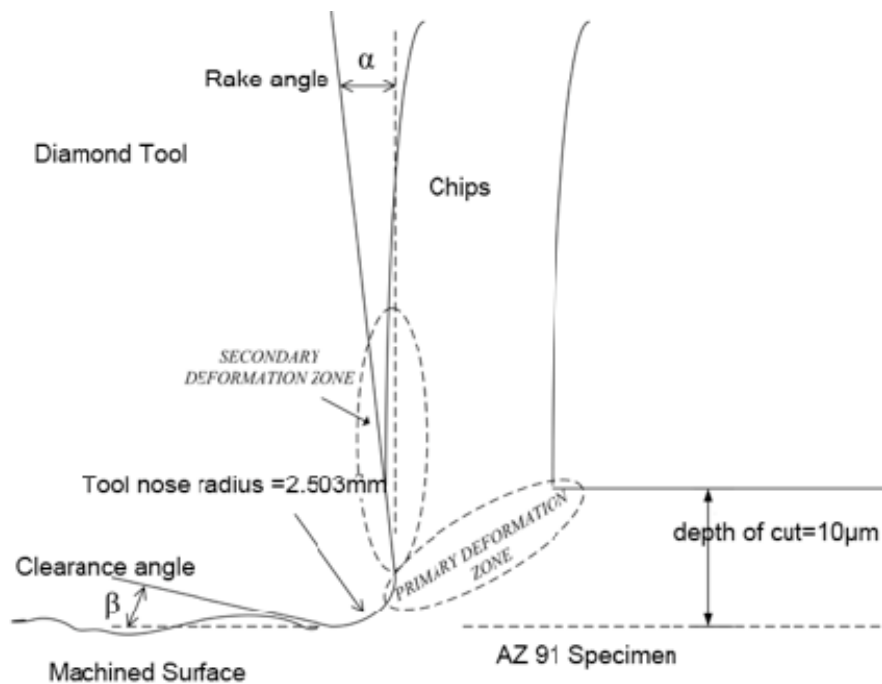


Fig. 5.21 Side view of chip morphology and principle of straight cutting

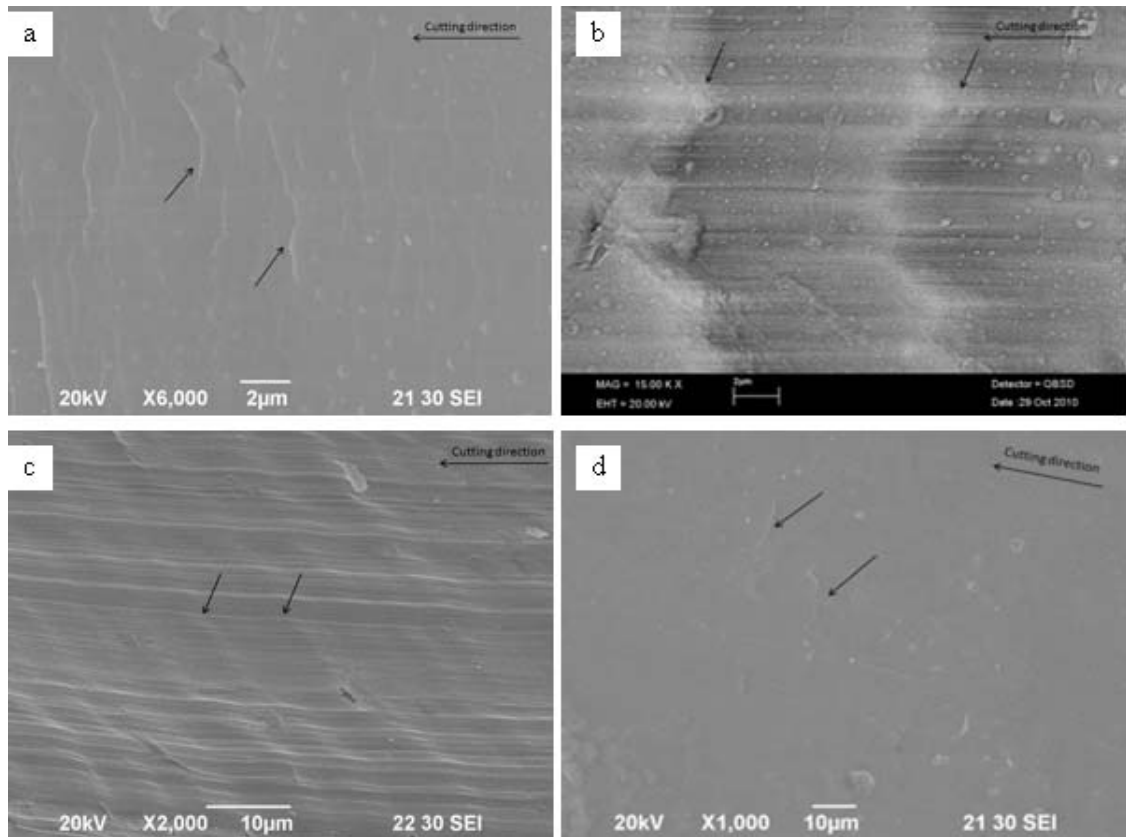


Fig. 5.22 SEM micrographs of tool-contact face of chips in straight cutting experiments under (a) non-EPT (b) 120 Hz-EPT (c) 183 Hz-EPT (d) 252 Hz-EPT

5.4 Summary

Face turning and straight cutting experiments have been conducted to study the machinability and microstructural changes with electropulsing treatment of AZ91. The work materials used in the experiments were treated with various EPT parameters. The effect of pre-machining EPT treatment on the micro-cutting process is identified by the measurement and study of surface roughness, cutting force, chip morphology and microstructural changes. The major findings in this chapter are summarized as below:

(1) With EPT treatment, the cutting force can be significantly reduced, and the surface roughness can be improved. Consistent results can also be correlated with the EPT induced microstructural change, as described in earlier chapters;

(2) On the other hand, segmented or serrated chip morphology is identified as one of the characteristics in the microcutting of as-tempered AZ91 alloy with static EPT. Differing in the serrated chips produced in the microcutting of most nonferrous materials, such as Al and Cu alloys, the shear band projection length is extremely high compared with the shear band thickness. This phenomenon can be attributed to the large elongation property of EPT treated material. In this regard, a relatively small volume of material deformation in the primary shear zone can accommodate the accumulated elastic stress in the chips; and

(3) The effect of super-plasticity in the treated specimen results in a seizing effect on the tool-chip interface, which results in a typical stick-slip phenomenon during chip-formation.

Chapter 6 Conclusions and Suggestions for Further Work

Work

6.1 Overall Conclusions

A study of the effect of electropulsing treatment (EPT) on the microstructural changes and machinability in single point diamond turning (SPDT) has been carried out on AZ91 alloy, focusing on the microstructural evolution, phase transformations and dislocation dynamics. The material characteristics are obtained using BSEM, XRD and TEM. The machining performance is evaluated by the surface roughness and the cutting force in SPDT. The chip morphology is also studied at the micro-scale of machining. Significant findings from this study include the followings:

(1) The microstructure of the as-tempered AZ91 specimen mainly consists of a primary α -Mg phase matrix and β phase particles ($\text{Mg}_{17}\text{Al}_{12}$). Under various frequencies of static EPT, two stages of phase transformations are found for β phase particles. From the non-EPT to 120 Hz-EPT and 183 Hz-EPT, amounts of β phase particles increase in a way of quenching. In the second stage, when the frequency further increases to 252 Hz-EPT, a decomposition of the β phase occurs in a way up-quenching. Moreover, judging from the TEM observations, the dislocations and atomic vacancies in the specimens are pushed towards the grain boundaries by the increasing EPT frequencies, while the dislocation arrays and nodes also decrease in the process. It

indicates that the accumulation and annihilation of dislocations occur at the grain boundaries, and achieve an adequate balance;

(2) For the cold-rolled specimens under various frequencies of static EPT, a way of up-quenching and quenching phase transformations are found for the β phase. From the non-EPT specimen to the 151 Hz-EPT specimen, decomposition of the β phase occurs, when the frequency of electropulsing further increases to 294 Hz, the precipitation of the β phase in a way of quenching is observed from both the SEM and TEM micrographs. By observing the optical micrographs of the specimens, it is also found that with increasing frequencies of static electropulsing, the amount of twins is decreased, with a relatively homogeneous microstructure of equi-axed grains obtained. The dislocations and nodes also decrease with increasing EPT frequency;

(3) For the dynamic EPT of rolling specimens, the decomposition of the β phase is observed, as the amounts of the β phase precipitates decrease with increasing EPT frequency. Under the conventional thermal process, it takes 20 hours of ageing in the range of 673-693 K to complete the decomposition process, while in EPT the phase transformation is accomplished in 10 seconds with a relatively low temperature 349-390 K. With examination of the TEM images, the aforementioned phase transformations are confirmed; meanwhile, the phenomena of dislocation movements and annihilation are found when the frequency of EPT increases. The twins immediately disappear as the electropulsing is applied, because the external stress resulting from the plastic deformation is reduced simultaneously in the dynamic electropulsing process, and a fine grain structure is developed with increasing EPT frequency;

(4) Different from conventional thermodynamics, in which the chemical Gibbs free energy is considered to be the dominant factor in determining the phase transformation, the total Gibbs free energy with EPT can be described as $\Delta G = \Delta G_{chem} + \Delta G_{surface} + \Delta G_{strain} + \Delta G_{orient} + \Delta G_{EPT}$. When $\Delta G < 0$, the EPT induced Gibbs free energy (ΔG_{EPT}) accelerates the decomposition of the supersaturated α phase and the precipitation of the β phase till the stable state when $\Delta G=0$; as ΔG_{EPT} continues to increase, resulting in the stable phases reverse-decomposed and the decomposition of the β phase. In all, the chemical Gibbs free energy and the EPT induced Gibbs free energy together accelerate the phase transformation process in a more efficient way than the conventional treatment;

(5) Under electropulsing, due to the transient stress caused by electron wind, dislocations move very quickly, even at ultrasonic speeds. The electron wind is formed by the knock-on collision of high-rate electrons with atomic nuclei. The transfer of energy from electrons to the atoms is also much more effective than that in the traditional thermal and thermo-mechanical processes. The sliding behavior of dislocations and phase transformations are significantly affected by electropulsing, and electron migration induced by electric current also plays an important role in the process. The effect of the atomic diffusion flux, on both the precipitation rate and on the motion of quench-in vacancies and dislocation to the grain boundaries and skins is important. Under electropulsing, the atomic flux consists of two main parts: the flux of diffusion atoms caused by the thermal effect, and the flux of diffusion atoms caused by the athermal effect. Both the thermal and athermal effect contribute to the acceleration of diffusional phase transformations and dislocation movements;

(6) Machinability of the electropulsing treated work materials is investigated in single point diamond turning process. Face turning and straight cutting experiments have been conducted with different cutting parameters, and the consequential microstructural changes and surface roughness of the machined surface, as well as cutting force variations are discussed. It is found that with pre-machining EPT treatment, the cutting force can be significantly reduced, the surface roughness is reduced, and the consistent results are also correlated with the EPT induced microstructural changes and dislocation annihilation; and

(7) Moreover, in studying the chip morphology, segmented or serrated chip morphology is identified as one of the characteristics in microcutting of AZ91 alloy with EPT treatment. Different from most nonferrous materials, including Al and Cu alloys, the electropulsing treated AZ91 alloy shows a high shear band projection length compared with the shear band thickness, which is attributed to the large elongation property of EPT treated materials; therefore a relatively small volume of material deformation in the primary shear zone can accommodate the accumulated elastic stress in chips. A seizing effect on the tool-chip interface is also found in a typical stick-slip phenomenon during chip formation, which is attributed to the effect of super-plasticity in the treated specimens.

All in all, EPT is more powerful and effective in accelerating the phase transformations and microstructural changes, which is thousands of times more efficient than the conventional thermal treatment. The incremental athermal effect during the process also provides sufficient energy for aggressive dislocation movements and annihilation. With increasing EPT frequency, the cutting force is

significantly reduced and surface roughness improved by SPDT, with the segmented or serrated chip morphology.

6.2 Suggestions for Further Work

The study confirms the importance of the EPT to the machinability improvements of Mg-Al alloy in ultra-precision single point diamond turning. The cutting force variations and surface roughness induced by EPT, and the microstructure and chips morphology changes also confirm the effect. However, in the design of the experiment for this study, only one material was selected, and the EPT and SPDT variables were controlled in a narrow range. Therefore, the following research topics are suggested for the further work:

(1) In the present study, when considering the EPT parameters, the frequency of EPT was changed while keeping other factors, including the current, voltage and duration time were kept fixed. Some existing research has reported that the variations of the current intensity and duration time would also induce significant microstructure and machinability changes in the materials, and the machinability under various EPT environments might also change. In the further study, therefore, the effect of other EPT parameters in mechanical properties and microstructural changes of work materials will be investigated;

(2) Cutting parameters in SPDT, including tool geometry, spindle speed, feed rate, depth of cut, material properties and relative vibration between the tool and the

workpiece all play an important role in determining the surface generation quality. These factors can be classified into two groups, which are the process factors and the materials factors. In this study, in order to obtain unbiased results of the machinability induced by EPT in SPDT, only the influence of materials factors on the surface generation is studied, while the process factors, such as spindle speed and feed rate, were kept unchanged. In the further study, the effect of various cutting parameters in SPDT should be investigated systematically, and an optimal cutting system could possibly be established for better surface generation;

(3) The AZ91 alloy was selected in this study due to its wide application in industry and the two-phase changes in the microstructure. Previous research on the effect of EPT in AZ31, AZ61, Zn-Al alloy, steel, and other metal materials has also provided other options for work materials, and the different phase transformations induced by EPT warrant further investigation. Besides, in SPDT, the material removal process and the surface generation are not only governed by the cutting tool, but also by the specific material properties. The study of the effect of material swelling, residual stress and crystallographic orientation for different workpiece materials will be conducted; and

(4) In the present study, due to the limitations of the machining equipment, the EPT and SPDT experiments were carried out independently. The specimens were firstly treated by electropulsing, and then machined by SPDT. On the basis of the results achieved, an integrated machining system, which incorporated with the EPT and SPDT, where the electropulsing can be applied to the specimen while the cutting is in progress, should provide a new investigation approach. Furthermore, the driving force of the

phase transformations in these circumstances should include the effect of EPT, the conventional thermal effect and the effect of ultra-precision diamond turning. The dislocation movements with the introduction of SPDT should also be different from the effect of EPT. The control experiments on the selection of both EPT parameters and SPDT parameters should provide an optimal solution, aiming at the best surface integrity of the final products.

References

- Albrecht P., “New development in the theory of the metal-cutting process Part II the theory of chip formation”, *Journal of Engineering for Industry*, Vol.83, pp.553-558 (1961).
- Albrecht P., “Dynamics of the Metal-cutting Process”, *Journal of Engineering for Industry*, Vol.87, pp.429-442 (1965).
- Benjamin R. J., “Diamond turning at a large optical manufacturer”, *Optical Engineering*, Vol.17, No.6, pp.574-577 (1978).
- Alia P., Andreone D., Turtelli R.S., Vinai F. and Rinontino G., “Structural relaxation and irreversible changes of electrical resistivity of Fe-Ni-Mo-B amorphous alloys”, *Journal of Applied Physics*, Vol.53(12), pp.8798-8804 (1982).
- Atasoy O.E. and Ozbilen S., “Pearlite spheroidization”, *Journal of Materials Science*, Vol.24, pp.281-287 (1989).
- Arcona C. and Dow Th.A., “An empirical tool force model for precision machining”, *Transactions of the ASME*, Vol. 120, Nov., pp.700-707 (1998)
- Asai S., Taguchi Y., Horio K. and Kasai T., “Measuring the very small cutting edge radius for a diamond tool using a new kind of SEM having two detectors”, *Annals of the CIRP*, Vol. 39, No. 1, pp.85-pp92 (1990).
- Asai S. and Kobayashi A., “Observations of chip producing behavior in ultra-precision diamond machining and study on mirror-like surface generating mechanism”, *Precision Engineering*, Vol.12, No.3, pp.137-143 (1990).
- Barghout J.Y., Lorimer G.W., Pilkington R. and Prangnell P.B., “The effects of second phase particles, dislocation density and grain boundaries on the electrical conductivity of aluminum alloys”, *Materials Science Forum*, Vol.217-222, pp.975-980 (1996).
- Barnak J.P., Sprecher A.F. and Conrad H., “Colony size reduction in eutectic Pb-Sn casting in electropulsing”, *Scripta Metallurgica et Materialia*, Vol.32(6), pp.879-884 (1995).
- Benjamin R. J., “Diamond turning at a large optical manufacturer”, *Optical Engineering*, Vol.17, No.6, pp.574-577 (1978).
- Bilyk S. R., Ramesh K. T. and Wright T. W., “Finite deformations of metal cylinders subjected to electromagnetic fields and mechanical forces”, *Journal of the Mechanics and Physics of Solids*, Vol.53, pp.525–544 (2005).
- Bishop J.F.W., Hill R., “A theory of plastic distortion of a polycrystalline aggregate

- under combined stresses”, *Philosophic Magazine*, Vol.42, pp.1298-1310 (1951).
- Black J.T., “Shear front-lamellar structures in large strain plastic deformation processes”, *Journal of Engineering for Industry*, No.2, pp.307-pp309 (1972).
- Black J.T., “On the fundamental mechanism of large strain plastic deformation”, *Journal of Engineering for Industry*, May, pp.507-512 (1971).
- Blackley W.S. and Scattergood R.O., “Ductile regime model for diamond turning of brittle materials”, *J. Prec. Eng.* 132. pp.95-102 (1991).
- Bryan J.B., “Design and construction of an ultra-precision 84 inch diamond turning machine”, *Precision Engineering*, Vol.1(1), pp.13-17 (1979).
- Cabibbo M. and Bardi F., “Eutectic microstructural evolution of a thixoformed AZ91 after solution heat treatment”, *Materials for Transportation Technology, Series: EUROMAT 99* (2000).
- Campbell J. and Conrad H., “Influence of electric current on the quench aging of a low carbon steel”, *Scripta Metallurgicaet Materialia*, Vol 31(1), pp.69-74 (1994).
- Cao W.D., Lu X.P., Sprecher A.F. and Conrad H., “Increased hardenability of steel by an external electric field”, *Materials Letters*, Vol.9(5.6), pp.193-197 (1990).
- Cao W.D., Sprecher A.F. and Conrad H., “Effect of strain rate on electroplastic effect in Nb”, *Scripta Metallurgica*, Vol.23, pp.151-155 (1989).
- Chattopadhyay S. and Sellars C.M., “Quantitative measurement of pearlite spheroidization”, *Metallography*, Vol.19, pp.89-105 (1997).
- Chattopadhyay S. and Sellars C.M., “Kinetics of peralite spheroidization during static annealing and during hot deformation”, *Acta Metallurgica*, Vol.30, pp.157-170 (1982).
- Cheung C.F., “Modelling and simulation of nano-surface generation in ultraprecision machining”, PhD. Thesis, The Hong Kong Polytechnic University, Hong Kong (2000).
- Cheung C.F., Chan K.C., To S. and Lee W.B., “Effect of reinforcement in ultra-precision machining of Al6061/SiC metal matrix composites”, *Scripta Materialia*, Vol. 47, pp.77-82 (2002a).
- Cheung C.F. and Lee W.B., “Prediction of the effect of tool interference on surface generation in single-point diamond turning”, *The International Journal of Advanced Manufacturing Technology*, Vol. 19, pp.245-252 (2002).
- Cheung C.F. and Lee W.B., “Study of factors affecting the surface quality in ultra-precision diamond turning”, *Materials and Manufacturing Processes*, Vol.15, No.4, pp.481-502 (2000).
- Cheung C.F. and Lee W.B., “Surface generation in ultra-precision diamond turning: modelling and practices”, *Professional Engineering Publishing*, (2003).

- Cheung C.F., To S. and Lee W.B., "Anisotropy of surface roughness in diamond turning of brittle single crystals", *Materials and Manufacturing Process*, Vol. 17, 2, pp.251-267 (2002b).
- Chiu W.M. and Lee W.B., "Development of ultra-precision machining technology, "5th International Conference on FACTORY", 2-4 April 1997, Conference Publication No. 435 0 IEE 1997, pp.486~490 (2000).
- Church E.L. and Takacs P.Z., "Survey of the finish characteristics of machined optical surfaces", *Optical Engineering*, Vol.24, No.3, pp.396-403 (1985).
- Chuzhoy L., Devor R.E. and Kapoor S.G., "Machining simulation of ductile iron and its constituents, part 2: numerical simulation and experimental validation of machining", *Journal of Manufacturing Science and Engineering*, Vol.125, May, pp.192-201 (2003a).
- Cotterell M. and Byrne G., "Dynamics of chip formation during straight cutting of titanium alloy Ti-6Al-4V", *CIRP Annals – Manufacturing Technology*, Vol.57, pp.93-96 (2008).
- Conrad H., Karam N. and Mannan S., "Effect of electric current pulses in the recrystallization of copper", *Scripta Metall.*, Vol.17(3), pp.411-423 (1983).
- Conrad H., Karam N. and Mannan S., "Effect of prior cold work on the influence of electric current pulses on the recrystallization of copper", *Scripta Metallurgica*, Vol.18, pp.275-280 (1984).
- Conrad H., Cao W.D., Lu S.P. and Sprecher A.F., "Effect of electric field on cavitation in superplastic aluminum alloy 7475", *Materials Science and Engineering A*, Vol.138, pp.247-258 (1991).
- Conrad H., Cao W.D., Lu S.P. and Sprecher A F., "Effect of electric field on superplasticity of 7475 Al", *Scripta Metallurgica*, Vol.23, pp.821-824 (1989).
- Conrad H., Guo Z. and Sprecher A.F., "Effect of an electric field on recovery and recrystallization of Al and Cu", *Scripta Metallurgica*, Vol.23, pp.697-702 (1989).
- Conrad H., "Effects of electric current on solid state phase transformations in metals", *Materials Science and Engineering A*, pp.227-273 (2000).
- Conrad H., Sprecher A.F., Cao W.D. and Lu X.P., "Electroplasticity: the effect of electricity on the mechanical properties of metal", *Journal Of Materials Science*, Vol. 9, pp.132-149 (1990).
- Cramer A., Eckert S. and Galindo V., "Liquid metal model experiments on casting and solidification processes", *Journal of Materials Science*, 39, No. 24, pp.7285-7290 (2004).
- Cullity B.D. and Stock S.R., "Elements of X-ray diffraction", 3rd Ed., Prentice Hall (2001).

- DeVries W.R., "Autogressive Time Series Models for Surface Profile Charactrization", *Annals of CIRP*, Vol. 30, No.1, pp.481-492 (1979).
- Dexter D.L., "Scattering of electrons in metals by dislocation", *Phys. Rev.*, Vol.86(5), pp.770-774 (1952).
- Ding F., Tang G., Xu Z. and Tian S., "A New Method for Improving Strength and Plasticity of Steel Wire", *Journal of Materials Sciences and Technology*, Vol. 23(02), pp.273-276 (2007).
- Di Y. and Conrad H., "Influence of an electric field in the plastic deformation of polycrystalline NaCl at elevated temperature". *Acta Materialia*. Vol.46(6) pp.1963-1968 (1998).
- Donaldson R.R. and Patterson S.R., "Design and construction of a large vertical axis diamond turning machine", *Proc. SPIE*, pp.433-442 (1983).
- Dong K.J., Liu R.S. and Zheng C.X., "Simulation study on formation characteristics of nano-clusters during rapid solidification process of liquid metal Al", *Journal of Rare Metal Materials and Engineering*.(in Chinese), 32,No.11. pp.893-901 (2003).
- Du X.N., Yin S.M. and Liu S.C., "Effect of the electropulsing on mechanical properties and microstructure of an ECAPed AZ31 Mg alloy," *Journal of Material Research*, Vol. 23(6), pp.1570-1577 (2008).
- Drescher J.D. and Dow T.A., "Tool force model development for diamond turning", *Precision Engineering*, Vol.12, No.1, pp.29-41 (1990).
- Drescher J.D., "Tool force, tool edge, and surface finish relationships in diamond turning", PhD Dissertation, North Carolina State University (1992).
- Engler O., Sacot E. and Ehrstrom J.C., "Recrystallisation and texture in hot deformation aluminium alloy 7010 thick plates", *Materials Science and Technology*, Vol.12, Sep., pp.717-729 (1996).
- Ernst H. and Merchant M.E., "Chip formation, friction, and high quality machined surfaces", *Surface Treatment of Metals*, ASM, pp.299-302 (1941).
- Evans C., "Precision Engineering: A Evolutionary view", Cranfield Press (1989).
- Evans C., "Cryogenic diamond turning of stainless steel", *Annals of CIRP*, Vol.40, pp.571-582 (1991).
- Furukawa Y. and Moronuki N., "Effect of material properties on ultra-precise cutting processes", *Annals of the CIRP*, Vol.37, No. 1, pp.113-116 (1988).
- Finnie I., "Review of metal cutting analyses of the past hundred years", *Mechanical Engineering*, Vol.78, pp.715-724 (1956).
- Goldman P. D., Motowidlo L. R. and Galligan J. M., "The absence of an electroplastic effect in lead at 4.2K", *Scripta Metallurgica*, Vol. 15, pp. 353–356 (1981).

- Grabec I., "Chaos Generated by the Cutting Process", *Physics Letters A*, Vol.117, pp.384-386 (1986).
- Inamura T., Suzuki H. and Takezawa N., "Cutting experiments in a computer using atomic models of a copper crystal and diamond tool", *Japan Soc. Precision Engineering*, 56m, pp.148-1488 (1990).
- Iida T. and Guthrie R.I., "The physical properties of liquid metals", Clarendon Press, Oxford, (1993).
- Ikawa N., Donaldson R. R., "Ultraprecision metal cutting—the past, the present and the future", *CIRP Annals - Manufacturing Technology*, Vol.40, Is.12, pp.587-594 (1990).
- Ikawa N., Shimada S., Tanaka H. and Ohmori G., "An atomistic analysis of nanometric chip removal as affected by tool-work interaction in diamond turning", *Annals of the CIRP*, Vol. 40, No.1, pp.551-554 (1991b).
- Ikawa N., Shimada S. and Tanaka H., "Minimum thickness of cut in micromachining", *Nanotechnology*, 3, pp.6-9 (1992).
- Ikawa N., Shimada S. and Morooka H., "Technology of diamond tool for ultraprecision Metal Cutting", *Bull. of Japan Soc. Of Prec. Eng*, Vol.21, pp.233-251 (1987).
- Ismail F., Elbestawi M.A., Du R. and Urbasik K., "Generation of milled surfaces including tool dynamic and wear", *Journal of Engineering for Industry*, Vol.115, pp.245-261 (1993).
- Jiang Y.B., Tang G.Y., Shek C.H. and Zhu Y.H., "On the thermodynamics and kinetics of electropulsing induced dissolution of β -Mg₁₇Al₁₂ phase in an aged Mg-9Al-1Zn alloy", *Acta Materialia*, Vol. 57(16), pp 4797-4808 (2009).
- Kelton K.F. and Spaepen F., "Kinetics of structural relaxation in several metallic glasses observed by changes in electrical resistivity", *Physical Review B*, Vol.30(10), pp.5516-5524 (1984).
- Kim J. D. and Kim D. S., "Theoretical Analysis of Micro-machining Characteristics in Ultra-precision Machining", *Journal of Materials Processing Technology*, Vol.49, pp. 387-398 (1995).
- Kim W.J., Park J.D. and Kim W.Y., "Effect of differential speed rolling on microstructure and mechanical properties of an AZ91 magnesium alloy", *Journal of Alloys and Compounds*, Vol.460, Iss.1-2, 28 July, pp. 289-293 (2008).
- Kiryanchev N.E. and Troitskii O.A., "Electroplastic drawing of trip steel", *Elektronnaya Obrabotka Materialov*, Issue 2, pp. 54-58 (1985).
- Kong M.C., Lee W.B., Cheung C.F. and To S., "A study of materials swelling and recovery in single-point diamond turning of ductile materials", *Journal of Materials Processing Technology*, pp.210 -215 (2006).

- Komanduri R., Chandrasekaran N. and Raff L.M., "Effect of tool geometry in nanometric cutting: a molecular dynamics simulation approach", *Wear*, Vol. 219(1), 4 August, pp.84-97 (1998).
- Languillaume J., Kapelski G. and Baudalet B., "Cementite dissolution in heavily cold drawn pearlitic steel wires", *Acta Materialia*, Vol.45(3), pp.1201-1212 (1997).
- Lasota A. and Rusek P., "Influence of random vibrations on the roughness of turned surfaces", *Journal of Mechanical Working Technology*, Vol.7, pp.277-284 (1983).
- Lawn B.R. and Evans A.G., "A model for crack Initiation in elastic/plastic indentation fields", *Journal of Material Science*, Vol. 12, pp.2195-2201 (1977).
- Lee E.H. and Shaffer B.W., "Theory of plasticity applied to a problem of machining", *Journal of Applied Mechanics*, Vol.18, pp.405-412 (1951).
- Lee S.J. and Lee Y.K., "Quantitative analyses of ferrite lattice parameter and solute Nb content in low carbon micro alloyed steels", *Scripta Materialia*, Vol.52, pp.973-976 (2005).
- Leo Prakash D.G. and Doris R., "Quantitative characterization of Mg₁₇Al₁₂ phase and grain size in HPDC AZ91 magnesium alloy", *Journal of Alloys and Compounds*, Vol. 461, pp.139-146 (2008).
- Lee W.B., "Prediction of microcutting force variation in ultra-precision machining", *Precision Engineering*, Vol. 12, No. 1, pp.25-28 (1990).
- Lee W.B. and Chan K.C., "Symmetry requirement in shear angle band formation", *Scripta Metallurgica and Materialia*, Vol. 25, pp.997-1012 (1990).
- Lee W.B. and Chan K.C., "A Criterion for the prediction of shear band angles in F.C.C. metals", *Acta Metall. Mater.*, Vol.39, No.3, pp.411-417 (1991).
- Lee W.B., "Design of meso-structures in material processing", *Journal of Materials Processing Technology*, Vol.48, pp.721-726 (1995).
- Lee W.B. and Cai M.J., "The development of a computer software system for the prediction for formability parameters of sheet metal from X-ray diffraction data", *Journal of Material Processing Technology*, Vol. 48, No. 1-4, pp.43-56 (1995).
- Lee W.B. and Cheung C.F., "Materials induced vibration in ultra-precision machining", *Journal of Materials Processing Technology*, Vol. 89-90, pp.318-325 (1999).
- Lee W.B., To S. and Cheung C.F., "Effects of crystallographic orientation in diamond turning of copper single crystal", *Scripta Materialia*, Vol. 42, No. 10, pp.77-87 (2000).
- Lee W.B., Cheung C.F., Chiu W.M. and Leung T.P., "An Investigation of residual form error compensation in the ultra-precision machining of aspheric surfaces", *Journal of Materials Processing Technology*, Vol.99, No.1-3, pp.129-142 (2000).
- Lee W.B. and Cheung C.F., "A dynamic surface topography model for the prediction

- of nano-surface generation in ultra-precision machining”, *International Journal of Mechanical Science*, Vol. 43, pp.961-991 (2001).
- Lee W.B., Cheung C.F. and Li J.G., “Applications of virtual manufacturing in materials processing”, *Journal of Materials Processing Technology*, Vol.113, No.1-3, pp.416-432 (2001).
- Lee W.B., Li J.G. and Cheung C.F., “Development of a virtual training workshop in ultra-precision machining”, *International Journal of Engineering Education*, Vol.18, No.5, pp.123-126 (2002).
- Li S. and Conrad H., “Electric field strengthening during superplastic creep of Zn-5wt% Al: a negative electroplastic effect”, *Scripta Materialia*, Vol.39(7), pp.847– 851 (1998).
- Liu W., Tang G.Y., “Effect of a magnetic field on phase transformation of steel”, *Journal of Materials Research* 16 (8), pp.2280-2282 (2001).
- Li Q.C., Li R.X., Chang G.W. and Zhai Q.J., “Research of microstructure of 97 spherical graphite iron by electropulsing annealing”, *Journal of Materials Sciences and Technology*, Vol.209(4), pp.2015-2020 (2009).
- Livesey S.J., Duan X., Priestner R. and Collins J., “An electroplastic effect in 3J4J silicon steel”, *ScriptaMaterialia*, Vol.44, pp. 803-809 (2001).
- Lv Z.Q., Jiang P., Wang Z.H., Zhang W.H., Sun S.H. and Fu W.T., “XRD analyses on dissolution behavior of cementite in eutectoid pearlitic steel during cold rolling”, *Materials Letters*, Vol.62, pp.2825-2827 (2008).
- Mandelbrot B.B., “*The Fractal Geometry of Nature*”, New York: Freeman (1977).
- Mallock A. “The action of cutting tools”, *Proceedings of the Royal Society of London*, Vol.33, pp.127-142 (1881).
- McKeown P.A., “From precision to micro and nano-technologies”, *Nanotechnology, UNIDO Emerging Technology Series*, pp.1-6 (1997).
- Mizumoto H., Matsubara T., Yamamoto H., Okuno K. and Yabuya M., “An Infinite-stiffness aerostatic bearing with an exhaust-control restrictor,” *Proc. 6th Int. Precision Engng. Smeniar, Braunschweig, Germany*, pp.315-342 (1991).
- Mohanty A.N. and Bhagat O.N., “Electrical resistivity and phase transformations in steel”, *Materialwissenschaft und Werkstofftechnik*, Vol. 34(1), pp.96-101 (2003).
- Moiseenko M.M. and Troitskii O.A., “Electroplastic deformation of lead cadmium and zinc crystals”, *Russian Metallurgy (Metally)*, Issue 1, pp. 159-161 (1987).
- Molotskii M. and Fleurov V., “Magnetic effects in electroplasticity of metals”, *Phys. Rev. B* Vol.52 (22), pp.35-46 (1995).
- Moronuki N., Liang Y. and Furukawa Y., “Experiments on the effect of material

- properties on microcutting processes”, *Precision Engineering*, Vol. 16 No.2, pp.124-131 (1994).
- Moriwaki T., Horiuchi A. and Okuda K., “Effect of cutting heat on machining accuracy in ultra-precision diamond turning”, *Annals of the CIRP*, Vol. 39(1), pp.81-84 (1990).
- Mulvaney D.J. and Newland D.E., “A Characterization of Surface Texture Profiles”, *Proc. ImechE*, Vol.200, pp.167-173 (1986).
- Nahm S.H., Kim Y.I., Yu K.M. and Kim A., “Evaluation of fracture toughness of degraded Cr-Mo-V steel using electrical resistivity”, *Journal of Materials Science*, Vol. 37, pp. 3549-3553 (2002).
- Nakao Y., Dornfeld D.A. “Diamond turning using position and AE dual feedback control system”, *Precision Engineering* 27, pp.117-124 (2003).
- Nakasuji T. and Kodera S., “Diamond Turning of Brittle Materials for Optical Components”, *Annals of the CIRP*, Vol.39, No.1 pp.89-112 (1990).
- Nakayama K. and Arai M. “On the storage of data on metal cutting forces”, *Annals of CIRP*, Vol. 25, pp.13-21 (1976)
- Nikolay A. Belov and Dmitry G., “Multicomponent phase diagrams: applications for commercial aluminum alloys”, Published by Elsevier, pp.134-142 (2005).
- Okuda K., Tanaka T. and Nunobiki M., “107 Study on surface integrity of magnesium alloys in ultra-precision diamond cutting”, *International conference on Leading Edge Manufacturing in 21st Century*, pp.33-38 (2003).
- Oxley PLB., “Mechanics of machining: an analytical approach to assessing machinability”, Chichester: Ellis Horwood Limited., pp.31-47 (1989).
- Ovchinnikov I.V., “Electroplasticity effect and the determination of ultimate plastic strain”, (Russian, English) *Mosc. Univ. Mech. Bull.* 47, No.2, pp.8-12 (1992); translation from *Vestn. Mosk. Univ.*, Ser. I 1992, No.2, pp.47-52 (1992).
- Ostafiev V., Ostafiev D., and Mukhmudov K., “Distribution of cutting tool contact loads along rake and flank surfaces”, *Annals of the CIRP*, Vol. 43, No.1, pp.55-62 (1994).
- Page D., “Wyko NT8000 setup and operation guide”, Veeco Instruments, Inc. (2003).
- Paul Ed., Evans C.J., Mangamelli A., McGlauflin M.L. and Polvani R. S., “Chemical aspects of tool wear in single point diamond turning”, *Precision Engineering*, Vol. 18(1), Jan., pp. 4-19 (1996).
- Park J.S. and Lee Y.K., “Determination of Nb (C,N) dissolution temperature by 98 electrical resistivity measurement in a low-carbon micro-alloyed steel”, *Scripta Materialia*, Vol. 56, pp. 225-228 (2007)
- Qi J.G. and Wang J.Z., “Casting structure of pure aluminium by electric pulse

- modification at different superheated temperatures”, *Journal of University of Science and Technology Beijing*, Vol.12, NO. 6, December, pp.527-612 (2005).
- Qin R. and Su S., “Thermodynamics of crack healing under electropulsing”, *Journal of Material Research*, Vol.17(8), pp.2048-2052 (2002).
- Qin R., Su S.X., Guo J.D., He G.H. and Zhou B.L., “Suspension effect of nanocrystalline grain growth under electropulsing”, *Nanostructured Materials*, Vol.10(1), pp.71-76 (1998).
- Qin R.S. and Zhou B.L., “Effect of electric current pulses on grain size in casting”, *International Journal of Non-equilibrium Processing*, Vol.11, pp.77-86 (1998).
- Raghavan V., “Al-Mg-Mn (Aluminum-Magnesium-Manganese)”, *Journal of Phase Equilibria and Diffusion*, Vol.28, No.2, Phase Diagram Evaluations:Section II (2007).
- Saito T., “Machining of optics: an introduction”, *Applied Optics*, Vol.14, No.8, pp.1773-1776 (1978).
- Sata T., “Surface finish in metal cutting”, *Annals of the CIRP*, Vol. 12, pp.190-213 (1964).
- Sata T. and Kubo M., “On forming of surface roughness in finishing processing”, *Bulletin of the JSPE*, Vol.1, No.4, pp.287-293 (1966).
- Sata T., Li M., Takata S., Hiraoka H., Li C. Q., Xing X. Z. and Xiao X. G., “Analysis of surface roughness generation in turning operation and its applications”, *Annals of the CIRP*, Vol.34, No.1, pp.473-482 (1985).
- Sato H. and O-hori M., “Characteristics of two dimensional surface roughness – Taking Self-excited Chatter Marks as Objective”, *Annals of CIRP*, Vol.30, No.1, pp.481-493 (1981).
- Sato M., Kato Y. and Tuchiya K., “Effect of material anisotropy upon the cutting mechanism”, *Trans. JIM.*, Vol.9, pp.530-536 (1978).
- Shaw M.C., “Metal cutting principles (3rd edition)”, MIT Press, Cambridge, MA (1954).
- Shaw M.C., “Historical aspects concerning removal operations on metals”, *Metal Transformations*, Gordon and Breach, N.Y., pp.211-232 (1968).
- Sprecher A.F., Mannan S.L. and Conrad H., “On the mechanisms for the electroplastic effect in metals”, *Acta Metal.* Vol. 34(7), pp.1145-1152 (1986).
- Sprecher A.F., Mannan S.L. and Conrad H., “On the temperature rise associated with the electroplastic effect in titanium”, *Scripta Metall*, Vol.17(6), pp.769-772 (1983).
- Suo Z., “Dislocation climb in the electron wind”, *Material Research Society Symposium Proceedings*, Vol.338, pp.379-390 (1994).

- Sugano T. and Takeuchi K., "Diamond turning of an aluminum alloy for mirror", *Annals of the CIRP*, Vol.36, No.1, pp.17-32 (1987).
- Tang G.Y. and Zhang J., "Electro-plastic effect and its engineering application", *Iron and steel*, Vol. 133 No.19 Sep., pp.89-112 (1998).
- Tang G.Y. and Zhang J., "The engineering application of the electroplastic effect in the cold-drawing of stainless steel wire", *Journal of Materials Processing Technology* 137, pp.96-99 (2003).
- Tang G.Y. and Zhang J., "Experimental study of electroplastic effect on stainless steel wire 304L", *Materials Science and Engineering A* 281, pp.263-267 (2000).
- Tang G.Y. and Zhang J., "Electroplastic effect of the stainless steel wire during different drawing velocities". The 3rd International Symposium on Electromagnetic Processing of Materials, Nagoya, Japan, ISIJ pp.590-595 (2000).
- Tang G.Y. and Zhang J., "Effect of a pulsed magnetic treatment on the dislocation substructure of commercial high strength steel". The 3rd International Symposium on Electromagnetic Processing of Materials, Nagoya, Japan, ISIJP. pp.606-611 (2000).
- Tang G.Y. and Zhang M.X., "The application of electroplastic technique in cold-drawing steel wires", *Journal of Master Process. Technol.* 84, pp.268-270 (1998).
- Tang G.Y., Wang J.Z., and Cang D.Q., "Effect of pulse electric discharging on solidification structure of high carbon steel", *Journal of Iron and Steel Research.*(in Chinese), Vol.11,No.4 pp.44-62 (1999).
- Taniguchi N., "Current status in, and future trends of, ultraprecision machining and ultrafine materials processing", *Annals of CIRP*, Vol. 32, 2, pp.573-603 (1983).
- To S., Cheung C.F. and Lee W.B., "Influence of material swelling upon surface roughness in diamond turning of single crystals", *Materials Science and Technology*, Vol.17, No. 1, pp.102-108 (2001).
- To S. and Lee W.B., "Deformation behavior of aluminum single crystals in ultra-precision diamond turning", *Journal of Materials Processing Technology*, Vol.113, pp.296-300 (2001).
- To S., Zhu Y.H., and Lee W.B., "Ultra-precision machining induced phase decomposition at surface of Zn-Al based alloy", *Applied Surface Science*, Vol.253, pp.132-142 (2006).
- To S, Lee W.B. and Chan C.Y., "Ultraprecision diamond turning of aluminum single crystals", *Journal of Materials Processing Technology*, Vol.63, pp.157-163 (1997).
- To S. Lee W.B. and Zhu Y.H., "Ultra-precision machining induced surface structural changes of Zn-Al alloy", *Materials Science and Engineering A*, Vol.325, pp.497-502 (2002).

- To S., "Effect of crystallographic orientation on material behavior in ultraprecision diamond turning of single crystals", PhD. Thesis, The Hong Kong Polytechnic University (2000).
- Troitskii O.A., "Electron plastic effect in metals", *Problemy Prochnosti*, Issue 2, pp. 176-182 (1984).
- Troitskii O.A. "Problem of the effect of electrical pulses on the process of drawing thin metal wires", *Russian Metallurgy (Metally)*, Issue 2, pp.192-195 (1984).
- Troitskii O.A. and Moiseenko M.M., "Action of series of electric pulses on deformation of zinc crystals", *Russian Metallurgy (Metally)*, Issue 6, pp.148-151(1985).
- Troitskii O.A., Savenko V.S., "Multistage electroplastic drawing of copper wire", Issue 5, pp.96-98 (1986).
- Timsit R. S., "Remarks on recent experimental observations of the electroplastic effect", *Scripta Metallurgica*, Vol.15, pp.461-464, (1981).
- Ueda K. and Iwata K., "Chip formation mechanism in single crystal cutting of brass", *Annals of CIRP*, Vol.29(1), pp.41-62 (1980).
- Ueda K. and Manabe K., "Chip formation mechanism in microcutting of an amorphous metal", *Annals of the CIRP*, Vol.41, No.1, pp.129-132 (1992).
- Ueda N., Matsuo T. and Hoshi T., "An Investigation of some shear angle theories", *Annals of the CIRP*, Vol.35, No.1, pp.27-30 (1986).
- Villars P., Prince A. and Okamoto H., "Handbook of ternary alloys phase diagram", *ASM int'l*, Vol. 3, pp.3891-3895, 3907-3910, 3938-3948, 3974 (1995).
- Wang H., To S. and Chan C.Y., "A theoretical and experimental investigation of the tool-tip vibration and its influence upon surface generation in single point diamond turning", *International Journal of Machine Tools & Manufacture*, Vol. 50, pp.241-252 (2010).
- Wang H., To S. and Chan C.Y., "Elastic strain induced shear bands in the microcutting process", *International Journal of Machine Tools & Manufacture*, Vol.50, Issue 1, pp.9-18 (2010).
- Wang H., To S. and Chan C.Y., "A study of regularly spaced shear bands and morphology of serrated chip formation in microcutting process", *Scripta Materialia*, Vol.63, pp.227-230 (2010).
- Wang J.S., Xue Q.G. and Wang J.Z., "Effect of EPM process on accelerated graphitization in solidification process of molten cast iron", *Foundry (in Chinese)* 50, No.11, pp.677-682 (2001).
- Wang J.Z., "Research of treating technology with electro-pulse modification and the Hypothesis of Liquid Metal Cluster Structure" (Dissertation in Chinese), University of

- Science and Technology Beijing, pp.54-68 (1998).
- Wang J.Z., Tang Y. and Cang D.Q., “Electro-pulse on improving steel ingot solidification structure”, *Journal of University of Science and Technology*. Beijing. Vol.6, No.2, pp.94-103 (1999).
- Wang X.L. and Guo J.D., “Segregation of lead in Cu-Zn alloy under electric current pulses”, *Applied Physics Letters*, Vol.89, pp.132-148 (2006).
- Watkins R., Ravi-Chandar K. and Satapathy S., “The mechanical behavior of conductors exposed to short-duration thermal loading”, *IEEE Trans. on Magn.*, Vol.41, pp.256–261 (2005).
- Wei-di C., Sprecher A.F. and Conrad H., “Effect of strain rate on the electroplastic effect in Nb”, *Scripta Metall.*, Vol.23(1), pp.151-155 (1989).
- Whitehouse D.J., “Handbook of surface metrology, Bristol, Philadelphia”, *Institute of Physics Pub* (1994).
- Whitehouse D. J., “Surface and their measurement”, *Hermes Penton Ltd: London* (2002).
- Wilks J., “Performance of diamonds as cutting tools for precision machining”, *Precision Engineering*, Vol. 2, No. 2, pp.57-71 (1980).
- Williams J.A. and Gare N., “Some observations on the flow stress of metals during metal cutting”, *Wear*, Vol.42, pp.341-352 (1977).
- Xiao S.H., Guo J.D. and Li S.X., “The effect of electropulsing on dislocation structures in [233] coplanar double-slip-oriented fatigued copper single crystals”, *Philosophical Magazine Letters*, Vol. 82(11), pp. 617-622 (2002).
- Xiao S.H. and Guo J.D., “Recrystallization in fatigued copper single crystals under electropulsing”, *ScriptaMaterialia* Vol. 46, pp.1-6 (2002).
- Xie J.Q., Bayoumi A.E. and Zbib H.M. “FEA modelling and simulation of shear localized chip formation in metal cutting”, *International Journal of Machine Tools and Manufacture*, Vol.38, pp.1067-1072 (1998).
- Yang D. and Conrad H., “Exploratory study into the effects of an electric field and of high current density electropulsing on the plastic deformation of TiAl, 100Intermetallics”, Vol. 9, pp.943-947 (2001).
- Yang W. and Lee W.B., “Mesoplasticity and its applications”, *Springer Verlag* (1993).
- Yao K.F., Wang J., Zheng M., Yu P. and Zhang H., “A research in electroplastic effects in wire drawing process of an austenitic stainless steel”, *ScriptaMaterialia*, Vol.45, pp. 533-539 (2001).
- Yao K.F., Yu P., Wang J., Fang W. and Zheng M.X., “Effect of high density current

pulses on work hardening behaviours of austenitic stainless steel in wire drawing deformation”, *Acta Metallurgica Sinica*, Vol.14(5), pp.341-346 (2001).

Yu K.M., Nahm S.H. and Kim Y.I., “Toughness degradation evaluation of 1Cr–1Mo–0.25V steel by electrical resistivity”, *Journal of Materials Science Letters*, Vol.18, pp.1175-1176 (1999).

Yuan Z. J., Zhou M., and Dong S., “Effect of diamond tool sharpness on minimum cutting thickness and cutting surface integrity in ultraprecision machining”, *Journal of Materials Processing Technology*, Vol.62, pp.327-330 (1996).

Zelin M., “Microstructure evolution in pearlitic steels during wire drawing”, *Acta Materialia*, Vol.50, pp.4431-4447 (2002).

Zhang J. and Tang G.Y., “Effect of current pulses on the drawing stress and properties of Cr₁₇Ni₆Mn₃ and 4J42 alloys in the cold-drawing process”, *Journal of Materials Processing Technology* 120, pp.13-16 (2002).

Zhang J.H., “Theory and technique of precision cutting”, Pergamon Press, 1 (1986).

Zhang W., Zhou Y.Z., Sui M.L., He G.H., Guo J.D. and Li D.X., “Formation of nanoscale α -Al in a superdralumin under high current density electropulsing”, *Journal of Material Science Letters*, Vol. 21, pp.1923-1925 (2002).

Zhang W., Sui M.L., Hu K.Y., Li D.X., Guo X.N., He G.H. and Zhou B.L., “Formation of nanophases in a Cu–Zn alloy under high current density electropulsing”, *Journal of Material Research*, Vol.15(10), pp.65-68 (2000).

Zhao M.C. and Liu M., “Influence of the β phase Morphology on the Corrosion of the Mg Alloy AZ91”, *Corrosion Science*, Vol.50, Issue 7, July 2008, pp.1939-1953 (2008).

Zhou M. and Clifton R. J., “Dynamic ductile rupture under conditions of plane strain”, *International Journal of Impact Engineering*, Vol.19, pp.189–206 (1997).

Zhou Y., Qiao D., He G. and Guo J., “Improvement of mechanical properties in a saw blade by electropulsing treatment”, *Material Letters*, Vol.57, pp.1566– 1570 (2003).

Zhou Y., Guo J., Gao M. and He G., “Crack healing in a steel by using electropulsing technique”, *Material Letters*, Vol.58, pp.1732– 1736 (2004).

Zhou Y., Zeng Y., He G. and Zhou B., “The healing of quenched crack in 1045 steel under electropulsing”, *Journal of Material Research*, Vol.16(1), pp.17-19 (2001).

Zhou Y., Zhang W., Sui M., Li D., He G. and Guo J., “Formation of a nanostructure in a low-carbon steel under high current density electropulsing”, *Journal of Material Research*, Vol.17(5), pp.921-924 (2002).

Zhou Y., Zhang W., Wang B., He G. and Guo J., “Ultrafine-grained microstructure in a Cu–Zn alloy produced by electropulsing treatment”, *Journal of Material Research*, Vol.18(8), pp.1991-1997(2003).

[Http://machine-tools.netfirms.com](http://machine-tools.netfirms.com)

[Http://www.sterlingint.com](http://www.sterlingint.com)

[Http://Zeus.plmsc.pus.edu](http://Zeus.plmsc.pus.edu)

Appendix I. List of Abbreviations

Advanced Manufacturing Optical Center (AMOC)

Amplitude Probability Density Function (APDF)

Autocorrelation Function (ACF)

Built-Up-Edge (BUE)

Coefficient of Anisotropy (COA)

Degree of Roughness Anisotropy (DRA)

Electropulsing Treatment (EPT)

Finite Element Analysis (FEA)

Magnesium-9Aluminum-1Zn alloy (AZ91)

Precision Ion Polishing System (PIPS)

Phase-Shifting Interferometry (PSI)

Root Mean Square deviation (RMS)

Scanning Electron Microscopy (SEM)

Single-Point Diamond Turning (SPDT)

Swelling Ratio (SR)

Transmission Electron Microscopy (TEM)

Ultra-Precision Machining (UPM)

Ultra-Precision Machining (UPM)

Ultra-Precision Grinding (UPG)

Ultra-Precision Raster Milling (UPRM)

X-ray Diffractometer (XRD)

Appendix II. Specification of Wyko NT8000

Work Parameters	Measurement System	Modular Optics Assembly equipped with a CCD camera and a Multiple Magnification Detector with Field of View lenses
	Supporting unit	Air anti-vibration system
	Work Table	Motorized stage with 8 inches of travel in x-y directions
	Maximum travel Length of Z axis	100mm
	Tip/tilt of cradle	$\pm 6^\circ$
Phase-shifting Interferometry (PSI)	Light Source	Monochromatic light source
	Range of surface roughness measurement	< 20-30nm
	Vertical surface roughness resolution	Sub-nanometer, adjacent pixel-height difference < $\lambda/4$
	Calibration routine	3-5 fringes at 45°
Vertical-scanning Interferometry (VSI)	Light Source	White light source
	Range of surface roughness measurement	Rough-surface object
	Vertical surface roughness resolution	Adjacent pixel-height difference > $\lambda/4$
	Calibration routine	3-5 fringes aligned perpendicular to the edge of step

Appendix III. Specification of Talysurf PGI 1240

Work Parameters	Measurement System	A stylus arm and a helium-neon laser interferometer of pick up system in x-y directions
	Supporting unit	Air anti-vibration system
	Traverse length of stylus	200mm traverse unit
	Straightness of the traverse	0.125 μ m over 200mm
	Work table	Motorized stage of y-axis 125mm travel in y-axis with 1 μ m resolution
	Maximum travel length of Z axis	450mm
Configuration settings	Available Measurement Speed	0.1mm/s 0.25mm/s 0.5mm/s 1mm/s 2mm/s
	Standard Stylus lateral resolution	0.8nm
	Standard Stylus tip/tilt of cradle	$\pm 90^\circ$